DEVELOPMENT OF SLOW-RELEASE NANO-COMPOSITE FERTILIZER USING BIODEGRADABLE SUPERABSORBENT POLYMER

By

Benard Kiplangat Rop

I80/50014/2015

Department of Chemistry,

University of Nairobi

A Thesis Submitted in Fulfillment of the Requirements for the Degree of Doctor of Philosophy in Chemistry of the University of Nairobi

November, 2019

DECLARATION

I declare that this thesis is my original work and has not been submitted elsewhere for examination, award of degree or publication. Where other people's work or my own has been used, this property has been acknowledged and referenced in accordance with the University of Nairobi's requirements.

Signature_____   Date_____

Benard Kiplangat Rop

I80/50014/2015

Department of Chemistry,

School of Physical Sciences,

University of Nairobi

This thesis has been submitted for examination with our approval as research supervisors.

1. **Dr. Damaris Mbui**   Signature_____   Date_____
   Department of Chemistry,
   University of Nairobi

2. **Dr. George N. Karuku**   Signature_____   Date_____
   Department of Land Resources &
   Agricultural Technology,
   University of Nairobi

3. **Dr. Njagi Njomo**   Signature_____   Date_____
   Department of Chemistry,
   University of Nairobi

4. **Dr. Immaculate Michira**   Signature_____   Date_____
   Department of Chemistry,
   University of Nairobi

DEDICATION

My wife Gladys for her constant love, support and encouragement throughout this journey; I couldn't have done it without you.

My sons, Brian, Ian and Allan

ACKNOWLEDGMENT

PUBLICATIONS

1. Kiplangat Rop, Damaris Mbui, Njagi Njomo, George N. Karuku, Immaculate Michira, Rachel F Ajayi (2019), Biodegradable water hyacinth cellulose-graft-poly(ammonium acrylate-co-acrylic acid) polymer hydrogel for potential agricultural application, *Heliyon,* **5**(3): e01416.

2. Kiplangat Rop, George N. Karuku, Damaris Mbui, Immaculate Michira, Njagi Njomo (2018), Formulation of slow release NPK fertilizer (cellulose-graft-poly(acrylamide)/nano-hydroxyapatite/soluble fertilizer) composite and evaluating its N mineralization potential, *Annals of Agricultural Sciences,* **63**: 163-172.

3. Kiplangat Rop, George N. Karuku, Damaris Mbui, Njagi Njomo, Immaculate Michira (2019), Evaluating the effects of formulated nano-NPK slow release fertilizer composite on the performance and yield of maize, kale and capsicum, *Annals of Agricultural Sciences,* **64**: 9-19.

Patent Application

Patent application No. 3319, Filed June, 2019, Kenya Industrial Property Institute (KIPI)

ABSTRACT

This work aimed at developing a slow release nano-composite fertilizer (SRF) for improved nutrient use efficiency in soil using a biodegradable superabsorbent polymer. Partially neutralized acrylic acid was grafted onto cellulose isolated from water hyacinth by radical polymerization reaction. The reaction conditions were optimized through assessment of grafting parameters namely, grafting cross-linking percentage (GCP), percentage grafting cross-linking efficiency (%GCE) and water absorption tests. The copolymer was characterized by Fourier transform infra-red (FTIR) spectroscopy, X-ray diffraction (XRD), Transmission electron microscopy (TEM) and Energy dispersive X-ray (EDX) spectroscopy. Water absorbency of the copolymer hydrogel was assessed in saline solutions and in solutions of various pH values. Degradation of the copolymer was tested by soil burial test and microbial culture isolated from agricultural soil. The optimized product exhibited superabsorbent qualities in distilled water and the water absorbency was influenced by pH and by the presence, nature and concentration of ions. The copolymer revealed the capacity to retain moisture in soil and degradation both in soil and microbial culture. A SRF was formulated by incorporating nano-hydroxyapatite (nano-HA), urea, $(NH_4)_2HPO_4$ and K_2SO_4 into the cellulose grafted copolymer, and the release of nutrients was assessed using laboratory incubation experiment. Significantly higher ($p \leq 0.05$) content of mineral nitrogen (mineral-N) was observed in the first 4 weeks in conventional fertilizer (CF) compared to SRF treatments and the control. Mineral-N content in SRF treatments increased considerably between the 8th and 12th week, and declined in the 16th week. The values of potentially mineralizable N estimated using single first-order kinetics model related well to the observed cumulative mineral-N at 16th week. Significantly higher P content was observed in CF compared to SRF treatment in the 4th week, whereas in the 8th week, some SRFs released significantly higher content than CF. The data revealed reduced chances of leaching losses and toxic effect to the plant roots, as well as synchronized nutrient release to cater for the requirement by crops. Effect of the formulated SRF on the performance and yield of maize, kale and capsicum was evaluated in a greenhouse experiment. SRF recorded higher dry matter and yields relative to CF with similar application rates, though statistically insignificant. The agronomic optimal application rates of SRF determined by quadratic function were higher than that of CF. SRF enhance growth and yields of crops just like CF and could potentially have greater benefits such as improving soil health and resilience. Therefore, a slow release nano-composite fertilizer has been fabricated and investigated under laboratory and greenhouse (controlled) conditions. It is recommended that the formulated SRF be tested under field conditions.

TABLE OF CONTENTS

LIST OF TABLES

LIST OF FIGURES

LIST OF SCHEMES

LIST OF ABBREVIATIONS, SYMBOLS AND ACRONYMS

d_{hkl}	Interplanar spacing
3-D	Three dimensional
AA	Acrylic acid
AAS	Atomic absorption spectroscopy
ANOVA	Analysis of variance
AOAR	Agronomic optimal application rate
APS	Ammonium persulphate
BC	Biochar
BP	Biopolymer
CAN	Calcium ammonium nitrate
CEC	Cation exchange capacity
CF	Conventional fertilizer
CMC	Carboxymethyl cellulose
CNC	Cellulose nano-crystal
CRD	Completely randomized design
CRF	Controlled release fertilizer
DAP	Diammonium phosphate
DM	Dry matter
DN	Degree of Neutralization
DNA	Deoxyribonucleic acid
EC	Ethyl cellulose
ECe	Electrical conductivity
EEF	Enhanced efficiency fertilizer
FTIR	Fourier Transform Infra-red
GCE	Grafting cross-linking efficiency
GCP	Grafting cross-linking percentage
GHG	Greenhouse gases
HA	Hydroxyapatite
HEC	Hydroxyethyl cellulose

HPMC	Hydroxypropylmethyl cellulose
HSD	Highest significant difference
IBDU	Isobutylidenediurea
K	Potassium
KeV	Kilo electric volts
MAP	Mono-ammonium phosphate
MBA	*N,N*-methylene-*bis*-acrylamide
MC	Methyl cellulose
MHC	Moisture holding capacity
Mineral-N	Mineral nitrogen
MT	Metric tones
MW	Molecular weight
MWD	Molecular weight distribution
N	Nitrogen
NaCMC	Sodium carboxymethyl cellulose
NUE	Nutrient utilization (use) efficiency
OC	Organic carbon
OECD	Organisation for Economic Co-operation and Development
OM	Organic matter
P	Phosphorus
PAA	Polyacrylic acid
PAM	Polyacrylamide
PBM	Phosphate buffered medium
PHG	Polymer hydrogel
PVA	Polyvinyl alcohol
RAM	Residual acrylamide monomer
ROS	Reactive oxygen species
rpm	Revolutions per minute
SAP	Superabsorbent polymer
SEM	Scanning electron microscopy
SEQ	Swelling equilibrium

SRF	Slow release fertilizer
SSA	sub-Saharan Africa
SSP	Single superphosphate
TEM	Transmission electron microscopy
TSP	Triple superphosphate
UAN	Urea ammonium nitrate
UF	Urea-formaldehyde
WH	Water hyacinth
WRB	World reference base
XRD	X-ray diffraction
θ	Angle
λ	Wavelength

APPENDICES

CHAPTER ONE

1.0 INTRODUCTION

1.1 Background information

Agriculture is the key driver to economic growth and source of livelihood in rural areas which is approximately 80% of the Kenyan population (Mauyo, *et al.,* 2011; Shoals, 2012; Kenya Economic Report, 2017). Soil fertility decline contributes to low crop yields due to lack of nutrient resources, imbalanced nutrient mining, reduced fallow periods, fewer rotations and soil erosion, among other factors (Kimetu *et al.,* 2007; Mucheru-Muna *et al*., 2014). To increase and sustain crop yields, farmers apply conventional fertilizers such as Diammonium phosphate (DAP), Nitrogen, Phosphorous and Potassium (NPK), Triple superphosphate (TSP), Calcium ammonium nitrate (CAN), urea (Mathenge, 2009; Shoals, 2012; Oseko and Dienya, 2015) and to some extent organic manure, to supply the most limiting nutrients (NPK).

Of the amount of fertilizers applied to the farms, only a small percentage is utilized by plants, while the rest is eventually washed into water bodies (Tolescu *et al.,* 2009) through leaching and surface run-off, or lost by volatilization under reduced conditions. Split application by top-dressing is known to improve nutrient use efficiency (NUE), but small-scale poor-resource farmers consider it a luxury, or apply below recommended rates (Mucheru-Muna *et al.*, 2014) leading to poor crop performance. The exclusive use of organic manure on the other hand, is hampered by bulkiness, low nutrient quality, low nutrient mineralization (Makokha *et al.,* 2001; Gaskell and Smith, 2007; Leye and Omotayo, 2014) and extra labour. Efforts have been made to minimize these challenges by developing new generation fertilizers, so-called "smart" fertilizers, and among them are slow release fertilizers (SRF).

SRF contains at least one nutrient that either delays its availability and utilization processes, or is available for plants' uptake for a longer period than a standard fertilizer considered "quickly available" (Zeroual and Kossir, 2012; Chen *et al.,* 2013). The availability of nutrients is prolonged by either slowing the release or altering reactions leading to losses (Olson-Rutz *et al*., 2011). SRF can be applied during planting and the need for split application is eliminated,

reducing production costs (Chao *et al.,* 2013). The use of SRF in crop production is considered beneficial due to reduced risk of environmental nutrient loss (Guertal, 2009; Li *et al*., 2017) but the relatively higher production cost currently compared to conventional fertilizers impedes their adoption for agronomic use (Noellsch *et al*., 2009; Liu *et al*., 2014).

Nano-technology has offered another possibility of utilizing nano-structured materials as fertilizer delivery vehicles for building "smart" fertilizers (Naderi and Danesh, 2013). Up till now, intensive research has been directed towards integrating nano-technology into fertilizer development or formulation. Due to high surface area to volume ratio, nano-fertilizers are anticipated to be more efficient than conventional polymer-coated SRF in enhancing NUE and minimizing the potential negative effects associated with excess fertilizer application such as water pollution (DeRosa *et al.,* 2010). Hydroxyapatite (HA) nano-particles are among the major candidates for potential agricultural nutrient sources (Kottegoda *et al.,* 2011; Kottegoda *et al.,* 2017). However, much of the available data on nano-HA mainly focus on biomedical application (Mateus *et al.,* 2007; Pang *et al.,* 2010; Costescu *et al.*, 2010; Pataquiva-Mateus *et al.,* 2013), while agricultural application is lacking.

More recently, there has been a growing interest to use polymer hydrogels (PHG) in agricultural production. PHGs are macro-molecular networks with the ability to swell in water due to hydrophilic groups such as $-SO_3H$, $-CONH-$, $-CONH_2$, and $–OH$, and slightly cross-linked structure which resists dissolution (Sannino *et al.,* 2009; Qiu and Hu, 2013; Laftah and Hashim, 2014). PHGs with high absorption capacities of up to 1000 times their own dry weight are referred to as super-absorbent polymer (SAP) hydrogels. They have wide applications in food industry, pharmaceuticals, agriculture, bio-medicine, bio-engineering and environmental remediation, among others (Shi *et al*., 2011; Laftah and Hashim, 2014; Ahmed, 2015).

Depending on the source, PHGs are often divided into; synthetic and natural hydrogels. Synthetic PHGs have excellent water absorbency, long shelf lives and high gel strength (Yu *et al*., 2011; Ahmed, 2015; Chai *et al*., 2017). However, non-biodegradability and toxicity in the environment limit their use in agriculture and consumer products (Yu *et al*., 2011; Laftah *et al*., 2011). Natural-based PHGs have been developed by amalgamating synthetic and natural substrates such as polysaccharides and polypeptides (Ahmed, 2015; Chai *et al*., 2017).

Polysaccharides have attracted much attention and cellulose, a polysaccharide, is rated as the best potential candidate for the production of bio-degradable PHGs due to its properties such as hydrophilicity, bio-degradability and good mechanical strength, among others (Shi *et al*., 2011). Cellulose is an active bio-polymer that can be chemically modified owing to the presence of -OH groups which participate in classical reactions such as oxidation and esterification (Roy *et al*., 2009; Sannino *et al*., 2009; Ambjörnsson, 2013; Qiu and Hu, 2013). Cellulose derivatives such as carboxymethyl cellulose and ethyl cellulose have been obtained by reacting –OH groups of cellulose repeat unit (Roy *et al*., 2009; Ambjörnsson, 2013; Qiu and Hu, 2013).

Synthesis of cellulose grafted polymers is another means of modifying physico-chemical properties of cellulose. Free radical polymerization is often used technique in grafting of monomers onto cellulose and/or its derivatives (Laftah *et al*., 2011; Ahmed, 2015). The free radicals are generated using initiation techniques such as UV, high energy irradiation (γ-ray or electron beams) and redox initiation with Mn or Ce (iv) ion. Cellulose-based PHGs are usually synthesized using cellulose derivatives such as carboxymethyl cellulose (Sadeghi *et al*., 2011; Sadeghi *et al*., 2013; Demitri *et al*., 2013). Polymerization reactions with these derivatives as substrates are performed in homogeneous reaction mixtures because of their solubility in various solvents. The -OH groups in cellulose chains enable grafting of vinyl monomers enhancing hydrophilicity, a feature useful in application prospects such as agriculture where biodegradability, and water retention and release is essential.

Despite exhibiting properties with potential application as fertilizer carriers and soil conditioners, high cost of producing bio-based hydrogels using cellulose derivatives limits their application. However, cellulose being the most abundant and renewable biopolymer, can be derived from a wide variety of biomass such as the water hyacinth (*Eichhornia crassipes*). Alkaline treatment of cellulose has an effect on supra-molecular structure, weakens molecular H-bonds and loosens the packing of its micro-fibrils, enhances swelling, resulting in improved accessibility of reactive –OH groups to the chemical reagents (Roy *et al*., 2009; Gupta *et al*., 2013; Pönni, 2014).

Water hyacinth (WH), an invasive non-native species in Kenya, infests rivers, dams, lakes and irrigation channels, causing serious economic and environmental problems. Due to the hyacinth's high growth rate, it has been a great challenge to control its invasion and proliferation.

The use of herbicide to eliminate this weed is effective, but herbicides' effects are hazardous to the environment. Water hyacinth has been utilized locally as compost manure, feed for animals and fish, paper-making, crafts (ropes, baskets, chairs, fibreboards) (Jafari, 2010; Istirokhatun at el., 2015), wastewater treatment (Zhu *et al*., 1999), production of biogas (Kivaisi and Mtila, 1997), ethanol (Aswathy *et al*., 2010) and charcoal briquettes (Rezania *et al*., 2016), among others. However, utilization of WH cellulose in the production of PHG has not been explored. The use of cellulose derived from WH can reduce the cost of production, impart biodegradability, and enhance the swelling and mechanical strength while at the same time helping to root out the weed.

Polyacrylamide (PAM) is a chemical intermediate in the production of super-absorbents PHGs such as diapers, medical and agricultural products, among others (Laftah and Hashim, 2014). High molecular weight PAM is added into the soil through irrigation water as anti-erosion additive (Kay-Shoemake *et al*., 1998a and 1998b**;** Charoenpanich, 2013) and it has been reported to be degraded by native soil bacteria such as *Pseudomonas* and *Bacillus sp.,* and fungi *(Aspergillus)* which are capable of accessing N through *amidase* activity (Guezennec *et al.,* 2015; Yu *et al.,* 2015). Extracellular amidase enzyme catalyzes the hydrolysis of amide (-$CONH_2$) group, resulting in generation of NH_3, NH_4^+ and -COOH group. The production of NH_3 under moisture conditions contributes to mineral N in the soil, whereas carboxylic acid is further degraded by micro-organisms as source of carbon (energy) to CO_2 and H_2O, thus being environmental friendly. PAM-treated agricultural soil has been experimentally demonstrated by Kay-Shoemake *et al.* (1998a and 1998b**)** to exhibit higher bacterial counts, high inorganic N concentration and amidase activity, hence considered healthier soil than the untreated ones.

This study aimed at producing biodegradable PHG by heterogeneously grafting acrylic monomers onto cellulose fibres isolated from WH, as an alternative means of managing its invasiveness coupled with economic gain. The cellulose grafted polymer hydrogel was utilized in the formulation of a slow release fertilizer composite and the release of nutrients was assessed using laboratory incubation experiment. The response of maize, kale and capsicum to the formulated slow release nano-NPK fertilizer (cellulose-graft-poly(acrylamide)/nano-hydroxyapatite/soluble fertilizer) composite was evaluated to establish their optimal application rates in a nitisol soil group in Kabete, Kiambu County, Kenya.

1.2 Statement of the problem

A major constraint to fertilizers use and profitable farming in Kenya has been high production cost. This is a function of a number of variables such as high cost of transport, fertilizer unavailability, lack of credit, poor markets, devaluation of domestic currencies, weak extension services and skewed agricultural policies that favor industrialists but not the farmers (Salami *et al*., 2010; Druilhe and Barreiro-Hurlé, 2012; Muthoni *et al*., 2013; Karuku *et al*., 2017). Thus, alternative sources of cheaper fertilizers are being sought.

The low nutrient use efficiency and hence higher losses of conventional fertilizers are great challenges which influence crop production and safety of the agricultural environment (Wang *et al*., 2013; Puntel *et al*., 2016). N and P nutrients are mostly applied to farms using conventional fertilizers. When nutrient use efficiency (NUE) by plants is low, these nutrients are lost through leaching below the root zone and surface run-off.

Biodegradable, environmental-friendly and sustainable, bio-based products are being sought due to increased environmental consciousness. Consumer awareness is increasing, and more and more people are inclined to buying eco-friendly products. Thus market pull for "greener" products has been the overriding force for product development, including fertilizers (Giroto *et al*., 2017).

Water Hyacinth (WH) grows at a rapid rate in fresh water bodies. It covers some parts of Lakes Victoria and Naivasha, and recently Nairobi dam, threatening the fishing industry and fresh water supply. In this study, cellulose isolated from the WH is utilized in the synthesis of biodegradable polymer hydrogel (PHG). A slow release fertilizer composite is then formulated by incorporating nutrients (NPK) into the polymer hydrogel in an effort to improve the NUE.

1.3 Objectives

1.3.1 General objective

The main objective of this research was to develop a slow-release nano-composite fertilizer for improved nutrient utilization efficiency in soil using a biodegradable superabsorbent polymer derived from water hyacinth.

1.3.2 Specific objectives

1. To synthesize and characterize Superabsorbent Polymer (SAP) hydrogel derived from the water hyacinth.
2. To assess and optimize the efficiency of the SAP.
3. To develop a Slow Release Fertilizer (SRF) by encapsulating NPK, urea, nano-hydroxyapatite onto the SAP
4. To determine the kinetics and mechanisms of nutrient release from SAP.
5. To assess the performance of SRF composite using selected crops in a greenhouse experiment.

1.4 Justification of the study

Fertilizers play a key role in promoting food security, especially in developing countries such as Kenya. It is well known that the yield of many crops is on the decline due to imbalanced nutrient replenishment and decrease in soil organic matter, among other factors (Kimetu *et al.,* 2007; Mucheru-Muna *et al*., 2014). About 40–70 % N and 80–90 % P of conventional fertilizers applied to the farms are lost to the environment causing economic and resource losses, and environmental pollution (Guo *et al*., 2005; Naderi and Danesh, 2013; Giroto *et al*., 2017). Excessive application of N and P fertilizers leads to contamination of underground water and eutrophication in surface water bodies (Guo *et al*., 2005; Jeng and Vagstad, 2009; Savci, 2012; Yuan *et al*., 2014). Further, excessive N fertilizer application can affect the climate by stimulating carbon storage in soils associated with increased production of crops, thus reducing CO_2 content in the atmosphere (Hanqin *et al*., 2012). Nonetheless, it can lead to increased production of N_2O, a potent greenhouse gas.

Research has demonstrated that slow release fertilizer formulations could improve NUE. The fact that the NUE is about 20-50 % for N, and 10-25 % for P fertilizers (Liu *et al*., 2007; Naderi and Danesh, 2013; Yuejin *et al*., 2013), improved nutrient use implies more efficient food production. Further, increasing NUE will have less, if any, negative environmental impacts and many positive impacts. It would also promote environmental conservation because of reduced pressure to convert forests and riparian lands for agricultural use.

N is rated as the key nutrient in the production of food and biomass in agriculture. Since, 50–70 % of N is supplied to the crops through conventional fertilizers; attempts to improve NUE in these fertilizers have resulted in little success (DeRosa *et al*., 2010; Kottegoda *et al*., 2011). Slow release fertilizers (SRF) are anticipated to enhance NUE and subsequently, improve crop yield, minimize economic losses and increase profits in crop production. The nutrient availability is increased by slowing their release or altering reactions that lead to losses (Fan and Xiaolin, 2009; Olson-Rutz *et al*., 2011).

The United Nations projects the world's human population to be about 9 billion by the year 2050 (Jaggard *et al*., 2010; Zeroual and Kossir, 2012; Naderi and Danesh, 2013). In order to feed this population, agricultural development can be realized through increased productivity by use of modern technologies such as nano-technology (DeRosa *et al*., 2010; Naderi and Danesh, 2013; Montalvo *et al*., 2015). Nano-fertilizers are predicted to be more efficient in nutrient delivery than conventional polymer-coated SRFs (DeRosa *et al*., 2010; Monreal *et al*., 2015).

Polysaccharides are eco-friendly, cheap, abundant, available and renewable organic material, and can be effectively used as raw materials for superabsorbent polymers (Zohuriaan-Mehr and Kabiri, 2008; Shi *et al*., 2011). The use of non-wood cellulose sources has been developed since wood is more expensive and also associated with environmental conservation. Water hyacinth is rated as one of the most invasive perennial aquatic weed and it has been regarded as a nuisance in many aquatic environments (Girisuta *et al*., 2008; Jafari, 2010; Reales-Alfaro *et al*., 2013; Istirokhatun at el., 2015). It can however serve useful purposes, among them being fertilizer production. Whereas controlling WH has proven to be a challenge, utilizing this plant for SRF production provides an alternative approach to deal with this invasive species, and with economic benefits. The cellulose derived from this plant can be used to produce biodegradable

polymer hydrogel which can act as a nutrient carrier in the formulation of a slow release fertilizer.

1.5 Hypotheses

i). Grafting a vinyl monomer onto WH cellulose through the –OH group forms a hydrophilic bio-degradable copolymer.

ii). Polymerization reaction and hydrophilicity of the copolymer is influenced by reaction conditions such as cellulose content, monomer to cross-linker ratio, initiator content, volume of the reaction mixture and temperature.

iii). Hydrophilic copolymer (PHG) encapsulates nutrients and absorbs moisture alongside micro-organisms in soil, initiating slow release of nutrients.

iv). The release of nutrients from superabsorbent polymer follows a kinetics model.

v). The performance parameters of crops receiving SRF treatment are higher than those of conventional fertilizer treatment with comparable application rates.

CHAPTER TWO

2.0 LITERATURE REVIEW

2.1 Fertilizers in agricultural production

Agriculture is Kenya's economic mainstay dominated by small-scale farmers in rural areas and hence, an important sector as regards food security and poverty alleviation. This sector is approximated to directly contribute 26 % of Gross Domestic Product (GDP) and indirectly about 27 % through manufacturing and service related industries (Mauyo, *et al.,* 2011; Kenya Economic report, 2017). The crop sub-sector accounts for 79% of agricultural GDP, generates about 50% of Kenya's export earnings, 18% of formal employment and 60% of total employment (Kenya Economic report, 2017). Farmers in Kenya face acute constraints such as unavailability and high cost of fertilizers, lack of credit and technical knowledge, poor crop markets, among other factors; hence, smallholder poor-source farmers may not be in a position to use fertilizers, or may apply below optimal rates (Salami *et al.*, 2010; Druilhe and Barreiro-Hurlé, 2012; Mucheru-Muna *et al.*, 2014; Muthoni *et al.*, 2013; Karuku *et al.*, 2017). Fertilizer subsidy programme has been effective in increasing fertilizer use and subsequently improving crop yields, but its success depends on implementation which is limited by administrative targeting, late delivery of fertilizer, leakages and fraud (Druilhe and Barreiro-Hurlé, 2012). Fertilizers are classified into two broad categories as inorganic and organic fertilizers, and they can supply macro-nutrients (N, P, and K), secondary nutrients (Ca, Mg, Na, and S) and micro-nutrients (Fe, Mn, Zn, B, Mo, Cu and Cl) (Fertilizer Manual, 1998; Leye and Omotayo, 2014).

2.1.1 Inorganic fertilizers

Inorganic fertilizers are commonly used by farmers because they are relatively easy to transport, store, apply and they exist in a variety of formulae that satisfy specific crop requirements. Nitrogenous fertilizers include NH_3, $(NH_4)_2HPO_4$, NH_4NO_3, $(NH_4)_2SO_4$, $CaCN_2$, $Ca(NO_3)_2$, $NaNO_3$, and N_2H_4CO. Phosphorous fertilizers are supplied as $(NH_4)_2HPO_4$, $Ca(H_2PO_4)_2$, and K fertilizers as K_2SO_4 or KCl (http://agritech.tnau.ac.in/agriculture/agri_nutrientmgt_fertilizers.html, 11 March, 2019).

Nitrogen is the most limiting nutrient in crop production due to high cost and demand by plants; hence, any luxurious application is unattractive to the farmers because of diminishing returns (Good and Beatty, 2011; Mullen, 2011). Unlike other nutrients, N undergoes several transformations in soil and may exist in the form of organic-N and mineral-N such as NH_4-N, NO_3-N, N_2O, NO_2, NO and NH_3, that can be lost in soil through surface run-off, leaching, denitrification and volatilization (Kimetu $et\ al.,$ 2007; Zaman $et\ al.$, 2008; Good and Beatty, 2011; Leye and Omotayo, 2014). Mineralization is one of the transformation processes in the soil involving conversion of organic-N into NH_3 which is rapidly converted to NH_4-N under acidic conditions (Leye and Omotayo, 2014; Karuku and Mochoge, 2016; Zhang $et\ al.$, 2017). NH_4-N is adsorbed onto soil particles (immobilized) because it is positively charged and hence leaching does not occur under normal soil conditions (Chen, 1997; Zaman $et\ al.$, 2008; Leye and Omotayo, 2014). However, it can be oxidized by nitrifying bacteria under aerobic conditions into highly soluble and mobile NO_3-N that can easily leach (Sahrawat, 2008; Zaman $et\ al.$, 2008). Application of N fertilizer into the soil increases soil pH, though the effect is temporary because an acid residue is formed during nitrification process (Zaman $et\ al.$, 2008).

Plants roots absorb P from the soil in the form of orthophosphate ions ($H_2PO_4^-$ or HPO_4^{2-}), with $H_2PO_4^-$ being absorbed more readily than HPO_4^{2-} (Leye and Omotayo, 2014). These anions highly react with cations such as Mg^{2+}, Ca^{2+}, Al^{3+} and Fe^{3+} in the soil (Reddy, 2014). P can be adsorbed in acidic soils by Al/Fe oxides and hydroxides, and precipitated in neutral pH to calcareous soil by Mg^{2+} and Ca^{2+} ions (Shen $et\ al.$, 2011). About 80 % of P in conventional fertilizers that is added to the soil is precipitated as metal ion complexes, suggestive of low nutrient use efficiency (NUE) (Abbasi $et\ al.$, 2015). Potassium exists in soil as water-soluble, exchangeable, non-exchangeable and mineral forms such as feldspar and micas. The water-soluble and exchangeable K are available for plants' uptake, while non-exchangeable K may contribute to plant's uptake at low levels of exchangeable K in certain types of soil (Basak and Biswas, 2009). It is adsorbed by negatively charged clay minerals and the organic matter, hence cannot easily leach and usually not deficient in tropical soils (Basak and Biswas, 2009; Leye and Omotayo, 2014). Soil pH, defined as the degree of acidity or alkalinity of soil, is among the conditions that contribute to the health and quality of soil. It influences soil physico-chemical properties and biological processes and subsequently, plants' growth. It plays a fundamental role

in the availability of essential nutrients, bio-activity of micro-organisms and solubility of phytotoxic elements such as Al and Mn which have greater solubility at pH < 5.5 (Kisinyo *et al*., 2014).

Small scale farmers occupying 70 % of land under cultivation in Kenya grow crops largely for subsistence and only participate in output market on surplus (Shoals, 2012). The recent trends on fertilizer use in Kenya by crops shows that maize consumes the largest portion (about 50%), followed by tea, sugarcane, wheat, beans and flowers as shown in Table 2.1 (Oseko and Dienya, 2015). Like most SSA countries, Kenya depends on the international markets for its fertilizers, which include USA, Europe, Asia, Middle East, South Africa, and more recently China, India and Singapore, as local production does not exist or is limited (Mathenge, 2009; Shoals, 2012; Oseko and Dienya, 2015; Nduati *et al*., 2015). Local firms such as Mea, Athi River Mining (Mathenge, 2009; Nduati *et al*., 2015) and Toyota Tsusho Fertilizer Africa, formulate blends using mainly imported inputs for various crops and soils. The four main fertilizers imported are DAP, CAN, Urea, and NPK (17:17:0). Others include soil- and crop-specific fertilizers such as NPK 17:17:17 for coffee, NPK 25:5:5 for tea and some specialized blends containing added nutrients and minerals meant for horticultural crops (Shoals, 2012; Oseko and Dienya, 2015; Nduati el., 2015). Due to high acidity levels of soil, and subsequent decrease in crop yields, the Government of Kenya and research institutions has spearheaded a shift towards soil-specific fertilizers. This trend is considered to have led to increased consumption of crop- and soil-specific fertilizers such as CAN and a range of Athi River Mining products (Nduati *et al*., 2015).

Table 2.1. Total quantity of fertilizer used by crop in 2011-2013

	Total quantity of fertilizer used per crop (MT)		
CROP	2013	2012	2011
Maize	268, 605, 229	273, 496, 424	268, 695, 741
Tea	101, 036, 570	99, 083, 200	98, 983, 935
Sugarcane	28, 103, 519	29, 193, 854	29, 175, 193
Wheat	25, 621, 563	29, 066, 258	24, 473, 674
Beans	20, 719, 820	21, 102, 929	20, 584, 107
Flowers	17, 123, 485	17, 058, 712	17, 715, 880
Other crops	67, 215, 003	64, 275, 113	52, 734, 695
Total Fertilizer Type	528, 425, 162	533, 276, 490	512, 363, 225

Note: Adapted from Oseko and Dienya (2015).

The use of conventional fertilizers, particularly N fertilizers may decrease soil productivity by increasing soil pH; reducing water-holding capacity, cation exchange capacity, base saturation, hydraulic conductivity, soil aggregation, porosity and microbial activity; and increasing soil bulk density and compaction (Savci, 2012; Ge *et al*., 2018). This can contribute to increased levels of greenhouse gases (GHG) such as N_2O which is rated as the third most significant GHG after CO_2 and CH_4 (Good and Beatty, 2011; Hanqin *et al*., 2012; Savci, 2012). Chemical N fertilizers used in China's cropland for more than 5 decades has been estimated to sequester 5.96 Tg C yr^{-1} (1 Tg = 1012 g), and the potential C sequestration rate was expected to reach a significant 'carbon benefit' value of 12.1 Tg C yr^{-1} (Hanqin *et al*., 2012). A study carried out over 6 decades (1949-2008) on food benefit and climate consequence of N addition showed that N fertilizer-induced crop yield and C sequestration have reached their peak, while N_2O emission continued rising (Hanqin *et al*., 2012). Excessive fertilizer application may lead to accumulation of N and P levels in the soil which is of environmental concern rather than agronomic benefit. The accumulated nutrients may be leached to underground aquifers or washed by surface run-off into rivers and lakes resulting in eutrophication (Good and Beatty, 2011; Jeng and Vagstad, 2009; Savci, 2012; Yuan *et al*., 2014). Excess nitrates and phosphates in water bodies boost excessive growth of algae which depletes dissolved oxygen in water leading to death of fish and other aquatic life. Elevated levels of nitrates in drinking water cause methemoglobinemia or "blue baby" disease (Savci, 2012).

2.1.2 Organic fertilizers

Organic materials used to improve fertility and conditions of soil include animal wastes, crop residues, farm yard manure, organic municipal wastes, microbial preparations, vermi-compost, sewage sludge, cover crop residues and some industrial wastes (Gaskell and Smith, 2007). The forms of N present in these materials are organic-N, NH_4-N and NO_3-N (Gaskell and Smith, 2007; Leye and Omotayo, 2014). The predominant form of N is organic-N which has to be decomposed and mineralized to ammonium/ammonia. NH_4^+ and NH_3 are rapidly interchangeable depending on the soil pH, in the sense that, increasing pH increases NH_3 content and decreases NH_4^+, and vice versa. The application of organic fertilizer into the soil improves nutrient status and structure, reduces use of chemical fertilizers and erosion hazards, and sequesters carbon, among others (Annicchiarico *et al*., 2011; Masunga *et al*., 2016). However, they usually contain

nutrients in low levels and cannot be exclusively relied upon for optimal crop yields. The nutrient contents are variable and mineralization may not synchronize crop demands. They may contain significant levels of P which can present environmental hazard if the soil P content is already high (Gaskell and Smith, 2007; Leye and Omotayo, 2014). They are bulky to deploy the right amount of nutrients and demanding to apply large fields. They can be source of noxious weed seeds and pathogens if not well decomposed, and can damage plants if the salt content is high (Leye and Omotayo, 2014).

2.1.3 Slow and controlled release fertilizers

The cost of conventional fertilizers, economic losses and environmental impacts, has stimulated research to explore ways of increasing nutrient use efficiency (NUE). New generation of fertilizers ("smart" fertilizers) which are more efficient have been developed and applied in modern agriculture (Zeroual and Kossir, 2012). Examples of such fertilizers include slow and controlled release fertilizers (SRF and CRF), water-soluble polymer coated fertilizers, stabilized fertilizers and bio-smart fertilizers (Zeroual and Kossir, 2012; Rop *et al.*, 2018).

Controlled release fertilizer (CRF) is a coated fertilizer in which the release of nutrients in soil is controlled by temperature and coating characteristics (Guertal, 2009; Fan and Xiaolin, 2009). The fertilizer granule (NPK or urea) is physically coated with sulfur, resin, wax, or some combination of these materials (Fan and Xiaolin, 2009; Guertal, 2009; Zeroual and Kossir, 2012). The release of nutrients from these fertilizers may depend on soil moisture, microbial activity, temperature, pore size and coating thickness, or a combination of some of these variables (Guertal, 2009). The rate of nutrient release from CRFs that are available in the market is vulnerable to change in soil moisture content and varies with soil types, among other factors. These complications may lead to improper synchrony of nutrient release with plants' requirement or plants may be starved of nutrients (Davidson *et al.*, 2013). Furthermore, some products such as polyurethane- polyolefin- and alkyd resin-coated fertilizers are not well degraded in soil and their accumulation may degrade the soil structure contradicting the purposes of sustainable agriculture (Yuejin *et al.*, 2013).

SRF can be a N fertilizer whose N availability period is prolonged in the soil through addition of nitrification inhibitors such as dicyandiamide, 3,4-dimethylpyrazone phosphate, or urease inhibitors such as hydroquinone and *N*-(*n*-butyl)-thiophosphoric triamide (Zaman *et al*., 2008; Fan and Xiaolin, 2009; Guertal, 2009; Zeroual and Kossir, 2012). It can also be a modified urea formulated product such as urea-formaldehyde, isobutylidene diurea and triazone (Guertal, 2009). The decomposition of urea formulated products is due to microbial activity and hence, the release of N strongly depends on soil properties such as aeration, pH, moisture content, clay content and temperature (Fan and Xiaolin, 2009; Guertal, 2009; Tolescu and Horia, 2010). The use of slow and controlled release fertilizers in crop production remains a challenge to date because of high cost of production and are mostly used in developed countries (Rahman *et al*., 2008; Guertal, 2009; Zeroual and Kossir, 2012; Yuejin *et al*., 2013; Liu *et al*., 2014). There has been an ever increasing interest to utilize polymer hydrogels as nutrient delivery vehicles in the formulation of SRFs (Guo *et al*. 2005; Liu *et al*., 2007; Rahman *et al*., 2008; Zhong *et al*., 2013; Fernandes *et al*., 2015)

2.2 Polymers in agricultural application

A polymer is a macro-molecule composed of a sequence of one or more types of monomer units (OECD, 1993a). A monomer refers to a molecule that forms a covalent bond with two or more like or unlike molecules (OECD, 1993b). Polymers can be classified based on the following considerations (Wang *et al.,* 2019):

i). Origin (source) of materials; natural (proteins, cellulose), synthetic (nylon-6, 6, polyesters) and semi-synthetic polymers (cellulose nitrate, cellulose acetate).

ii). Polymer chain structure; linear, branched, cross-linked and network (3-D) polymers

iii). Mode of Polymerization; addition (chain-growth) and condensation (step-growth) polymers.

iv). Polymer composition; homopolymer and heteropolymer (or copolymer). Copolymers are further classified into alternating, random, block and graft copolymers.

v). Molecular forces; elastomers, fibres, thermoplastics and thermosetting polymers.

Polymerization reactions in the synthesis of polymers are often categorized based on the reaction mechanism, into chain-growth and step-growth polymerizations (Hacker *et al.,* 2019). Chain-growth (addition) polymerization involves initiation, propagation and termination steps. Depending on the nature of the active center of propagating chains, addition polymerizations are further classified into radical, ionic (cationic and anionic) and co-ordinative (transition-metal mediated) polymerizations. Step-growth polymerization is a repetitive condensation reaction between bi-functional monomers that result in elimination of molecules such as alcohol, water, HCl, etc., during polymerization reaction (Hacker *et al.,* 2019).

Polymers are versatile materials that have been used in agriculture as matrices for controlled delivery of agrochemicals such as fertilizers and pesticides, superabsorbent polymer hydrogels in soil conditioning and adsorbents in the removal of heavy metals ions in contaminated water and soil (Ekebafe *et al.,* 2011; Milani *et al.,* 2017).

2.2.1 Polymer hydrogels

Polymer hydrogels (PHGs) are hydrophilic materials with a 3-D network structure. They are able to undergo substantial swelling (or shrinking) in the presence (or absence) of water, and can maintain the swollen state even under pressure (Laftah *et al*., 2011; Laftah and Hashim, 2014; Ahmed, 2015). The absorption of water is attributed to hydrophilicity of functional groups such as $-SO_3H$, $-CONH-$, $-CONH_2$ and $-OH$ attached to polymeric chains, while resistance to dissolution is attributed to chemical or physical cross-links between the chains (Laftah *et al*., 2011; Laftah and Hashim, 2014; Ahmed, 2015). PHG with high absorption capacity in the order of 10 to 1000 times its own dry weight in water free of ions, is called a superabsorbent polymer (SAP) (Ekebafe *et al.,* 2011; Yu *et al*., 2011; Ahmed, 2015; Laftah and Hashim, 2014; Milani *et al.,* 2017). PHG that respond to external stimuli such as pH, heat and electric field, are referred to as "smart" or "intelligent" hydrogels (Sannino *et al*., 2009; Laftah *et al*., 2011; Ahmed, 2015; Chai *et al*., 2017).

Polymer hydrogels have been attracting much interest due to positive properties such as hydrophilicity and soft tissue-mimicking (Ren *et al*., 2014). These characteristics has enabled extensive applications as thickening agents (food), artificial organs (bio-medicine), controlled release agents (drugs, fertilizers, pesticides), moisture retention aids (agriculture) and as

adsorbents (environmental remediation), among others (Zohuriaan-Mehr and Kabiri, 2008; Ekebafe *et al.,* 2011; Laftah *et al*., 2011; Shi *et al*., 2011; Laftah and Hashim, 2014; Ren *et al*., 2014; Ahmed, 2015; Chai *et al*., 2017). The most important properties that enable wide application of PHGs are the swelling behavior and absorption capacity (Laftah *et al*., 2011; Laftah and Hashim, 2014). They are available in our daily lives as sanitary napkins, baby diapers, shampoo, soap, hair gel, toothpaste and contact lenses, among others (Zohuriaan-Mehr and Kabiri, 2008; Laftah *et al*., 2011; Laftah and Hashim, 2014; Ahmed, 2015).

The structural integrity of PHGs depends on the cross-links established between polymeric chains (Laftah *et al*., 2011; Ahmed, 2015). PHG networks can either be chemically bonded where irreversible links such as covalent bonds are formed between molecules, or physically bonded where the networks are held together by physical molecular entanglements and reversible molecular interactions such as H-bonds, charge and hydrophobic interactions (Laftah *et al*., 2011). The precursors in the synthesis PHG include the monomer, initiator and cross-linker. The free radical polymerization technique is often used to produce PHGs by reacting vinyl monomers with multi-functional cross-linkers (Zohuriaan-Mehr and Kabiri, 2008; Laftah *et al*., 2011; Ahmed, 2015).

The functional features of an ideal PHG include high water absorbency in saline solution, desired absorption rate, high water absorbency under load (AUL), low residual monomer, low cost, durable and stable in swelling environment and during storage, biodegradable, pH-neutrality, photo-stable, colorless, odourless and non-toxic, and re-wetting ability depending on the application requirement (Zohuriaan-Mehr and Kabiri, 2008; Ahmed, 2015). It is however, not possible for PHG to simultaneously fulfill all these features because the synthetic components which assist in achieving the maximum level of some of them lead to inefficiency of the rest. Thus, reaction variables have to be optimized to achieve appropriate balance between the properties (Zohuriaan-Mehr and Kabiri, 2008; Ahmed, 2015). For example, PHGs for hygiene application must have high absorption rate, low re-wetting and low residual monomer, whereas for agricultural application, high absorption rate is not necessary but, it must have high AUL and low sensitivity to saline solution (Zohuriaan-Mehr and Kabiri, 2008).

Based on the source, PHGs are often divided into synthetic and natural hydrogels. Synthetic PHGs such as polyacrylate and polyacrylamide have excellent water absorbency, long shelf life and high gel strength (Yu *et al*., 2011; Ahmed, 2015; Chai *et al*., 2017). However, non-biodegradability, high cost of production and their toxicity in the environment limit their use in agriculture and other consumer products (Yu *et al*., 2011; Laftah *et al*., 2011). Bio-based PHGs are usually prepared by adding some synthetic part to natural substrates and sources of natural materials include polysaccharides and polypeptides (Zohuriaan-Mehr and Kabiri, 2008; Ahmed, 2015; Chai *et al*., 2017). Polysaccharide-based hydrogels attracts much attention as they are eco-friendly, cheap, abundant, available and renewable organic materials (Zohuriaan-Mehr and Kabiri, 2008; Shi *et al*., 2011).

There have been attempts to graft vinyl monomers onto bio-polymers such as starch, cellulose, chitosan, agar, dextrin and gum to produce eco-friendly PHGs (Zohuriaan-Mehr and Kabiri, 2008; Yu *et al*., 2011; Shi *et al*., 2011). Among them, cellulose is the most potential candidate because of its biodegradability, good mechanical strength and linear structure of its macro-molecule that enables synthesis of PHGs with reinforced networks. Other properties attracting numerous applications in vast array of fields include biocompatibility, hydrophilicity, relative thermo-stabilization and alterable optical appearance (Shi *et al*., 2011; Qiu and Hu, 2013). Low cost inorganic compounds have also been incorporated into PHG structures as fillers to lower the cost of production and enhance mechanical strength that limit their wide application. The interest has been on clay minerals such as hydrated alumino-silicates due to small particle size and intercalation properties (Yu *et al*., 2011; Hosseeinzadeh and Sadeghi, 2012; Rashidzadeh *et al*., 2014).

2.2.1 Structure of cellulose

Cellulose is the most abundant bio-polymer of glucose found as the main constituent of plants and natural fibres such as cotton, and synthesized by bacteria such as *Acetobacter xylinum* (Sannino *et al*., 2009; Goetz, 2012; Qiu and Hu, 2013; Ambjörnsson, 2013; Abdel-Halim, 2014). Structurally, it is a linear polymer composed of β-D-glucopyranose ring monomers in $^4C_1$ chair conformation. The β-D-glucopyranose ring monomers are linked by 1,4-β-glycosidic bonds with each D-glucose monomer rotated 180° from its neighboring unit (Goetz, 2012; Ambjörnsson,

2013). The repeat unit in the cellulose chain is called cellobiose and often described as having reducing (aldehyde) end group and non-reducing (alcoholic) end group (Scheme 2.1) (Goetz, 2012; Ambjörnsson, 2013; Qiu and Hu, 2013). The linear structure of cellulose can extend to molecules containing 1000 - 1500 β-glucose units with high cohesive energy due to -H units (in axial vertical plane) and –OH units (in equatorial ring plane) that stabilize the polymer by forming extensive intra- and inter-molecular H-bonds (Roy *et al*., 2009; Goetz, 2012). The glucosidic linkages and H-bonding account for the high crystallinity and insolubility in common solvents such as water (Roy *et al*., 2009; Sannino *et al*., 2009; Ambjörnsson, 2013). Hydrophobic interaction has been proposed to exist between cellulose molecules and also linked to insolubility of cellulose in aqueous solutions (Ambjörnsson, 2013).
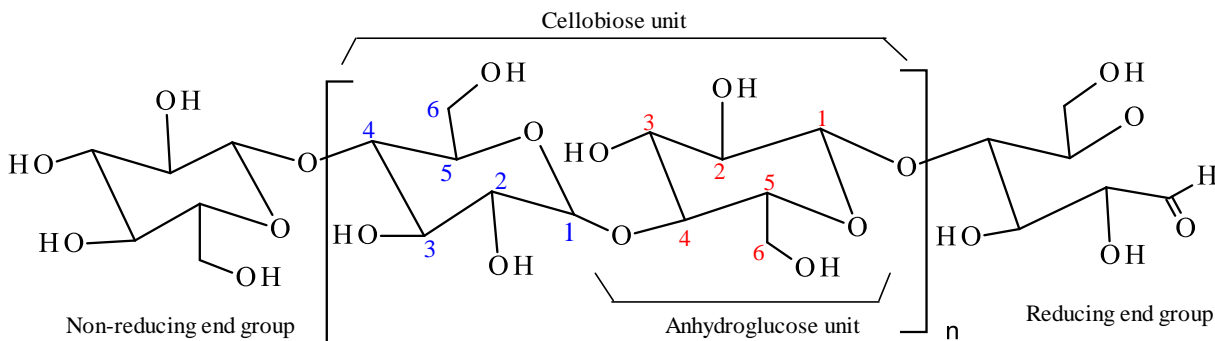
Scheme 2.1. Structure of cellulose (Goetz, 2012; Qiu and Hu, 2013)

Cellulose is the main constituent of plant's cell wall in lignocellulosic materials. Its fibre is embedded in a composite structure, which is composed lignin, hemicellulose, pectin and other carbohydrate polymers (Goetz, 2012; Abdel-Halim, 2014). The two structural regions found in cellulose fibres are the crystalline (ordered) and amorphous (disordered) regions (Roy *et al.,* 2009; Goetz, 2012; Ambjörnsson, 2013; Rambo *et al*., 2015). The polymorphs of crystalline cellulose include cellulose I, II, III and IV. Cellulose I (also referred to as native cellulose) is the crystalline form of cellulose naturally produced by trees, tunicates, plants, algae and bacteria. Cellulose I has two allomorphs, namely; cellulose Iα (triclinic) and Iβ (monoclinic) structures, which exist in various proportions depending on the source of cellulose (Roy *et al*., 2009; Ambjörnsson, 2013; Poletto *et al*., 2014; Rambo *et al*., 2015). Generally, cotton, ramie and wood cellulose fibres are rich in Iβ, while bacterial and algal celluloses are rich in Iα. Both cellulose Iα

18

and Iβ form sheets of dense H-bonded parallel chains arranged in stacks, but they differ in H-bonding pattern in stacking of the sheets, a difference displayed in the chain direction (Roy *et al*., 2009; Chen *et al*., 2011; Goetz, 2012; Poletto *et al*., 2014; Nam *et al*. 2016). Cellulose I is transformed to cellulose II by mercerization with aqueous NaOH, regeneration (dissolving and re-precipitating), ball-milling and supercritical water treatment (Gupta *et al*., 2013; Ago *et al*., 2004; Chen *et al*., 2011). The crystalline structure of cellulose II consists of H-bonded anti-parallel chains, but relatively less dense than those of cellulose I (Roy et al*.*, 2009; Ambjörnsson, 2013). Cellulose III is obtained from cellulose I (or II) by supercritical NH_3 or amine treatment, while cellulose IV is obtained by treating cellulose III with glycerol at 260 °C (Wada *et al*., 2004). Cellulose II is considered thermodynamically the most stable allomorph of cellulose (Wada *et al*., 2004; Ago *et al*., 2004; Goetz, 2012; Ambjörnsson, 2013; Pönni, 2014; Nam *et al*., 2016).

2.2.2 Sources of cellulose; the water hyacinth

Cellulose can be derived from a wide variety of biomass that include wood, cotton, sisal, ramie, rayon, hemp, kapok and flax (Malmström and Carlmark, 2012), as well as the water hyacinth (WH) (*Eichhornia crassipes*), among others. WH is non-native in Kenya and has infested fresh water bodies such as rivers, dams, lakes and irrigation channels causing serious economic and environmental problems (Jafari, 2010; Istirokhatun *et al*., 2015). It grows on the surface of water forming large impenetrable mats (>60 kg/m^2) with an intensity of spread that can double the infested area within a period of 6-15 days (Reales-Alfaro *et al*., 2013). The specific impacts of its infestation include; elimination of native aquatic plants, reduced penetration of sunlight, altered temperature, oxygen and pH levels of water, reduced gas exchange at water surface, increased water loss through transpiration, altered habitats of aquatic organisms, restricted transport and recreational use of waterways, reduced water quality by decomposing plants, among others (Girisuta *et al*., 2008; Jafari, 2010; Istirokhatun *et al*., 2015). These negative environmental impacts of WH invasion have stimulated research for control measures including the use of herbicides which is very effective but hazardous to the environment. Mechanical and manual harvesting is costly, though the cost of removal is considered to reduce through commercial utilization of WH as a whole or partly. Chemical characterization reports that, WH

contains 18-31 % cellulose, 18-33 % hemicelluloses and 7-26 % lignin (Girisuta *et al*., 2008; Reales-Alfaro *et al*., 2013; Saputra *et al*., 2015; Mukaratirwa-Muchanyereyi *et al*., 2016)

2.2.3 Purification and accessibility of cellulose

Cellulose fibres can either be isolated from lignocellulosic materials by mechanical or chemical means, or combination of both methods. Fibres can be separated mechanically by defibrating cellulosic material into fibres and fibre fragments, and fibre bundles. The chemical components in mechanical pulps remain almost in the same proportion as they were in the original material, while chemical pulping removes lignin, hemicellulose and other materials releasing cellulose fibres (Goetz, 2012; Swantomo *et al*., 2013; Pönni, 2014). Cellulose fibre accessibility depends on crystalline-amorphous structure. The penetration of chemical reagent is limited to disordered regions which range from low degree of disorder to completely disordered (or amorphous) regions, but not the crystalline regions unless disrupted (Roy *et al*., 2009; Swantomo *et al*., 2013; Ambjörnsson, 2013). Activation treatments such as swelling (in acids, bases, etc.) and mechanical pulping, of lignocellulosic material, open the surface cannulae, internal pores and cavities, disrupt fibrillar aggregations and crystalline order, altering H-bonding system and relative availability of -OH groups (Roy *et al*., 2009; Gupta *et al*., 2013).

Accessibility of cellulose can be improved by swelling it in acids, bases and salts, and some organic solvents. Swelling agent penetrates the crystalline regions of cellulose, breaking the bonds between chains and fibrils (Roy *et al*., 2009; Ambjörnsson, 2013; SiunChee *et al*., 2013; Pönni, 2014). The most often used swelling agent is aqueous NaOH, a process referred to as mercerization. The fibrillar structure of cellulose is maintained after mercerization, but the degree of crystallinity decreases (Roy *et al*., 2009; SiunChee *et al*., 2013). The extraction of hemicellulose and lignin from lignocellulosic material by chemical pulping creates pores between cellulose micro-fibrils. However, drying of cellulose enables molecular segments to approach each other due to dehydration, and the fibres cannot regain the swollen state because of irreversible micro-fibrillar coalescence (Ambjörnsson, 2013; Pönni, 2014). The most acceptable explanation to this is the formation of strong H-bonds between adjacent cellulose micro-fibrils which is considered to occur mainly in the amorphous regions. Another possible reason is the

cross-linking between crystalline domains in the adjacent cellulose micro-fibrils i.e., co-crystallization (Pönni, 2014).

2.2.4 Cellulose fibre modifications

It is difficult to make cellulose into other useful materials due to its poor solubility in common solvents such as water, poor dimensional stability and lack of thermo-plasticity (Roy *et al*., 2009; Ambjörnsson, 2013). Nevertheless, physical and chemical properties of cellulose can be modified to achieve the desired properties such as water absorbency, mechanical strength, thermal resistance, hydrophobicity and antimicrobial activity. The major types of approaches in cellulose fibre modification include physical treatments, physico-chemical treatments and chemical modifications. Cellulose is an active biopolymer due to the presence of 3-OH groups in each of its *D*-anhydroglucopyranose units that can be chemically modified. The primary -OH at C-6 and two secondary ones at C-2 and C-3 (Scheme 2.1) can participate in reactions such as esterification, etherification and oxidation (Sannino *et al*., 2009; Roy *et al*., 2009; Qiu and Hu, 2013; Ambjörnsson, 2013). Cellulose derivatives are obtained by reacting some (or all) –OH groups of cellulose repeat unit with an organic species such as methyl and ethyl units to generate water-soluble derivatives known as cellulosics. The most commonly produced cellulose derivatives are cellulose ethers such as ethyl cellulose, carboxymethyl cellulose, hydroxyethyl cellulose, hydroxypropyl cellulose (Scheme 2.2), and cellulose esters such as cellulose acetate and cellulose acetate propionate (Sannino *et al*., 2009; Carlmark *et al*., 2012; Qiu and Hu, 2013; Ambjörnsson, 2013). The degree of substitution which is defined as the average number of etherified -OH groups per anhydroglucose unit, can be controlled to a certain extent so as to obtain a derivative with a specific solubility and viscosity in water (Sannino *et al*., 2009; Ambjörnsson, 2013).

Chemical modification of cellulose can be carried out under both homogeneous and heterogeneous reaction mixtures. However, reactions mainly take place under heterogeneous mixtures due to poor solubility of cellulose in common solvents (Roy *et al*., 2009; Carlmark *et al*., 2012; Qiu and Hu, 2013). The modifications under heterogeneous mixtures are usually performed after allowing native cellulose such as cotton and wood fibres, to swell in a suitable solvent. The reaction of cellulose in this condition only occurs at the surface layer hence, its

gross structure can be largely maintained (Qiu and Hu, 2013; Ambjörnsson, 2013). The modification under this condition is often performed in the form of cellulose nano-crystals, films or membranes, fibres and cellulose particle suspensions (Qiu and Hu, 2013). The inherent chemical reactivity and steric effects from the chemical reagent and supra-molecular structure of cellulose may however, influence reactivity of –OH groups (Roy *et al.*, 2009). The –OH at C6 has been found to react ten times faster in esterification reaction than other –OH groups, while -OH at C2 has been found to react twice faster in etherification reaction than –OH at C3, and generally, the relative reactivity of –OH follows the order; OH-C6 >> OH-C3 > OH-C2 (Roy *et al.*, 2009; Ambjörnsson, 2013).

MC	R = H,CH$_3$
NaCMC	R = H,CH$_2$COONa
EC	R = H,CH$_2$CH$_3$
HPMC	R = H,CH$_3$,CH$_2$CH(OH)CH$_3$
HEC	R = H,CH$_2$CH$_2$OH
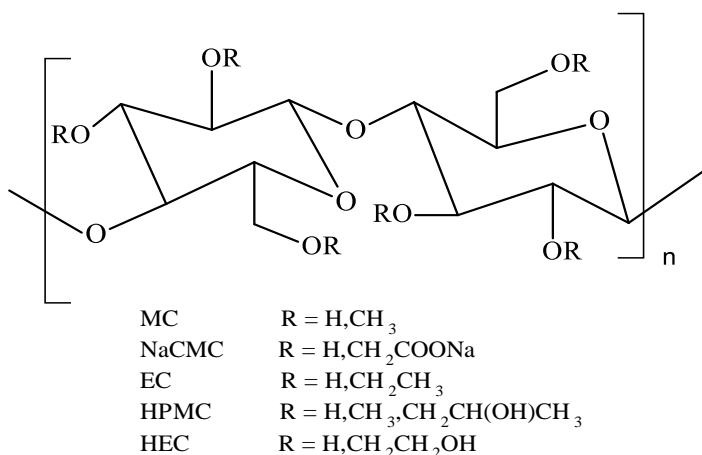
R denotes; methyl cellulose (MC), sodium carboxymethyl cellulose (NaCMC), ethyl cellulose (EC), hydroxypropylmethyl cellulose (HPMC) and hydroxyethyl cellulose (HEC)

Scheme 2.2. Repeat unit of cellulose derivatives (Sannino *et al.*, 2009).

Cellulose modification under homogeneous reaction mixtures can be achieved by dissolving it in non-derivatizing solvents such as *N,N*-dimethyl acetamide/LiCl, derivatizing solvents such as N$_2$O$_4$/DMF, or by dissolving its derivatives in appropriate solvents, employing substituents as starting, protecting or leaving groups for consecutive reactions (Ambjörnsson, 2013; Qiu and Hu, 2013). The original supra-molecular structure of the sample is destroyed under this condition, but the reaction of cellulose chains is higher than that of heterogeneous condition (Gürdağ and Sarmad, 2013; Qiu and Hu, 2013). However, the solvents that can dissolve cellulose may be toxic (*e.g.* N$_2$O$_4$/DMF) or difficult to remove (*e.g. N,N*-dimethyl acetamide/LiCl). Thus,

modifications in these conditions are often started with cellulose derivatives such as hydroxyethyl cellulose, hydroxypropyl cellulose and cellulose acetate due to their solubility in common solvents such as water (Carlmark *et al*., 2012; Ambjörnsson, 2013; Qiu and Hu, 2013).

2.2.5 Cellulose-based hydrogels and cross-linking strategies

Physical and chemical properties of cellulose can be modified by grafting synthetic polymers, to obtain PHGs composite with improved mechanical and biodegradable characteristics (Roy *et al*., 2009; Sannino *et al*., 2009). Grafting of vinyl monomers onto cellulose (or its derivatives) has been performed using free radical polymerization, ionic or ring opening polymerization and 'living' or controlled radical polymerization techniques (Roy *et al*., 2009; Carlmark *et al*., 2012). The techniques of graft polymerization can be based on one (or more) of the following three approaches; i) "grafting to" in which pre-formed polymer with its reactive end-group is coupled with functional groups located on the cellulose backbone (Scheme 2.3a), ii) "grafting from" where polymer chains are grown from initiating site on cellulose backbone (Scheme 2.3b), and iii) "grafting through" where the substrate bears a polymerizable group, hence acts as a macro-monomer, and polymerization of monomers takes place in the presence of this substrate, Scheme 2.3c (Roy *et al*., 2009; Carlmark *et al*., 2012; Malmström and Carlmark, 2012).

Free radical polymerization is often preferred technique because of relative insensitivity to impurities and moderate reaction conditions. Grafting of vinyl monomers to pre-existing polymeric backbone by radical polymerization generally involves "grafting from" approach (Roy *et al*., 2009). The "grafting from" approach is often preferred because of the high grafting density achieved, "grafting to" often suffers from steric hindrance limiting the final grafting density, while "grafting through" is relatively convenient but requires synthesis of cellulose derived macro-monomers (Malmström and Carlmark, 2012). The use of ring opening polymerization method is limited by demanding experimental conditions such as low temperature, use of high purity reagents, inert atmosphere, anhydrous conditions, and direct use of carbocations that require protection of -OH groups in cellulose to avoid side reactions. The disadvantages of free radical polymerization are; poor control over composition, architecture and molecular weight distribution of the copolymer. To overcome these drawbacks, controlled radical polymerization techniques such as atom transfer radical polymerization, reversible addition-fragmentation chain

transfer polymerization and nitroxide-mediated polymerization have been developed (Roy *et al*., 2009).
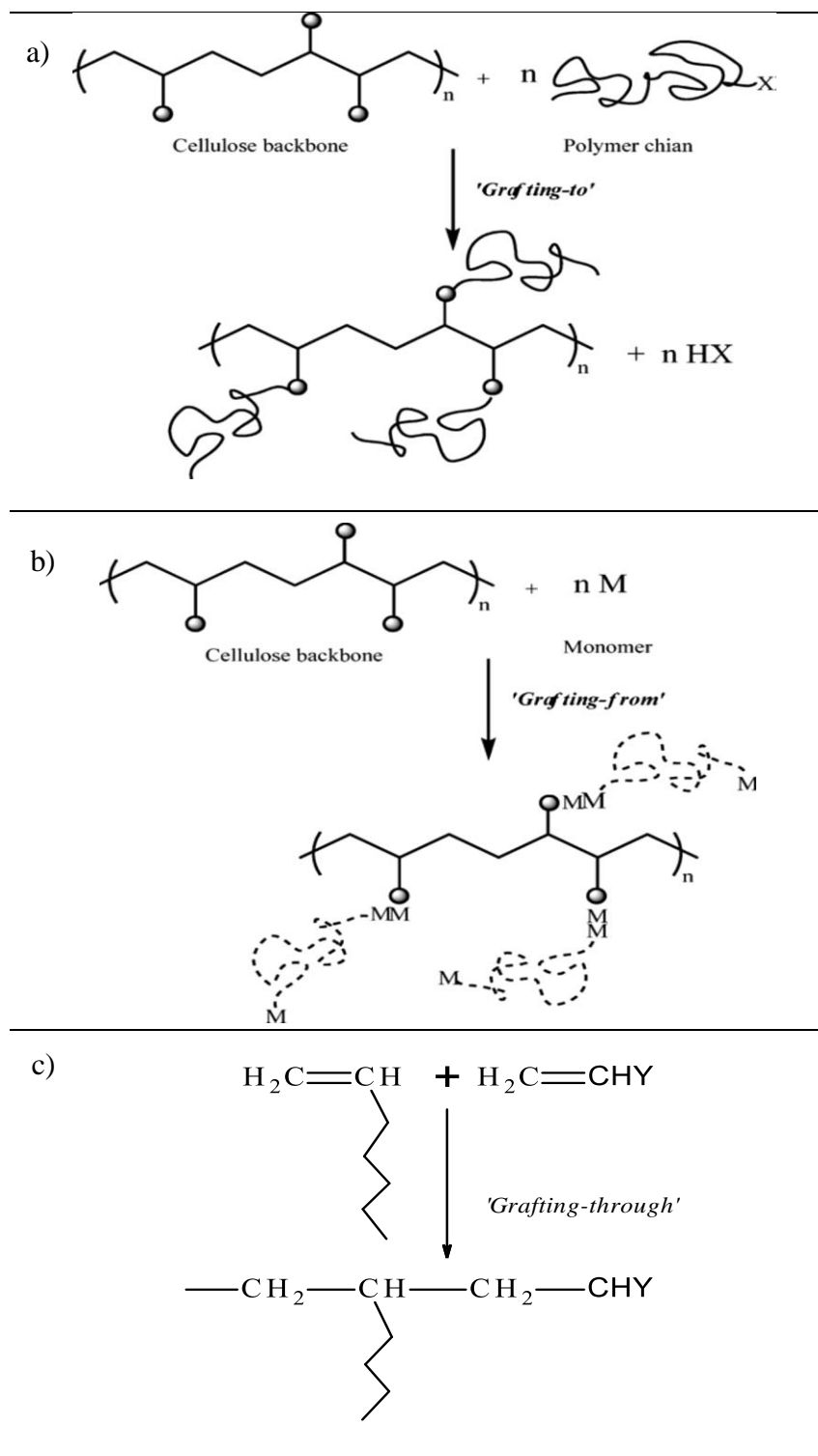
Scheme 2.3. (a) 'grafting to', (c) 'grafting from', and (d) 'grafting through' approaches (Roy *et al*., 2009)

Cellulose-based hydrogels are commonly synthesized using cellulose derivatives such as carboxymethyl cellulose (Sannino *et al*., 2004; Sadeghi *et al*., 2011; Sadeghi *et al*., 2013: Demitri *et al*., 2013) by free radical polymerization technique. Polymerization reactions with these derivatives as substrates are performed under homogeneous reaction mixtures because of their solubility in various solvents. The most common multi-functional vinyl monomers used in radical polymerization include acrylic acid (and its salts), methyl acrylate, ethyl acrylate, methyl methacrylate, acrylamide, methacrylamide, vinyl acetate, acrylonitrile, 2-acrylamido-2-methylpropane sulphonic acid, vinyl sulphonic acid, N-vinyl pyrrolidone, among others (Zohuriaan-Mehr and Kabiri, 2008; Laftah *et al*., 2011; Ahmed, 2015). They contain C=C bonds through which an active center propagates to generate polymeric chains (Ahmed, 2015; Ren *et al*., 2014). Free radicals are generated using appropriate initiation technique such as ionizing high energy irradiation (γ-rays and electron beams), plasma; redox initiation with Mn or Ce (iv) ion, Fe^{2+}-H_2O_2; thermal initiation (UV-irradiation, ammonium persulphate and potassium peroxidisulphate), among others (Zohuriaan-Mehr and Kabiri, 2008; Laftah *et al*., 2011; Gürdağ and Sarmad, 2013; Ahmed, 2015). The cross-link agents employed include aldehydes, epichlorhydrin, carbodiimides, urea derivatives and multi-functional carboxylic acids, though some of them such as aldehydes are toxic in their unreacted state (Sannino *et al*., 2009).

2.2.6 Porosity and swelling of hydrogels

Amongst the desired features in the design and development of PHGs are high swelling capacity and high swelling rate. These features are enhanced by creating porous structures to enable penetration of water molecules through diffusion and capillarity (Shi *et al*., 2011). Porous polymeric networks have been created using various techniques such as salt leaching, freeze-drying and hydration techniques, surfactants self-assembly templating, phase inversion and foam techniques.

Salt leaching technique has been extensively used to generate porous bioactive degradable substrates (scaffolds) for cell growth, proliferation and support for the formation of new tissues (Chiu *et al*., 2010). Salt crystals of definite size are added to salt-saturated polymer precursor solutions before polymerization and then leached out after polymerization. Surfactant molecules self-assemble in aqueous environment to form micelles that act as templates during

polymerization. Shi *et al*. (2011) used surfactant templating technique to prepare micro-porous guar gum-g-poly (sodium acrylate-co-styrene)/attapulgite PHG and observed enhanced swelling capacity and swelling rate. Sannino *et al*. (2004) used phase inversion desiccation technique in acetone to introduce micro-pores into PHG and observed improved water absorbency and swelling kinetics due to capillary effects. Acid dependent foaming agent such as $NaHCO_3$ is used to generate gas bubbles in foam technique (Ahmed, 2015). A surfactant such as polyethylene oxide-polypropylene oxide tri-block copolymer is added as a stabilizer to prevent the foam from collapsing. The foamed product is soaked in ethanol to dehydrate, stabilize and prevent shrinkage.

2.2.7 Biodegradation of acrylamide polymers

Biodegradation is a process by which complex organic materials in the environment are broken down to simple molecular compounds such as carbon dioxide, water, mineral salts (mineralization) and biomass (new cellular constituents), through the action of enzymes produced by micro-organisms (Joutey *et al.,* 2013; Bandyopadhyay-Ghosh *et al.,* 2015). Several microbes including bacteria, fungi and yeast are involved in biodegradation owing to their large numbers, wide diversity, metabolic versatility and exceptionally high metabolic rates (Joutey *et al.,* 2013; Bandyopadhyay-Ghosh *et al.,* 2015). The rate and degree of biodegradation depend on several factors that include chemical structure and concentration of the substrate, diversity of microbial communities involved and their adaptive response, numbers of microbes present and their catabolism evolution, substrate concentration and the presence of multiple substrates, toxicity of end-products, availability of additional carbon sources and inorganic nutrients, moisture content, temperature and pH of the environment, and the presence of oxygen though it can occur under both aerobic (with oxygen) and anaerobic (without oxygen) conditions (Joutey *et al.,* 2013; Sihag *et al.,* 2014; Bandyopadhyay-Ghosh *et al.,* 2015).

Acrylamide monomer is used as a precursor in the synthesis of polyacrylamide (PAM) and other polymers. PAM is used as a binding agent in seed coatings, adhesives, emulsion stabilizers, printing ink; thickening agent in pesticide formulation, cosmetics, latex dispersion, printing paste; flocculating agent in grout, sewage treatment and beet sugar juice clarification, among others. It is also used as a chemical intermediate in the synthesis of superabsorbent materials

such as diapers, medical and agricultural products (Bologna *et al.*, 1999; Charoenpanich, 2013; Guezennec *et al.* 2014; Chen *et al.*, 2015).

A diversity of bacterial species isolated from soil such as *Bacillus, Pseudomonas, Rhodococcus, Arthrobactor, Xanthomonous, Ralstonia, Enterobacter,* among others, and also fungi such as *Aspergillus sp.,* have been reported to degrade PAM (Kay-Shoemake *et al.*, 1998b; Charoenpanich, 2013). They utilize acrylamide as nitrogen (N) source under both aerobic and anaerobic conditions by producing acrylamide induced-*amidase* enzyme. Aliphatic *amidase* (*amidohydrolase*) from *nitrilase* superfamily catalyze the hydrolysis of C-N bond of the amide to acrylic acid and NH_3/NH_4^+ (Kay-Shoemake *et al.*, 1998a; Charoenpanich, 2013; Chen *et al.*, 2015). These microbes are also capable of utilizing PAM as carbon (C) source under anaerobic conditions by breaking down the C chain to form volatile fatty acids. Bacteria enrichment cultures derived from agricultural soils have been reported to gain N benefit from PAM and *amidase* activity has been detected in enrichment cultures (Nawaz *et al.*, 1991; Kay-Shoemake *et al.* 1998a and 1998b; Sojka *et al.*, 2006). Conversely, PAM-specific *amidase* activity could not be detected in cultures supplemented with NH_4NO_3, which is an easily assimilated source of N (Kay-Shoemake *et al.*, 1998b).

Kay-Shoemake *et al.* (1998a and 1998b) reported altered mineral-N pools in PAM-treated soils due to polyacrylamide degradation by soil micro-organisms. Kay-Shoemake *et al.* (1998a) evaluated the possibility of PAM bio-transformation and its effects on bacterial counts and mineral-N content. The data revealed elevated bacterial counts and mineral-N content in PAM-treated field soils compared to untreated soils. PAM-treated potatoes planted soil contained a significantly higher NO_3-N and NH_4-N contents (36.7 and 1.3 mg kg^{-1}, respectively) relative to untreated soil (10.7 and 0.50 mg kg^{-1}, respectively). The content of mineral-N in beans planted soil showed insignificant variation between PAM treated and untreated soil, which was attributed to leguminous N fixation. Microbial cultures obtained from PAM treated and untreated soil utilized PAM as sole source of N, but not sole source of C, whereas its monomers (acrylamide and acrylic acid) supported their growth as sole source of C. Kay-Shoemake *et al.* (1998b) evaluated *amidase* activity and substrate specifity in PAM-treated and untreated field soils. The enzyme activity increased with increase in cell growth and removal of N from acrylamide. The growth of cells, removal of N and production of amidase depended on readily available C in the

culture medium. Based on the absence of *Amidase* activity in the cultures supplemented with NH₄NO₃ as the sole N source relative to significant activity observed in PAM amendments with or without NH₄NO₃, PAM-specific amidase activity was considered inducible and not constitutive. Though the N content in PAM supplied to the soil through irrigation water, 10 mg L^{-1} (0.2-1.7 N ha^{-1}y^{-1}), is a fraction of N added through fertilizers per season, it may result in a slight shift in microbial communities and soil mineral-N content (Kay-Shoemake *et al.*, 1998a and 1998b). *Amidase* activity has also been linked to degradation of amide containing pesticides and herbicides in culture media and soil (Nawaz *et al.*, 1991).

Chen *et al.* (2015) isolated bacterial strain *Pseudomonas putida* from dewatered sewage sludge that could metabolize PAM as its sole source of N. The degradation efficiency of PAM was recorded as 31.1 % in 7 days and surpassed 45 % under optimal culture conditions of pH 7.2, 39 °C and 100 revolutions per minute. Degraded PAM samples showed high molecular weight (MW) PAM to have been partly reduced to low MW oligomer derivatives. PAM-induced extra cellular *amidase* enzyme converted a portion of -CONH₂ to -COO^{-} and the monomer did not accumulate. Culture medium supplemented with mineral N, sucrose and liquid paraffin contributed to PAM degradation and biomass, relative to medium without nutrients. Yeast extract was also shown to improve both cell growth and PAM degradation to 47.2 % in 5 days, while glucose improved degradation efficiency to 56.8 %, but lower biomass was obtained than with yeast extract. This was attributed to utilization of glucose as the only C source, whereas yeast extract metabolizes (prior to PAM) as C and N source for cell growth.

Though PAM is stable and considered safe, its monomer (acrylamide) is a neurotoxin and a carcinogen to animals (Bologna *et al.*, 1999; Charoenpanich, 2013). Bologna *et al.* (1999) analyzed corn, sugar beets, potatoes and beans for residual acrylamide monomer (RAM) that was grown in PAM treated soil. All tested crops showed RAM content < 10 ppb and it appeared unstable when in contact with plant tissues. The recovery was found to be 22 % for beans treated with 100 ppb acrylamide monomer for 10 min and 7 % for a bean sample soaked with 500 ppb monomer solution for 18 h. Fresh corn and soaked beans were found to be more bio-active compared to mature potatoes and sugar beets. Based on the rate at which spiked acrylamide monomer disappeared and the fact that it has to survive various biological and chemical activities inside plant tissues for several months to remain intact, the authors believe bio-accumulation is

unlikely. Sojka *et al*. (2006) evaluated the effect of massive rates of anionic PAM (2691 and 5382 kg active ingredient PAM ha^{-1}) containing 18 % negative charge density on soil microbial biomass and metabolic potential. Despite large accumulative PAM addition over a period of 3-6 years, little effect was observed on microbial biomass and metabolic potential. The use of PAM to control erosion (or to improve soil structure) was considered most unlikely to negatively influence soil microbial population and diversity. A slight shift observed in soil microbial biomass was attributed to N enrichment by PAM addition rather than PAM chemistry.

2.2.8 Formulation of slow release fertilizers

Slow release properties and mechanical strength of efficiency fertilizers are commonly improved through cross-linking to introduce a 3-D network structure (Chao *et al*., 2013). The active ingredient can be loaded into the PHG by; (i) adding the active ingredient into the reaction mixture and polymerizing *in situ,* where it gets entrapped within the polymer matrix, or (ii) swelling dry PHG in a solution of the active ingredient (Liu *et al*., 2007). However, each of the methods has a limitation; in the former, the active ingredient may affect polymerization reaction and the network structure of the polymer, while in the latter, it may accumulate at the surface in the course of drying the loaded hydrogel leading to "bust effect". The quantity of the loaded compound may also be low if it strongly affects water absorbency of the hydrogel (Liu *et al*., 2007).

Guo *et al*. (2005) prepared a slow-release N and P fertilizer with superabsorbent and moisture retention features using carboxylmethyl starch, acrylic acid, NH_3, urea and DAP. The water absorbency of the product was about 85 g/g, contained 22.6% N and 7.2% P and water retention experiment showed excellent moisture holding capacity in soil. Rahman *et al*. (2008) covalently immobilized urea in a biodegradable poly(acrylamide-co-maleic acid)/urea matrix. It was found to contain 32.85% N and the dissolution in water reduced by 297 times as compared to urea. Assessment was carried out on growth and yield of green chilli (*Capsicum annuum)* plants. The release behavior of N in soil and plant uptake suggested that this fertilizer formulation could be used as a SRF.

Tolescu *et al*. (2010) synthesized polymeric microstructures for slow release using urea-formaldehyde (UF) resins through cross-linking impregnation method. The solid fertilizer obtained slowed the release of nutrients and had a much higher activity (>40%, minimum imposed value for a product to be considered as a "SRF") compared to similar products. Zhong *et al*. (2013) incorporated phosphate rock (PR) into sulphonated maize starch (SMS)/ poly(acrylic acid) (PAA) PHG. The dispersion of PR in the medium (SMS-PAA) was found to be satisfactory and that, the ratios of components (SMS, PAA and PR) influenced water absorbency. The system provided sustained release of P and also exhibited excellent water retention capacity. Fernandes *et al*. (2015) produced a co-polymer of urea, acrylic acid and glycerol by radical polymerization. Chemical characterization results showed urea to have been incorporated into the final product and glycerol acted as a multi-functional chain transfer agent in cross-linking. The product could be used as a fertilizer where N could be released slowly through hydrolysis of the amide-N and diffusion through polymeric network.

Other strategies for increasing NUE include the use of nano-clays and zeolites (Naderi and Danesh, 2013). The zeolite network can be filled with nutrients as slow release fertilizer formulation. Ammonium-charged zeolites have been demonstrated to have the capacity to enhance solubilization of phosphate minerals improving P uptake and crop yield (Alberto *et al*., 2010). Yuejin *et al*. (2013) prepared slow-release urea using bentonite and polymer to form a 3-D lattice structure by melting urea directly. 75 % of 12 g sample could be released in 1 L of water for about 14 h, longer than that of conventional urea (<0.5 h).

2.2.9 Nano-technology

Nano-technology refers to design, characterization, production and application of structures, devices and systems by controlling shape and size at nano-meter scale, < 100 nm (Naderi and Danesh, 2013). Nano-structured materials are classified as follows:

i). Zero-dimensional such as quantum dots

ii). One-dimensional such as nano-tubes, nano-rods, nano-wires

iii). Two-dimensional such as nano-sheets, nano-plates, nano-discs, and

iv). Three-dimensional such as nano-balls, nano-pillars (Tiwari *et al.,* 2012).

Nano-materials exist in single, fused or agglomerated forms with spherical, tubular and irregular shapes. They often present properties that are different from those of bulk materials due to exceptionally small size, high specific surface area to volume ratio, high fraction of surface atoms and high surface energy. Such properties include optical, electronic, magnetic and chemical properties (Mourdikoudis *et al.,* 2018). These unique characteristics give nano-particles the capacity to interact with each other and other chemical structures (Naderi and Danesh, 2013; Montalvo *et al*., 2015; Sagadevan and Koteeswari; 2015; Mourdikoudis *et al.,* 2018).

2.2.9.1. Characterization of nano-particles

2.2.9.1.1 X-ray diffraction (XRD)

X-ray diffraction is one of the most extensively used techniques in characterization of crystalline materials. It provides information on nano-particle crystal structure, lattice parameters, grain size, phase composition, preferred orientation and crystal defects (Lin *et al.*, 2014; Bunaciu *et al.*, 2015; Mourdikoudis *et al.*, 2018). This technique is based on Bragg's law (Equation 2.1); in that, reflected beam of X-rays from different layers of a crystalline material undergo constructive interference.

$$n\lambda = 2d_{hkl}\sin\theta \qquad\qquad (2.1)$$

Where, n is the integer, λ is the wavelength of the incident X-ray beam (1.5418 Å for Cu target), d_{hkl} is the interplanar spacing of the crystal layers and θ is the angle of incidence.

The X-rays generated by a cathode ray tube are filtered to produce a monochromatic beam which is incident on the sample (Figure 2.1). The constructive interference of monochromatic beam scattered at specific angles from each set of lattice planes in a crystalline material produce diffraction patterns which describe the sample (Bunaciu *et al.*, 2015).
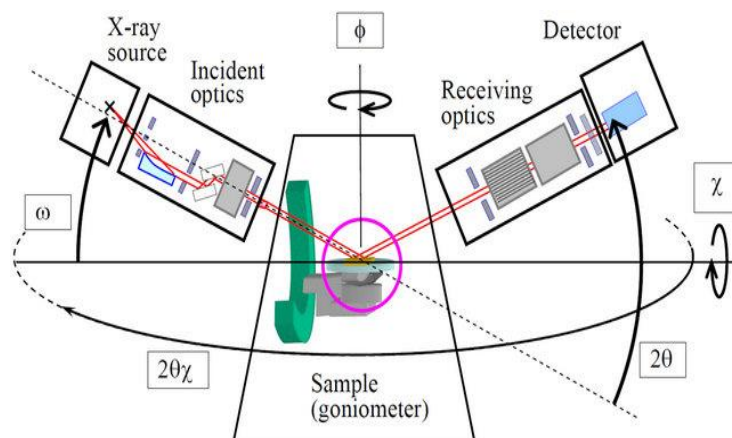
Figure 2.1. Schematic diagram of 5-circle X-ray diffractometer (Inaba *et al.,* 2013)

2.2.9.1.2 Fourier transform infra-red (FTIR) spectroscopy

Fourier transform infra-red (FTIR) spectroscopic technique is widely used to study the interaction of matter with electromagnetic radiation falling within 4000-400 cm^{-1} (Ojeda and Dittrich, 2012). The position of a band in FTIR spectrum is characteristic of a functional group, thus providing information on the molecular structure and the chemical interactions in a compound. The core of FTIR is the interferometer which is composed of a beam splitter, a moving and a fixed mirror (Figure 2.2). Infrared radiation is projected onto the beam splitter where it is divided into two beams which recombined after being reflected (Åmand and Tullin, 1999; Ojeda and Dittrich, 2012). The movement of one of the mirrors changes the path difference to the fixed mirror causing constructive and destructive interference that generates an interferogram, which is Fourier transformed to produce a spectrum (Doyle, 1992; Åmand and Tullin, 1999; Ojeda and Dittrich, 2012).
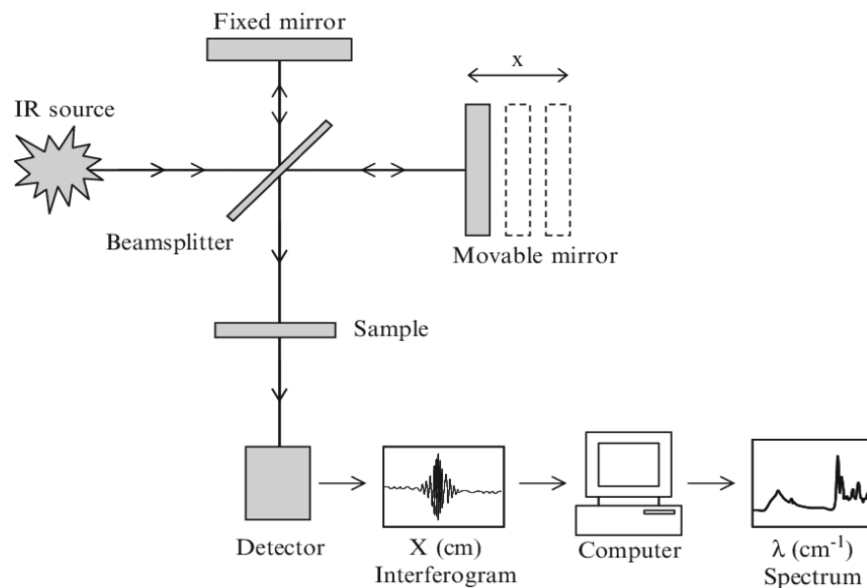
Figure 2.2. Schematic diagram of Fourier transform infra-red spectrometer (Ojeda and Dittrich, 2012)

2.2.9.1.4 Scanning Electron Microscopy (SEM)

Scanning electron microscopy (SEM) is a non-destructive technique often used to image the microstructure of materials (Tayebi and Moharamzadeh, 2017). The technique is used to derive characteristic information of nano-particles including, size, shape, aggregation, elemental composition and their relative ratios, crystal structure and orientation (Lin *et al.,* 2014; Mourdikoudis *et al.,* 2018). A beam of electrons from the electron gun (source) are accelerated through electromagnetic lenses and apertures which focus and shape the beam to form a concentrated spot on the sample (Figure 2.3). The condenser lens controls the intensity of the electron beam, while the objective lens focuses the scanning beam onto the sample. The deflection (scanning) coils guide the beam to scan the sample surface in a raster pattern (https://blog.phenom-world.com/what-is-sem, Available 23rd August, 2019). The electron-sample interaction generates signals including the secondary and backscattered electrons (https://serc.carleton.edu/research_education/geochemsheets/techniques/SEM.html, Available 23rd August, 2019). Other signals generated are the X-rays, visible light and heat. These signals are detected using different detectors which depend on the mode of SEM used, such as secondary electron imaging and backscattered electron imaging (Tayebi and Moharamzadeh, 2017).
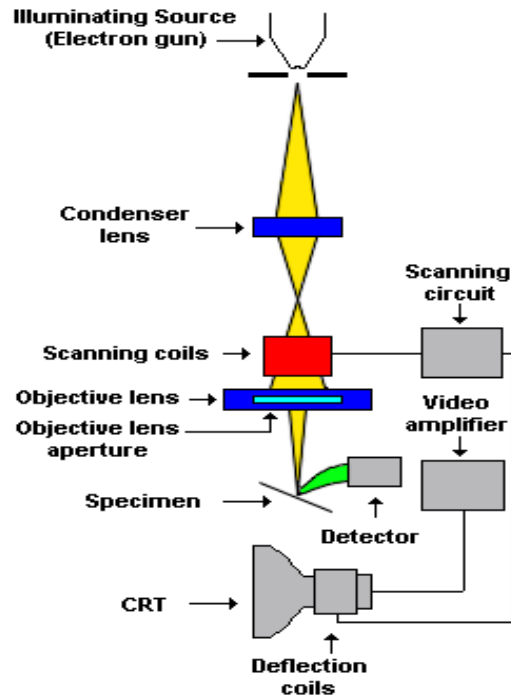
Figure 2.3. Schematic diagram of Scanning electron microscope
(https://www.innerfidelity.com/content/hard-core-diy-scanning-electron-microscope)

2.2.9.1.3 Transmission electron microscopy (TEM)

Transmission electron microscopy (TEM) is technique often used to characterize nano-particle size and shape, size distribution, aggregation, heterogeionity, detection and quantifying nano-particles in matrices, growth kinetics (Lin *et al.*, 2014; Mourdikoudis *et al.,* 2018). TEM technique exploits the interaction between electron beam and a thin sample. An electron beam from the source passes through a condenser lenses which focuses it into a thin beam (Figure 2.4). The condenser aperture excludes high-angle electrons from the beam which then strikes the sample and part of it is transmitted, while the rest is scattered. The objective lens focuses the transmitted portion of the beam into an image on the screen. The image contrast can be enhanced by eliminating high-angle electrons using objective apertures. The intermediate and projector lenses enlarge the image on the screen (Marturi, 2013; Mourdikoudis *et al.,* 2018).

34
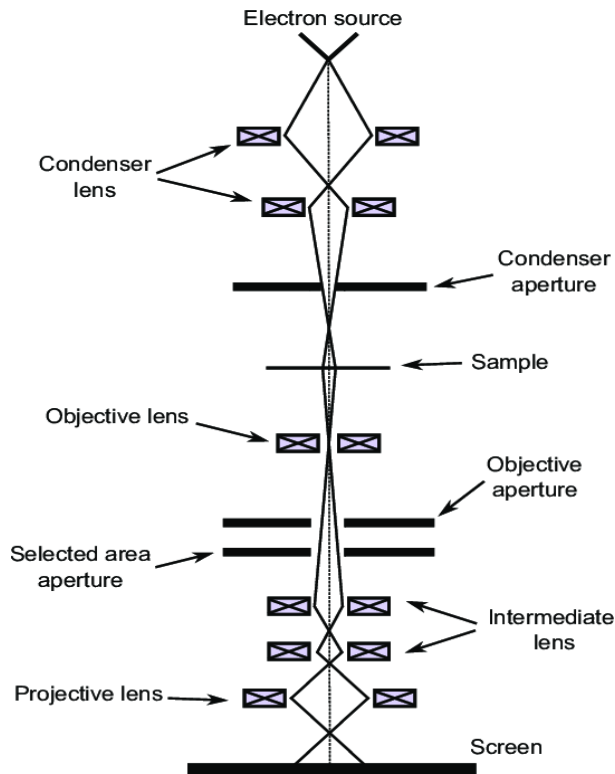
Figure 2.4. Schematic diagram of Transmission electron microscope (Marturi, 2013)

The resolution of TEM is however, limited by chromatic and spherical aberrations of electromagnetic lenses. An aberration-corrected high resolution TEM (HRTEM) that can produce resolutions below 0.5Å has been developed. The correctors used are the monochromator and objective lens with minimum spherical coefficient values (Cs) (Smith, 2008; Krivanek *et al.,* 2009). HRTEM creates images from the interference in the image plane, while conventional TEM uses absorption to create images. The electrons interact with the sample and the electron beam passes through the imaging system of the microscope where phase change and interference occur. The image recorded is however, not a direct representation of crystallographic structure of the sample (Kumar *et al.,* 2016; Titus *et al.,* 2019). High resolution TEM provides all the characteristic information obtained using conventional TEM, and also crystal structure of a single particle and distinguishes mono-crystalline, poly-crystalline and amorphous nano-materials (Mourdikoudis *et al.,* 2018).

2.2.9.1.4 Energy dispersive X-ray (EDX) spectroscopy

Energy dispersive X-ray (EDX) spectroscopy is a micro-analysis technique utilizing the X-rays emitted from the sample during bombardment with a beam of electrons. The EDX detector is connected to SEM or HRTEM to quantify the emitted X-rays against the energy. The peak intensity in the spectrum quantifies the element present in the sample while the peak position identifies the element (Oleg and Yefimov, 2019).

Other techniques mainly used to characterize nano-particles are presented in Table 2.2.

Table 2.2. A Summary of the techniques often used to characterize of nano-particles

Technique	Main Characterization information
Small-angle X-ray scattering (SAXS)	size distribution, structure and growth kinetics
Branuaer-Emmet-Teller (BET)	Surface area
Zeta potential	Surface charge
UV-visible spectroscopy	Optical properties, size, agglomeration state and concentration
Neuclear magnetic resonance (NMR)	Structure, composition, purity and conformational change
Dynamic light Scattering (DLS)	Hydrodynamic size distribution and detection of agglomerates
ICP-MS	size distribution, elemental composition and concentration
Ferromagnetic resonance (FMR)	size distribution, shape, defects, composition, magnetic properties
Atomic force microscopy (AFM)	size distribution, structure, shape, aggregation, dispersion, sorption and surface properties

(Lin *et al.,* 2014; Mourdikoudis *et al.,* 2018)

2.2.9.2 Formulation of nano-fertilizers

Nano-technology has enabled numerous biomedical, biological, optical, electronic and quantum size domain applications (González-Henríquez *et al*., 2014). It has also provided feasibility of utilizing nano-structured materials as fertilizer carriers for building "smart" fertilizers. Encapsulation of fertilizers within a nano-particle is achieved through; i) encapsulating nutrients inside nano-porous materials such as nano-tubes, ii) coating nutrients with a polymeric film, or iii) delivering nutrients as emulsions or nano-particles (Naderi and Danesh, 2013). There have been attempts to develop nano-devices that can control the release of nutrients in response to environmental signals such as moisture and heat, etc. (DeRosa *et al*., 2010). Under nutrient

limitation, plant roots exudate carbonaceous compounds into the rhizosphere environment that enable biotic mineralization of nitrogen and phosphorous. These exudates are considered environmental signals that can be selected to produce biosensors for fertilizer delivery (DeRosa *et al*., 2010; Mastronardi *et al*., 2013; Monreal *et al*., 2015).

Hydroxyapatite $[Ca_{10}(PO_4)_6(OH)_2]$ nano-particles (nano-HA) are visualized as appropriate candidates for surface modification (Jayachandran and Kwon, 2010; Mechay *et al*., 2012). They are considered to play a vital role in fields such as drug delivery, tissue engineering, artificial bone synthesis, biosensors, and more recently in fertilizer formulation. It can be derived from natural source such as calcium apatite, though good results have been achieved through synthetic methods such as chemical precipitation, hydrothermal emulsion method and surfactant-assisted methods, among others (Mateus *et al.,* 2007; Wang *et al*., 2010; Montazeri *et al*., 2010; Mechay *et al*., 2012; Tiwari *et al.,* 2012; Kottegoda *et al*., 2011 and 2017). The morphology and crystallinity level of nano-HA however, depends on the preparation method and reaction conditions. For example, the chemical precipitation is the simplest synthetic method with high yield, while the hydrothermal method is environmentally benign, consumes low energy and produces homogeneous powders with higher crystallinity level and better control over size and shape.

The introduction of polymers or surfactants into synthetic methods has been found to influence the morphology and size of HA nano-particles. Salariana *et al*. (2008) obtained nano-rods with uniform morphology and controlled size in the presence of a cationic surfactant (cetyl trimethylammonium bromide) and a non-ionic surfactant (polyethylene glycol) under hydrothermal conditions. SEM and TEM images revealed nano-rods with diameter ranging from 60-80 nm with an aspect ratio ranging from 10-12. Surfactant mixture was thought to be acting as a soft template that regulates nucleation and growth of nano-HA crystals. Yusong and Dangsheng (2010) synthesized nano-HA reinforced poly(vinyl alcohol) (PVA) gel composite. Nano-HA synthesized in PVA solution showed a decrease in size and crystallinity, compared to that synthesized in distilled water. The diameter of nano-rods ranged from 30-60 nm and length ranged from 160-220 nm. FTIR spectrum indicated the existence of a chemical bond between nano-HA and PVA, and the interaction between them improved the interfacial strength of the composite. Iyyappan and Wilson (2013) using non-ionic surfactant (tritonX-100) obtained

relatively smaller particles than those prepared in the absence of the surfactant. TEM micrographs of calcined nano-HA without TX-100 showed agglomerated particle assuming almost spherical morphology, while those of surfactant-assisted method existed as discrete particles assuming rod-like morphology. The surfactant was considered to control agglomeration of nano-HA through physical interaction with primary particles prior to agglomeration.

Nano-hydroxyapatite is rated as one of the potential candidates for potential agricultural application (Kottegoda *et al.*, 2011; 2017). The use of phosphate minerals such as apatite, strengite and veriscite is generally limited by release of low quantities of P to satisfy crop requirement, though application of apatite has been proven to be effective in acidic soils (Shen *et al.*, 2011). Nano-HA is thought to be more effective in supplying P, minimizing the losses associated with conventional fertilizers and delivery problems associated with phosphate mineral. Kottegoda *et al.* (2011) synthesized nano-HA surface modified with urea and encapsulated into micro-porous cavities of *Glyricidia sepium*. It was hypothesized that incorporation of this nano-fertilizer composite into the soil would absorb moisture initiating slow release of N by diffusion and microbial degradation. The release profile showed an initial burst followed by slow-release to the 60th day, while CF released heavily at first, followed by low and inconsistent quantities to about the 30th day.

Montalvo *et al.* (2015) evaluated the efficacy of nano-HA in strong P-sorbing Andisol and Oxisol soils. Saturated soil column and pot experiments were carried out to evaluate the transport of nano-HA (20 nm) and bulk HA (600 nm), and P uptake by wheat (*Triticum aestivum*) derived from nano-HA, bulk HA and triple superphosphate (TSP). The column experiments showed limited mobility of nano-HA in both soils, i.e., about 5 % was recovered in the leachate for the Andisol and < 1 % for the Oxisol, an observation attributed to aggregation in the soil. The greater mobility in Andisol was related to porosity of soil and carbon content which acted as electrostatic barrier hindering the attachment of negatively charged nano-HA. P could not be recovered in the leachates in both soils for bulk HA, a phenomenon related to large particle size. The pot experiment for both soils showed plant P uptake and the % P in the plant derived from the fertilizers to follow the order; TSP> nano-HA > bulk HA. The better performance of nano-HA over bulk HA was attributed to faster dissolution, though it was a less effective P source compared to TSP.

The –OH group at nano-HA surface has been reported to interact with the active sites of vinyl monomers resulting in the formation of polymer composite. Wang *et al*. (2010) synthesized sodium acrylate/nano-HA polymer composite by radical polymerization and observed enhanced swelling rate and swelling capacity. FTIR spectra revealed participation of nano-HA in grafting through the -OH groups. TEM micrograph revealed nano-scale dispersion of needle-like crystals with diameter of about 40 nm and length of about 270 nm. Lui and Lal (2014), synthesized carboxymethyl cellulose (CMC) stabilized nano-HA fertilizer suspension and carried out soil column tests. CMC–stabilized nano-HA could pass through the column and mix with soil, while nano-HA without CMC were retained on the column surface. The better mobility CMC–stabilized nano-HA in the soil suggested a more efficient delivery of P to the root system. The nano-fertilizer formulation promoted growth and yield of soybeans in a greenhouse test, higher than those under $CaHPO_4$ treatment.

It has been reported that, roots of some plant species and soil micro-organisms are effective in solubilizing and mineralizing complex P compounds. Roots induce chemical changes that involve release of proton to decrease the pH of the rhizosphere which results in dissolution of sparingly soluble P (Shen *et al*., 2011; Abbasi *et al*., 2015). The cation/anion uptake ratios and N assimilation mainly influences the pH change in the rhizosphere. Supply of NH_4^+ to the roots causes rhizosphere acidification, whereas NO_3^- supply causes alkalization. Carboxylate exudates e.g. citrate, malate and oxalate, enhance P solubility through chelation and ligand exchange. Rhizosphere micro-organisms have the capacity to solubilize P compounds such as $CaHPO_4$, $Ca_3(PO_4)_2$, phosphate rock and HA (Shen *et al*., 2011; Reddy, 2014). Plant growth promoting rhizobacteria and fungi can mobilize P by acidifying the soil, releasing enzymes such as Phytases and phosphatases, or by producing carboxylates such as gluconate, oxalate and citrate.

2.3 Evaluating fertilizers on the performance and yield of crops

The amount of fertilizers supplied to the crops should be sufficient and efficient to increase the yield and returns without degrading the environment. This can be achieved by establishing optimal fertilizer application rate, which is defined in both agronomic and economic perspective (Hartinee *et al.,* 2010; Puntel *et al.,* 2016). Agronomically, it is the rate of fertilizer application beyond which extra addition produces no change in crop yield, and economically, it is the

minimum rate of fertilizer application required to maximize returns (Bélanger *et al*., 2000; Luce *et al*., 2015). The effect of fertilizer on crop yield can be evaluated using fertilizer response functions that are usually fitted to the data from fertilizer rate trials through regression analysis (Bachmaier and Gandorfer, 2012) and also in forecasting. Curve fitting techniques such as linear, quadratic, quadratic-plus-plateau, exponential and square root models, among others, have been used to estimate optimal application rates (Hartinee *et al.,* 2010; Bachmaier and Gandorfer 2012; Wang *et al.,* 2014; Puntel *et al.,* 2016).

In this work, a slow release nano-composite fertilizer (water hyacinth cellulose-graft-poly(acrylamide/nano-HA/soluble fertilizer) was formulated and its efficacy assessed on growth and yield of some selected crops specifically, maize, kale and capsicum, relative to a conventional fertilizer in a greenhouse experiment. Maize (*Zea mays*), kale (*Brassica oleracea var. sabellica*) and capsicum (*Capsicum annuum*) are among important crops grown in Kenya by smallholder farmers due to their strong impact on food security and farm income. Maize accounts for 40% of cultivated area and more than 51% of staple food produced. More than 75% of maize production is by smallholder farmers who produce more than 65% of maize consumed in the country (Abate *et al*., 2015). Kale locally known as *sukuma wiki* is grown by 90% of smallholder farmers and locally consumed by households. It plays a significant role in nutritional balance and provides employment mostly to youth and women who are involved in its production (http://www.nafis.go.ke/vegetables/kales/, 25th March 2019). Capsicum also called bell pepper or sweet pepper is cultivated as a subsidiary crop, but it has a high export potential. Its local consumption has been increasing due to demand by urban consumers and many farmers have developed interest for the crop (Edgar, *et al*., 2017).

CHAPTER THREE

3.0 MATERIALS AND METHODS

3.1 Materials

Cellulose was isolated from water hyacinth; Acrylic acid and *N,N*-methylene–*bis*-acrylamide, were obtained from ACROS Organics, Germany. Triton X-100 was obtained from Sigma Aldrich, while other chemicals such as phosphoric acid, hydrochloric acid, sulphuric acid, sodium hypochlorite, acetone, toluene, methanol, sodium hydroxide, calcium hydroxide, ammonia, ammonium hydroxide, ammonium persulphate, ammonium acetate, potassium chloride, calcium chloride, aluminium chloride, were from Loba Chemie, Mumbai, India. All the chemicals used in the experiments were analytical grade.

3.2 Preparation of biodegradable water hyacinth cellulose-graft-poly(ammonium acrylate-co-acrylic acid) polymer hydrogel

3.2.1 Sample preparation

Fresh water hyacinth (WH) plants were collected from Nairobi dam (Figure 3.1; Appendix 1a), then washed with water to remove dirt and any other material attached to the surface. They were separated into leaves, stems and roots for use during characterization. The plant parts were chopped into small pieces and air-dried in the shade. The particle size of dried material was further reduced (to particle size ≤ 450 μm) through milling so as to increase its surface area for reaction with chemicals. Samples were stored in air-tight polythene bags ready for use in the experiments.

3.2.2 Characterization of water hyacinth

The characterization method was adopted from Istirokhatun *et al*. (2015), Abdel-Halim (2014) and Kaco *et al*. (2014). The moisture and ash content of the air-dried WH samples were determined gravimetrically. Hemicellulose was isolated by treating the samples with KOH (10 % w/v) and the resulting mixture was precipitated with ethanol. For lignin content determination,

the air-dried WH sample was first treated with a toluene/ethanol mixture (2:1 v/v) to extract any compound in the WH other than cellulose, hemicellulose and lignin. The solvent-extracted samples were treated with 72 % v/v H_2SO_4 at low temperature to hydrolyse the cellulose and hemicellulose. The resultant extract was solubilized through heating, and insoluble lignin retained. The cellulose content was determined by subtracting the sum of moisture, ash, hemicellulose and lignin content from 100 %.
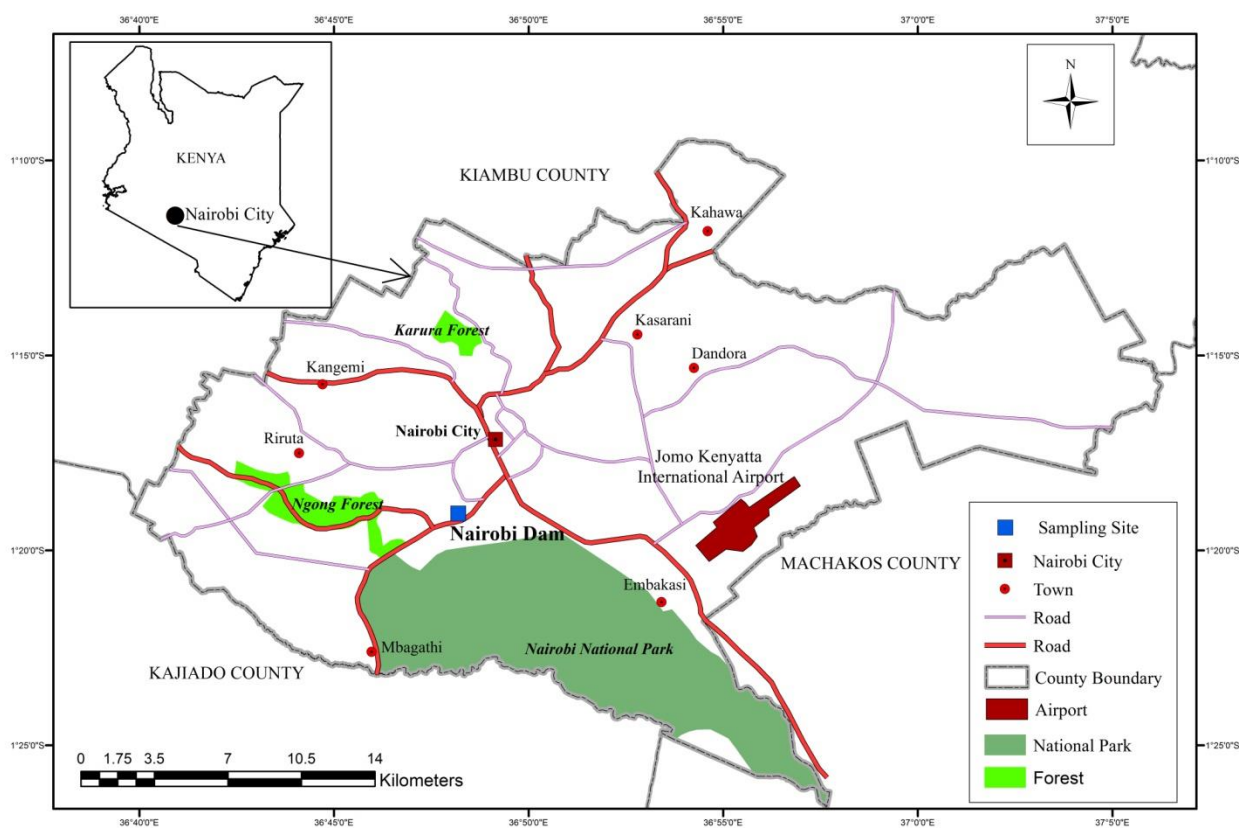
Figure 3.1. Geographical location of Nairobi dam, Nairobi, Kenya

3.2.3 Isolation of cellulose from water hyacinth

The cellulose fibres were isolated from WH using the method adopted from Istirokhatun *et al*. (2015). Air-dried WH samples were refluxed in a toluene/ethanol solvent mixture (2:1 v/v) for 3 h and then allowed to cool to room temperature, after which they were filtered and air-dried. The solvent-extracted samples were bleached to remove lignin using 3 % NaOCl in a water bath at 80

°C for 2 h. Hemicellulose was removed by alkaline hydrolysis using 2 % NaOH at 60 °C for 2 h. Samples were then bleached for the second time to remove the remaining lignin by heating in 2 % NaOCl with stirring at 75 °C for 3 h. The last stage was acid hydrolysis, using 5 % HCl as the catalyst at 65 °C for 6 h. The isolated cellulose was washed with water and the pH adjusted to 13 by adding 0.1 M NaOH to avoid microbial degradation over time (Appendix 1b, 2a and b, 3a and b, 4a). This alkaline cellulose was neutralized with 0.1 M HCl, washed with distilled water and then used in subsequent experiments.

3.2.4 Determination of dry weight of cellulose in swollen cellulose fibres

30 mL of swollen cellulose fibres (Appendix 4b) were drawn using a syringe, transferred onto a filter cloth, allowed to drain and then oven-dried at 105 °C to a constant weight. This was replicated three times and the average dry weight value was determined using an analytical balance with a precision of ±0.01 g. This procedure was repeated regularly so that the water content in the swollen fibres could be maintained.

3.2.5 Synthesis of water hyacinth cellulose-g-poly(ammonium acrylate-co-acrylic acid) polymer hydrogel

3.2.5.1 Partial neutralization of acrylic acid

The degree of neutralization (DN) is defined as molar percentage of carboxylic acid groups neutralized by a base, usually NaOH, KOH or NH$_3$ (Guo *et al*., 2005; Liu *et al*., 2007). In this work, the carboxyl groups in acrylic acid were partially neutralized with NH$_3$. For a weak acid, the relationship between the pH and the dissociation equilibrium constant (K_a) is given by the well-known Henderson–Hasselbach (Equation 3.1).

$$pH = pK_a + \log\left[\frac{\alpha}{1 - \alpha}\right] \qquad\qquad (3.1)$$

where α is the DN. From the pK_a value of acrylic acid (4.25 at 25 °C) and the desired degree of neutralization, the pH can be calculated.

The acrylic acid was neutralized using ammonia to pH values of 4.07, 4.25, 4.42, 4.62, 4.85 and 5.20 which is equivalent to degree of neutralization of 40, 50, 60, 70, 80 and 90%, respectively. The neutralization reaction between NH_3 and acrylic acid is exothermic, thus dropwise addition of NH_3 to acrylic acid was done in a beaker placed in ice-cold water to avoid polymerization of the monomer.

3.2.5.2 Heterogeneous grafting of partially neutralized acrylic acid monomer onto cellulose fibres

The method followed was adopted from Soleimani and Sadeghi (2012). Swollen cellulose fibres containing 0.6-1.25 g dry weight of cellulose, were transferred using a syringe into a 3-necked flask. The flask was then fitted with a reflux condenser and nitrogen line, and then placed in a temperature-controlled water bath equipped with a magnetic stirrer. Nitrogen gas was bubbled through the mixture for 10 min, as the temperature was gradually raised to 70 °C. Ammonium persulphate (APS) (0.05-0.25 g) was added into the mixture and stirred for 30 min to generate free radicals. Acrylic acid (AA) partially neutralized using NH_3 solution and *N,N*-methylene-*bis*-acrylamide (MBA) were blended, stirred to dissolve and then introduced into the reaction flask. The total volume of the reaction mixture was varied between 40 and 50 mL, by adding distilled water. The mixture was stirred for 1 min after which it was left to stand for 2 h. The polymer hydrogel formed was allowed to cool to room temperature, removed from the flask and then cut into small pieces. These were soaked in distilled water and a 1:1 NH_3 solution was added dropwise to adjust the pH to 8. They were then washed with water and oven dried at 60 ºC to a constant weight.

3.2.5.3 Extraction of homopolymer

A 0.5 g dry PHG sample (from section 3.2.5.2) of particle size ≤ 2 mm was soaked overnight in about 100 mL of distilled water in a beaker. It was soxhlet extracted with acetone for 2 h to remove the homopolymer and other impurities (Appendix 6b). The copolymer obtained was oven dried at 60 °C to a constant weight, pulverized and then kept in air-tight polyethylene bottles for subsequent experiments.

3.2.6 Optimization of reaction conditions

The optimum reaction conditions were obtained by changing one synthetic variable at a time. The synthetic variables that influenced the radical polymerization reaction included monomer to cross-linker ratio, degree of neutralization, initiator concentration, cellulose content, total volume of reaction mixture and the reaction temperature. Grafting of the monomer onto cellulose was monitored gravimetrically, where the weight gain in cellulose after extracting the homopolymer was used to determine grafting parameters (Sadeghi and Soleimani, 2011; Gürdağ and Sarmad, 2013; Thombare *et al*., 2014). It also confirmed that grafting was successful. The grafting parameters, *i.e.,* grafting cross-linking percentage (GCP) and percentage grafting cross-linking efficiency (% GCE), were determined using Equation 3.2 and 3.3, respectively.

Grafting cross-linking percentage (GCP) is the weight ratio of grafted polymer to original cellulose expressed as a percentage.

$$GCP = \left(\frac{W_g - W_c}{W_c}\right) \times 100 \qquad (3.2)$$

where W_g is the weight of the copolymer after extracting the homopolymer, W_c is the weight of cellulose used for the reaction.

Percentage grafting cross-linking efficiency (% GCE), is the portion of synthetic polymer grafted onto cellulose in the total polymer expressed as percentage.

$$\% \, GCE = \left(\frac{W_g - W_c}{W_{cp} - W_c}\right) \times 100 \qquad (3.3)$$

where W_g is the weight of the copolymer after extracting the homopolymer, W_c is the weight of cellulose used for the reaction and W_{cp} is the weight of the copolymer before extracting the homopolymer**.**

3.2.7 Characterization of crude WH, isolated cellulose and cellulose grafted copolymer

3.2.7.1 FTIR spectroscopy

An FTIR spectrophotometer, Shimadzu IRAffinity-1S, was used to characterize the crude WH, isolated cellulose and cellulose-grafted polymer hydrogel.

Sample analysis

    i). The FTIR instrument and the computer were switched on.

    ii). The instrument was initialized and ATR accessory mounted into the FTIR compartment.

    iii). The sample area in the ATR was cleaned with absolute ethanol and soft swipes.

    iv). The instruments settings (e.g. number of scans, apodization, etc.) were confirmed.

    v). The anvil was lowered to cover the samples area and the background scanned without the sample.

    vi). The details of the sample (sample name and identity) were input under a file name.

    vii). A finely ground sample was placed on the sample area and the anvil lowered to press the sample against the diamond crystal.

    viii). The sample was scanned between 4000-400 cm^{-1} to obtain its spectrum.

3.2.7.2 Transmission electron microscopy (TEM) and energy dispersive X-ray (EDX) analysis

The morphology of copolymers was assessed using high resolution transmission electron microscope (HRTEM), Tecnai G2 F20 X-TWIN MAT instrumentation at an operating voltage of 200 kV, fitted with energy dispersive X- ray (EDX) spectrometer.

Sample preparation

    i). The sample was cut to size measuring 5 X 5 mm and glued onto the sample disc using a low melting point wax.

    ii). The glued sample was heated at 120°C using the heater.

iii). The sample disc was placed on SiC paper fixed on a rotating polishing machine to reduce the thickness to about 20 μm.

iv). The sample disc was removed from the disc grinder and heated to melt the glue and then mounted on the grid for further thinning.

v). The thinned sample was glued with a mixture of hardener and resin and then heated at 120°C.

vi). The thinned sample was loaded onto a low angle ion polishing machine to create a high quality electron transparent TEM sample.

3.2.7.3 X-ray diffraction (XRD) analysis

1 g of the sample was placed in a disc with an internal diameter of 2.5 cm. X-ray diffractograms were recorded using D2 PHASER (Bruker) with Cu Kα radiation (1.54184 Å) and a generator working at a voltage of 30 kV and a filament current of 10 mA. The samples were scanned from $2\theta = 8°$ to $40°$ at the rate of $0.090°$/min.

3.2.8 Evaluating the swelling of polymer hydrogel

3.2.8.1 Swelling in water

A 0.1 g powdered PHG sample (250-350 μm) was weighed into a porous bag, immersed in distilled water and then allowed to attain the swelling equilibrium overnight at room temperature. The surface water was removed by gently dabbing with filter paper and the mass of the swollen PHG determined. The swelling ratio (water absorbency) at equilibrium (SEQ) was determined using Equation 3.4 (Shi *et al.*, 2011; Laftah and Hashim, 2014).

$$SEQ = \left(\frac{M_{eq} - M_\circ}{M_\circ} \right) \tag{3.4}$$

where $M_\circ$ (g) is the weight of dry PHG, M_{eq} (g) is the weight of swollen PHG and *SEQ* (g/g) is the swelling ratio at equilibrium.

3.2.8.2 Swelling in salt solution

A 0.2 g powdered PHG sample was weighed into a porous bag and then immersed in different concentrations of NaCl, CaCl$_2$ and AlCl$_3$ solutions. It was left overnight at room temperature in order to achieve swelling equilibrium, weighed and water absorbency calculated using Equation 3.4.

3.2.8.3 Influence of the pH on swelling

Several 0.2 g powdered PHG samples were weighed into porous bags and immersed in buffered solutions at pH values of 3, 4, 5, 6, 7, 8, 9, 10 and 11. They were allowed to attain swelling equilibrium and then weighed. Potassium dihydrogen phosphate, potassium hydrogen phthalate, and sodium tetraborate were used to prepare the buffer solutions, while HCl and NaOH were used to adjust pH to the desired values.

3.2.8.4 Moisture holding capacity in soil

The method followed was adopted from Thombare *et al*. (2018). A soil sample was air-dried in the shade and passed through a 2 mm sieve. Sub-samples of air-dried soil weighing 100 g each were transferred into plastic beakers with perforations and filter paper lining at the base. They were amended with 0.5, 1.0 and 1.5 g dry PHG (250-350 μm) and mixed to homogenize, while the untreated soil served as the control. The amendments were placed in a water tub and allowed to absorb water by capillarity for 12 h. They were then removed, allowed to drain excess gravitational water and kept under the same temperature and humidity. The weights of the moistened soil in the beakers were recorded at intervals of 2 days until there was no noticeable change. After subtracting the weight of empty beaker and filter paper, the moisture holding capacity (MHC) of soil was calculated using Equation 3.5.

$$MHC = \left(\frac{W_{wet} - W_{dry}}{W_{dry}}\right) \times 100 \qquad (3.5)$$

where W_{wet} is the weight of wet soil at a particular time interval and W_{dry} is the weight of air-dried soil.

3.2.9 Biodegradation test

3.2.9.1 Biodegradation of polymer hydrogel in soil

The method was adopted from Laftah and Hashim (2014), where soil burial tests were used to simulate natural degradation of PHG samples. Dry PHG samples (1 g each) of particle size ≤ 2 mm were placed in porous nylon bags that allowed the entry of micro-organisms and invertebrates. They were then buried in normal garden soil moistened to field capacity (30% w/w). Degradation was monitored through unearthing of the samples at 2-week intervals for a period of 14 weeks. The compost materials attached onto the surface of unearthed samples were removed, washed with distilled water and oven-dried to a constant weight at 60 °C. The percentage dry matter remaining at each sampling period was determined using Equation 3.6.

$$Dry\ matter\ remaining\ (\%) = \left(\frac{W_t}{W_o}\right) \times 100 \qquad (3.6)$$

where W_o is the initial weight of the sample and W_t is the weight of the sample at a particular incubation time t.

The decomposition rate constant (k) was determined using Olson single exponential model adopted by Thombare *et al.* (2018), (Equation 3.7).

$$W_t = W_o e^{-kt} \qquad (3.7)$$

where W_o is the initial weight of the sample, W_t is the weight of the sample at incubation time t and k is the decomposition rate constant.

The half-life ($t_{1/2}$) was calculated using Equation 3.8.

$$t_{1/2} = 0.693/k \qquad (3.8)$$

3.2.9.2 Microbial culture and test for degradation of copolymer by soil microbial isolates

The methodology was adopted from Nawaz *et al.* (1993; 1994). Acrylamide degrading microbes were isolated from the soil with a history of exposure to alachlor (Roundup®), in a phosphate

buffered medium (PBM) supplemented with 10 mM acrylamide. 5 soil samples were collected from randomly selected points in a coffee farm at the College of Agriculture and Veterinary Science, University of Nairobi, Kenya. 5 g of each sample was placed in a 250 mL conical flask containing 50 mL PBM. This was covered with cotton wool and aluminum foil, and incubated for 10 days at 30°C. 2 mL aliquot of microbial suspension was drawn from each of the flasks, transferred to a fresh 50 mL PBM (pH 7.5) and incubated for another 10 days. After 5 similar transfers, a 10 mL aliquot of each sample was centrifuged at 15,000 g × 10 min at 4 °C and the supernatant measured colorimetrically for liberated ammonia using indophenol blue method described by Hall (1993). Samples which tested positive for ammonia revealed acrylamide degradation (Nawaz *et al.*, 1993; 1994). The pellet (microbial cells) was suspended in 10 mL PBM and after one wash; the suspension was sonicated for 5 min at intervals of 15 sec. At the same time, free NH_4^+ ions were leached out of the copolymers using distilled water and oven-dried at 60 °C to constant weight. 2 mL of microbial suspension was inoculated into a 100 mL PBM supplemented with 0.2-0.6 g of cellulose-grafted copolymer and copolymer without cellulose in separate flasks, then incubated at 30°C. 10 mM acrylamide monomer and PBM without the substrate served as the reference and the blank, respectively. A 5 mL aliquot of the suspension was drawn at intervals of 20 h for 12 days, centrifuged and the supernatant tested for liberated ammonia.

3.3 Formulation of slow release NPK fertilizer composite and evaluating its N mineralization potential

3.3.1. Synthesis of hydroxyapatite (HA) nano-particles

The methodology used in the synthesis was adopted from Kottegoda *et al.* (2011) with some modification namely, introducing a surfactant. 7.716 g $Ca(OH)_2$ was weighed into a beaker and 0.22 mM TX-100 (non-ionic surfactant) solution added to make a total volume of 100 mL and the mixture stirred for 30 min with a motorized stirrer. A 100 mL of 0.6 M H_3PO_4 was added into the suspension of $Ca(OH)_2$, drop-wise (15 mLmin^{-1}) from the burette while stirring vigorously at 1000 rpm. After the reaction, the dispersion was stirred for 10 min and then allowed to age for 2 h. It was then oven-dried at 105 °C to constant weight (Appendix 7a) and

then pulverized into fine powder. The surfactant was removed by washing the powder with methanol.

3.3.2 Preparation of cellulose-g-poly(ammonium acrylate-co-acrylic acid)/nano-HA composite

30 mL of swollen cellulose (containing 0.8 g dry weight) and 0.25 to 3.0 g HA nano-powder was transferred into a 3-necked flask. The flask was fitted with a reflux condenser and nitrogen line, and then placed in a thermostated water bath equipped with a magnetic stirrer. Nitrogen gas was bubbled through the mixture for 10 min, as the temperature was gradually raised to 70 °C. A 0.1 g of ammonium persulphate was added into the mixture, while stirring for 30 min to generate radicals. 2.7 mL of acrylic acid neutralized with NH_3 to 70 % and 0.25 g of *N,N*-methylene–*bis*-acrylamide were mixed, stirred to dissolve and then introduced into the reaction flask. The total volume of the reaction mixture was adjusted to 40 mL using distilled water. Stirring was allowed to continue for 1 min and then stopped to allow the reaction to proceed for 2 h. The reaction product was allowed to cool to room temperature, removed from the flask and cut into small pieces. These were soaked in distilled water and 1:1 NH_3 solution was added drop-wise, to adjust the pH to 8. It was soxhlet extracted with acetone for 2 h, oven-dried at 60 °C to a constant weight, pulverized and tested for water absorption.

3.3.3 Formulation of cellulose-g-poly(acrylamide)/nano-HA/soluble fertilizer composite

30 mL (predetermined volume containing 0.8 g dry weight) of cellulose fibres, 1.0 g nano-HA and varied amounts of soluble NPK fertilizer blend ($(NH_4)_2HPO4$, urea and K_2SO_4 weight ratio 3:5:2, respectively, were transferred into a 3-necked flask. The flask was fitted with a reflux condenser and nitrogen line, and then placed in a thermostated water bath equipped with a magnetic stirrer. Nitrogen gas was bubbled through the mixture for 10 min, as the temperature was gradually raised to 70 °C. 0.1 g of ammonium persulphate (APS) was added into the mixture and stirred for 30 min to generate radicals. 2.7 mL of acrylic acid (AA), partially neutralized with NH_3 to 70 % degree of neutralization and 0.25 g of *N,N*-methylene–*bis*-acrylamide (MBA) were mixed, stirred to dissolve and then introduced into the reaction mixture. The total volume of the reaction mixture was adjusted to 40 mL. The mixture was stirred for an additional 1

minute after which the reaction was allowed to proceed for 2 hours. The reaction product was then cooled to room temperature, removed from the flask and then cut into regular pieces. 1:1 NH_3 solution was added drop-wise to adjust the pH to 8. Fertilizer composite was then oven-dried at 60 ºC to constant weight and then pulverized to pass through a 1 mm sieve.

3.3.4 Chemical characterization of nano-HA and the fertilizer composite

Nano-HA and cellulose-g-poly(acrylamide)/nano-HA/soluble fertilizer composite were characterized using Fourier Transform Infra-red (FTIR) spectrophotometer, Shimadzu IRAffinity-1S, by scanning the samples between 4000 and 400 cm^{-1}. The morphology was assessed by transmission electron microscopy (HRTEM, Tecnai G2 F20 X-TWIN MAT) equipped with energy dispersive X-ray (EDX) spectrometer. The X-ray diffraction (XRD) analysis was carried out using D2 PHASER (Brucker) with Cu Kα radiation (1.5418 Å) by scanning the samples from $2\theta = 8°$ to $40°$ at the rate of $0.090°$/min. The procedures in section 3.2.7 were followed in sample preparation and analysis.

3.3.5 Soil sampling for incubation and greenhouse experiments

3.3.5.1 Study site

The study was carried out at the College of Agriculture and Veterinary Science, University of Nairobi, located in Kiambu County, coordinates 1° 15′ S and 36° 44′ E, and an altitude of 1940 m above sea level (Figure 3.2). The site is representative of large areas of the Central Kenya highlands in terms of soils and climate, and the geology is composed of the Nairobi Trachyte of the Tertiary age. The soils are very deep (>180 m), well-drained, dark-red to dark-reddish-brown, friable clays with moderate to high inherent fertility (Gachene, 1989; Kimetu *et al*., 2007; Karuku *et al*., 2012; Mucheru-Muna *et al*., 2014) and are classified as humic nitisols (WRB, 2015). The climate is characterized as semi-humid according to the Kenya Soil Survey agro climatic zonation (Sombroek *et al*., 1982). The annual average rainfall to annual potential evaporation (r/Eo) is 58% (Karuku *et al.,* 2012; Karuku *et al*., 2014a and 2014b). The average monthly maximum and minimum temperatures are 23.8 and 12.6°C, respectively. The area experiences bimodal rainfall distribution (long rains from mid-March to May and short rains from October to December) and the average annual precipitation is 1000 mm (Jaetzold *et al*.,

2006). Crops grown in the area include; kale (*Brassica olesarea*), tomatoes (*Lycopaersicon esculentum*), cabbage (*Brassica olesarea*), carrots (*Daucus carota*), onions (*Allum fistulosum*), beans (*Phaseolus vulgaris*), maize (*Zea mays*) and coffee (*Coffea Arabica*).
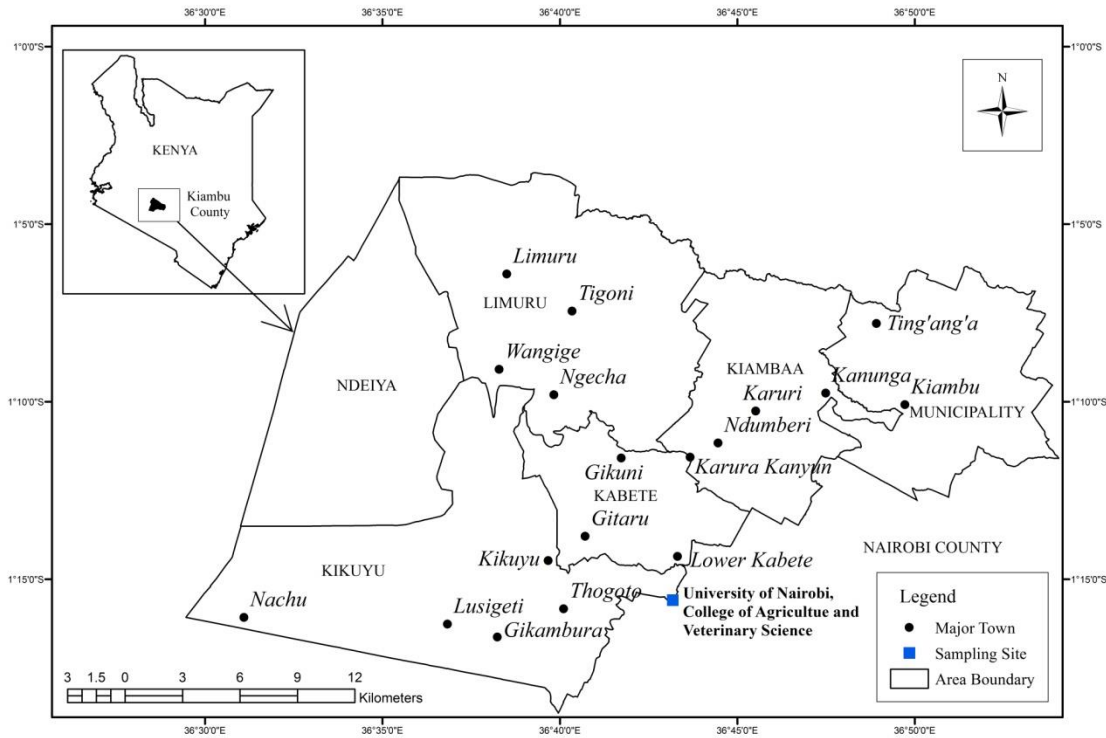
Figure 3.2. Geographical location of Kiambu County, Kenya

3.3.5.2 Soil sampling and preparation

The surface litter that included leaves, sticks, stumps and other materials were removed gently to expose the surface soil. Soil samples at a depth of 0-20 cm were randomly collected at selected points in a field measuring 50 x 50 m using a 600 cm^3 soil auger and bulked to make a composite sample. The composite sample was air-dried in the laboratory, crushed to pass through a 4 mm sieve to remove large pieces of surface materials. A portion of the composite sample was set aside for chemical characterization and the other portion for incubation experiments.

The soil samples for greenhouse experiment were sampled at a different time from that of incubation experiment at the same site. A field measuring 5 x 5 m was identified and cleaned of trash and plant debris. Soil samples were collected at a depth of 0-40 cm with 600 cm^3 soil auger,

bulked to form a composite and a sub-sample taken for selected physico-chemical characterization. Extra soil was collected for potted greenhouse experiment.

3.3.5.3 Soil characterization before onset of incubation and greenhouse experiments

A sub-soil sample was air-dried in the laboratory and crushed to pass through <1mm sieve. Total N was determined by micro-Kjedahl method (Bremner, 1996), available P by Mehlich 1 method (Mehlich, 1953). Exchangeable cations (Ca, K and Mg) were extracted with 1M NH_4OAc; Ca and Mg contents were then determined in the leachate by atomic absorption spectroscopy (AAS) and K by flame photometry. Organic carbon (OC) was determined using wet oxidation method (Nelson and Sommers, 1996) and organic matter (OM) calculated by multiplying the % OC by 1.724. Soil texture was determined by hydrometer method (Glendon and Doni 2002). Soil pH-H_2O was determined with a pH meter (with glass electrodes) at a 1:2.5 soil to water (salt) ratio, while electrical conductivity (ECe) was measured at a 1:2.5 (soil to water ratio) extract using a conductivity meter. Cation exchange capacity CEC was determined by leaching the soil with NH_4OAc at pH 7 and the NH_4^+ concentration in the leachate determined through steam distillation by micro-Kjeldahl method (Bremner, 1996).

3.3.6 Fertilizer composite samples and laboratory incubation experiment

Table 3.1 shows the composition of the fertilizer composite and the amount of NPK added to the soil for incubation experiments. T1 is cellulose-g-poly(acrylamide) polymer hydrogel (PHG) and T2-T6 was formulated to contain cellulose-g-poly(acrylamide)/nano-HA/soluble fertilizer. The amount of soluble fertilizer (SF) in the composites was increased from T2 to T6 while the content of PHG and nano-HA decreased, and T7 represented conventional fertilizer.

The formulated fertilizer composite (<1 mm) was added to the soil at the rate of 50 mgNkg^{-1}, thoroughly mixed and then put into plastic incubation bags. This corresponded to 100 kgN/ha, recommended for N application for maize in Kiambu County (planting, 250 kg/ha NPK 23:23:0; top dressing with CAN, 125 kg/ha) (Ministry of Agriculture, 2014). The amount of the fertilizer added to 1 kg of soil include; T1 – 397 mg, T2 – 362 mg, T3 – 325 mg, T4 – 298 mg, T5 – 250 mg, T6 – 235 mg and T7 – 227 mg. The treatments were replicated three times, with untreated soil serving as the control. Distilled water was added to field capacity (30 % w/w) and the bags

sealed and incubated in the dark at 20 °C for 16 weeks. The amount of mineral N (NH_4-N and NO_3-N), P and K were followed bi-weekly from the onset of incubation. The soil was kept moist at field capacity throughout the incubation period by adding distilled water where the feel method was used to establish the necessity. Aerobic conditions were maintained by opening plastic bags periodically to allow aeration. Each of the samples was divided into two portions at the time of sampling. For one portion, available N (NH_4-N and NO_3-N) was extracted and quantified. The other portion was air dried, before analyzing for total N, available P and K.

Table 3.1. The composition of the formulated fertilizer composite and the amounts of N, P and K, in the treatments

Treatment	Composition of the Fertilizer Composite (% w/w)				Soil Treatment (mgkg^{-1})		
	N- P_2O_5 -K_2O	PHG	SF	Nano-HA	N	P_2O_5	K_2O
T1	14: 0: 0	100	0	0	50	0	0
T2	13.8: 18.8: 4.6	68.8	16.0	16.0	50	68.1	16.6
T3	15.4: 20: 4.8	62.7	22.3	15.0	50	65.0	15.6
T4	16.8: 21.5: 6.2	57.7	28.5	14.3	50	64.0	18.4
T5	20: 24: 9.7	44.5	44.4	11.1	50	60.0	24.2
T6	21.3: 25.2: 11.6	25.0	66.0	9.0	50	58.5	27.2
T7	22: 24: 11	0	100	0	50	54.5	24.9

Legend: PHG = polymer hydrogel, SF = soluble fertilizer, nano-HA = nano-hydroxyapatite

3.3.7 Estimation of nitrogen mineralization potential (No)

Potentially mineralizable-N (N_o), which is the fractional quantity N susceptible to mineralization, was estimated using single first order kinetics employed by Stanford *et al.* (1974) and later adopted by Karuku (1989), and Karuku and Mochoge (2018), Equation 3.9.

$$\frac{dN}{dt} = -kN \qquad (3.9)$$

Integration gives Equation 3.10,

$$Log\ (N_\circ - N_t) = \log N_\circ - kt/2.303 \qquad (3.10)$$

Where, N_t is the cumulative N mineralized at time t (days), N_o is the amount of potentially mineralizable N and k is the first order rate constant (day^{-1}). Stanford *et al.* (1974) and Karuku and Mochoge (2018) found the rate constant k, to be reasonably equal for large number of soils and a period of 2 weeks incubation following a short term pre-incubation was sufficient to estimate mineralization potential (N_0) using simplified Equation 3.11.

$$N_0 = 9.77 \, N_t \hspace{3cm} (3.11)$$

Where, N_0 is nitrogen mineralization potential and N_t is nitrogen mineralized in 2 weeks.

3.4 Evaluating the effects of formulated nano-NPK slow release fertilizer composite on the performance and yield of maize, kale and capsicum

3.4.1 Greenhouse experiment

4 kg of soil were placed into experimental pots, water added to field capacity (30% w/w) and amended with SRF 17:22:6 which composed of 57% cellulose-g-poly(acrylamide), 14.3% nano-HA, 8.6% $(NH_4)_2HPO_4$, 14.3% urea and 5.7% K_2SO_4 (w/w) (Table 3.1). Alongside SRF treatments, the soil was amended with CF in the rates shown in Table 3.2. Maize, kale and capsicum all from certified seeds were planted as test crops; where, in the first set of pots, 2 maize seeds (var. H513) were sown at a depth of 4cm. In the other two sets, 2, 4 weeks-old seedlings of kale and capsicum were transplanted. The experiment was laid out in completely randomized design (CRD) consisting of 7 treatments and the control, replicated thrice. The plants were sprinkled with water every 3 days and thinned to one, 3 weeks after planting. Weeds were uprooted whenever they emerged, pests managed with application of Imidacloprid twice, every 10 days at 1mL/2L of water and diseases controlled with Metalaxy-m+Mancozeb, every 10 days at 5g/2L of water.

Table 3.2. Fertilizer application rates at planting

Treatments	Maize (106, 667 plants/ha)		Kale (74, 074 plants/ha)		Capsicum (59, 259 plants/ha)	
	Appl. rates (kg ha^{-1})	N:P$_2$O$_5$:K$_2$O (kg ha^{-1})	Appl. rates (kg ha^{-1})	N:P$_2$O$_5$:K$_2$O (kg ha^{-1})	Appl. rates (kg ha^{-1})	N:P$_2$O$_5$:K$_2$O (kg ha^{-1})
Control	0	0:0:0	0	0:0:0	0	0:0:0
S1	266	45:57:17	185	31:40:11	148	25:32:9
S2	532	89:114:33	370	62:79:23	296	50:64:18
S3	798	134:171:50	556	93:119:34	444	75:95:27
S4	1064	178:228:66	741	124:159:46	592	100:127:36
S5	1333	223:285:83	926	155:199:57	740	125:159:45
CF1	532	90:90:90	370	63:63:63	296	50:50:50
CF2	1064	180:180:180	741	126:126:126	592	100:100:100

Legend: S1- S5 are SRF treatments, CF1 and CF2 are commercial fertilizer treatments, N - Nitrogen; P$_2$O$_5$ – Phosphorous; K$_2$O - Potassium

3.4.2 Data collection

Plant performance was monitored from the 4th week after planting. It involved counting the number of leaves and measuring plant height, stem thickness, as well as length and maximum width of the leaves. The plant girth was determined from stem diameter measured at half the plant height using Vernier caliper, while the plant height, leaf length and maximum width were measured with a tape measure. The leaf area of harvested kale was measured using a millimeter graph paper (Pandey and Singh, 2011). The leaf was spread over a millimeter graph paper, outline drawn and the area covered by the outline cut and weighed. A 1 cm^2 of the graph paper was also cut and weighed, and the leaf area calculated using Equation 3.12.

$$Leaf\ area\ (cm^2)\ =\ a/b \qquad (3.12)$$

where, a is the weight of the graph paper covered by the leaf outline and b is the weight of the 1 cm^2 graph paper (Pandey and Singh, 2011).

For maize and capsicum, the length and maximum width of all the leaves were measured in a growing plant and the leaf area estimated using the Equation 3.13.

$$Area\ (cm^2) =\ b \times length\ \times max.width \qquad (3.13)$$

where, b is a coefficient found to be 0.602 for capsicum (Ray and Singh, 1989) and 0.75 for maize according to Montgomery (1911) and adopted by Maddonni and Martínez-Bercovich (2014).

Kale leaves were harvested bi-weekly from the 7th week after transplanting on 4 occasions and mature capsicum fruits harvested continuously from the 12th week for a period of 6 weeks. The fresh weights measured in the day of harvest were each used to determine cumulative yields. Maize was harvested on the 20th week after emergence, grains were air-dried to adjust the moisture content to the recommended 13% and then weighed. For dry matter, above ground biomass of maize and capsicum was cut at final harvest and oven dried to constant weight at 60 °C. For kale, cumulative dry weight of harvested leaves was summed up with that of the stem at final harvest. A sub-sample was taken from dry matter, pulverized and NPK extracted by wet oxidation method (Anderson and Ingram, 1993). N content was then determined using micro-Kjedahl method (Bremner, 1996), P with molybdenum blue method (Murphy and Riley, 1962) and K by flame photometry.

3.4.3 Estimation of optimal fertilizer application rates

The yield response quadratic function was used to determine the optimal fertilizer application rates (Equation 3.14). For a quadratic function, the yield increases to a maximum with increase in the amount of fertilizer and then declines in a mirror image of the increments (Hartinee *et al*., 2010). The agronomic optimal fertilizer application rate (x_{agr} kg ha^{-1}) was determined using Equation 3.15 (Bélanger *et al*., 2000; Wang *et al*., 2014; Luce *et al*., 2015; Puntel *et al*., 2016).

$$y_{fer} = y - y_0 = a + bx + cx^2 \qquad (3.14)$$

$$x_{agr} = -\frac{b}{2 \cdot c} \qquad (3.15)$$

where, y_{fer} is the increase in crop yield response with the addition of fertilizer (fertilizer-derived yield, Mg ha^{-1}), y and y_0 are the crop yields (Mg ha^{-1}) with and without fertilizer application, respectively, x is the fertilizer application rate (kg ha^{-1}), a is the intercept, b and c are linear and quadratic coefficients, respectively.

3.4.4 Statistical data analysis

The data was subjected to ANOVA using IBM SPSS Statistics Version 20. Tukey honest significant difference (HSD) post hoc test was used to compare and assess the significance of the mean values at a probability level of $P \leq 0.05$.

CHAPTER FOUR

4.0 RESULTS AND DISCUSSION

4.1 Biodegradable water hyacinth cellulose-graft-poly(ammonium acrylate-co-acrylic acid) polymer hydrogel

Water hyacinth was characterized and cellulose fibres isolated. Partially neutralized acrylic acid was grafted onto cellulose, reaction conditions optimized and the resulting copolymer characterized. The copolymer was assessed for water absorption in saline solution and in solutions of various pH values, and tested for biodegradability in soil and soil microbial isolates.

4.1.1 Composition of water hyacinth

The composition of air-dried water hyacinth is given in Table 4.1. Cellulose content ranged from 26.1 to 33.3 %, with the highest amount obtained from the stem, though not significantly different from the amount obtained from the leaves. The moisture content ranged from 9.2 to 9.3 %, ash from 13.0 to 24.1 %, hemicellulose from 16.1 to 22.0 % and lignin from 20.6 to 23.1 %. No significant difference in moisture content was observed amongst the plant parts. Significantly higher ash content ($P \leq 0.05$) was obtained in the roots, relative to the leaves and stem. Lignin and hemicellulose content was significantly higher ($P \leq 0.05$) in the leaves, compared to the stem and roots.

Table 4.1. Composition of air-dried water hyacinth (%)

Plant Part	Moisture content	Ash	Hemicellulose	Lignin	Cellulose
Leaves	9.3(0.21)[a]	13.0(0.10)[a]	22.0(0.45)[c]	23.1(0.25)[b]	31.7(0.25)[bc]
Stem	9.3(0.15)[a]	20.2(0.35)[c]	16.1(0.40)[a]	20.8(0.60)[a]	33.3(0.42)[c]
Roots	9.3(0.10)[a]	24.1(0.45)[d]	19.7(0.80)[b]	20.6(0.80)[a]	26.1(0.49)[a]
Whole Plant	9.2(0.15)[a]	18.4(0.69)[b]	20.8(0.40)[bc]	21.3(0.26)[a]	30.5(1.30)[b]

Note: The values in the parentheses are standard deviations (n=3), different letters in the same column are significantly different (Tukey test; $P \leq 0.05$ level)

The results are within the range of values obtained by other researchers. For example, Girisuta *et al*. (2008) reported 7.4 % moisture, 18.2 % ash, 47.7 % holocellulose (cellulose + hemicellulose) and 26.7 % lignin in leaves. Similarly, Reales-Alfaro *et al*. (2013) characterized a 1:1 ratio of leaves to stem and reported 9.3 % moisture, 31.7 % cellulose, 27.3 % hemicellulose and 3.9 % lignin. Saputra *et al*. (2015) obtained values ranging from 8.3 to 9.2 % for moisture, 15.2 to 19.8 % ash, 62.2 to 64.2 % holocellulose and 7.3 to 10.0 % lignin in the stem. Mukaratirwa-Muchanyereyi *et al*. (2016) reported 17.4 to 18.4 % ash and 17 to 23 % lignin in the roots. The slight variation in the composition may be attributed to the different methodologies used and the geographical location (source) of water hyacinth.

The isolated cellulose fibres were dispersed in water (Appendix 3b and 4a) due to the exposure of hydrophilic -OH groups; however, the dispersion (swelling) was irreversibly lost upon dehydration either by air- or oven-drying. This irreversible swelling was related probably to the collapse of spaces where hemicellulose and lignin were embedded leading to the restoration of strong inter- and intra-molecular H-bonds (Roy *et al*., 2009; Pönni, 2014). The swelling of cellulose is a vital pre-condition for rendering the system accessible to the reagents. Bleaching with NaOCl decreases the crystallinity of cellulose, thus expanding the amorphous region where most grafting occurs (Swantomo *et al*., 2013). Alkaline treatment also loosens the inter-molecular interactions to allow competing interactions with the swelling agent, *i.e.,* H_2O, where these interactions are restricted to the amorphous regions and pores (Roy *et al*., 2009; Pönni, 2014). Consequently, the accessibility and reactivity of cellulose is improved in heterogeneous chemical reactions (Pönni, 2014).

4.1.2 Mechanism of graft polymerization and extraction of homopolymer

The reaction Scheme 4.1 shows a possible mechanistic pathway for the synthesis of water hyacinth cellulose-graft-poly(ammonium acrylate-co-acrylic acid) polymer hydrogel. The reaction is thought to initiate through thermal decomposition of APS to generate a sulphate anion radical which then abstracts H from an alcoholic –OH group in cellulose to form the corresponding macro-radical (Scheme 4.1a). Ammonium acrylate and acrylic acid (monomers) then become macro-radical receptors. The macro-radical initiated monomers in turn donate free radicals to the neighbouring molecules (chain propagation) (Scheme 4.1b) and subsequently, the

grafting of the monomers onto cellulose chains leads to the formation of the graft copolymer. The chain terminates through combination of two growing polymer chains (Scheme 4.1c) (Sadeghi *et al*., 2011).

a)

$$S_2O_8^{2-} \xrightarrow{\Delta\ (70\ ^oC)} 2S\dot{O}_4^{-}$$

$$\sim\!\!\sim\!\!\sim ROH\ +\ S\dot{O}_4^{\cdot-} \longrightarrow \sim\!\!\sim R\dot{O}\ +\ HSO_4^{-} \longrightarrow$$

b)

c)

(R denotes cellulose chain)
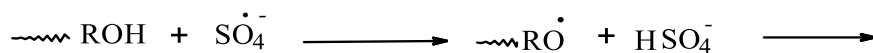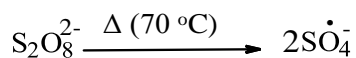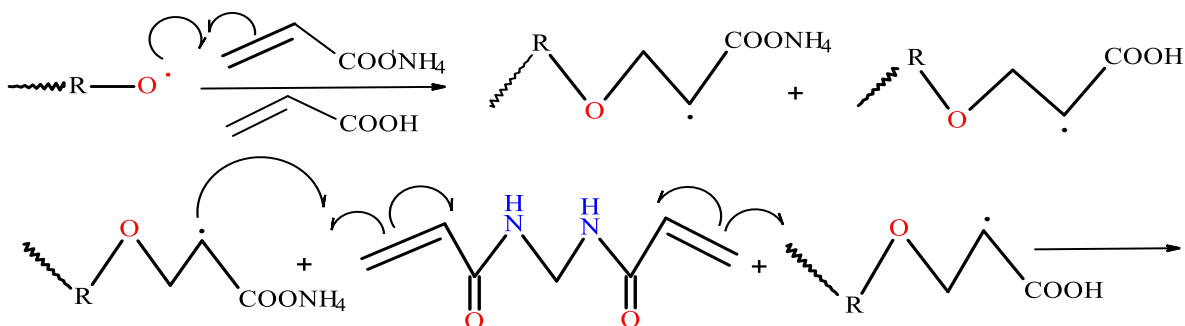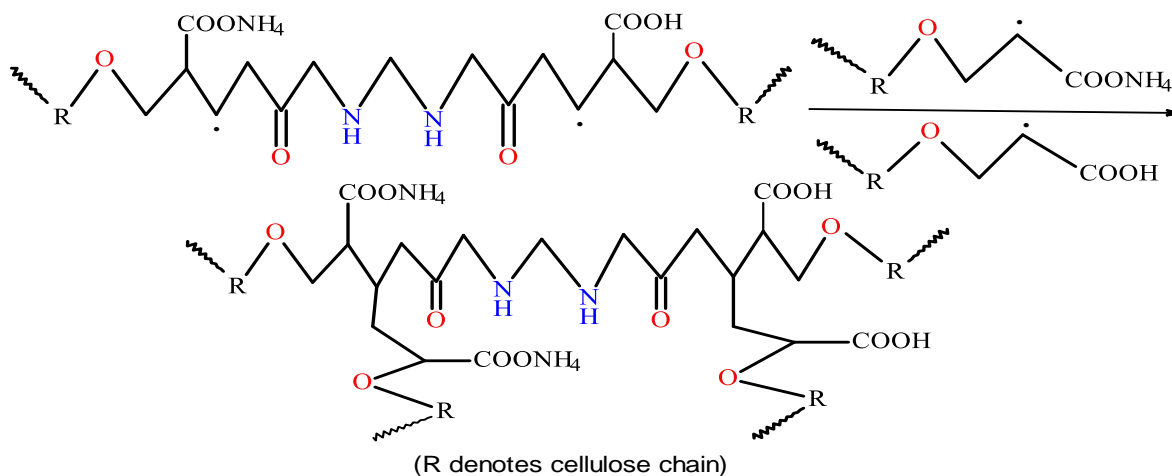
Scheme 4.1. Proposed mechanistic pathway for the synthesis of water hyacinth cellulose-g-poly(ammonium acrylate-co-acrylic acid) polymer hydrogel; (a) thermal initiation, (b) chain propagation, and (d) termination steps

The copolymer product was then transformed from cellulose-g-poly(ammonium acrylate-co-acrylic acid) to cellulose-g-poly(acrylamide-co-acrylic acid) {or cellulose-g-PAM-co-AA} upon heating (oven drying), according to Scheme 4.2.

$$R\!-\!\!-\!COO^-\,NH_4^+ \xrightarrow[\text{-H}_2\text{O}]{\Delta\,(60\,^oC)} R\!-\!\!-\!CONH_2$$

polyammonium acrylate   polyacrylamide
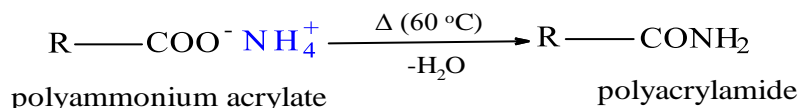
Scheme 4.2. Transformation of ammonium acrylate to acrylamide on heating

The homopolymer was extracted from the graft copolymer using several solvents including; acetone, water, methanol, ethanol and an ethanol/acetone mixture. It was found that use of water alone took long (about 3 days) and alcohols impacted negatively on the hydrophilicity of the polymer hydrogel material. Dehydration with ethanol or an ethanol/acetone mixture at normal temperatures generated heat, an indication of the formation of an exothermic chemical bond. It was likely that the unneutralized acrylic acid or ammonium acrylate groups in the copolymer network caused the protonation of the -OH group in the alcohol, leading to the formation of an ester according to Scheme 4.3. Acetone was adopted as the solvent of choice because it did not influence the swelling property of the PHG and it also shortened the time taken to extract the homopolymer.

(R = Polymer macro-molecule)
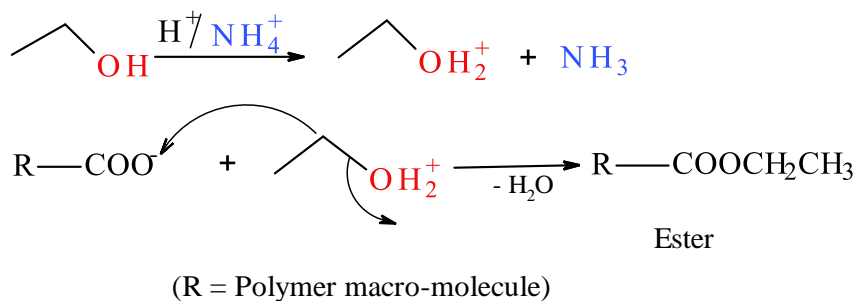
Scheme 4.3. Protonation of alcohol by unneutralized acrylic acid or ammonium acrylate, leading to the formation of an ester

Figure 4.1 shows photographs of oven-dried cellulose-g-PAM-co-AA and acetone-extracted cellulose-g-PAM-co-AA polymer hydrogels. The homopolymer was extracted effectively when dry PHG samples were swollen in water to enable the penetration of acetone. The acetone-extracted sample transformed from a tough, brown solid material (Figure 4.1a) to a white

sponge-like solid product (Figure 4.1b), which could be easily pulverized into fine powder. The white colour observed in Figure 4.1(b) may be due to micro-porous polymeric network structure. This is consistent with the observation made by Kabiri and Zohuriaan-Mehr (2004) who induced porosity into PHG composite (kaolin as inorganic component) using $NaHCO_3$, acetone and a combination of both porogens. They obtained a foamy PHG composite with high swelling capacity and swelling rate due to porosity of PHG network. Zhang *et al.*, 2007 obtained higher water absorbency in methanol and ethanol dehydrated chitosan-g-poly(acrylic acid)/attapulgite composites compared to acetone dehydrated sample. The water absorbency of oven-dried PHG composite was lower than those of methanol, ethanol and acetone dehydrated samples. The organic porogens were considered to protect the porous structure easing penetration of water molecules, while oven-drying was linked to interaction between polymer chains that collapsed the porous structure, increasing the cross-link density. These authors used NaOH to neutralize acrylic acid, implying that, protonation of alcohol could most likely be due to NH_4^+ ions (Scheme 4.3).

a)   b)
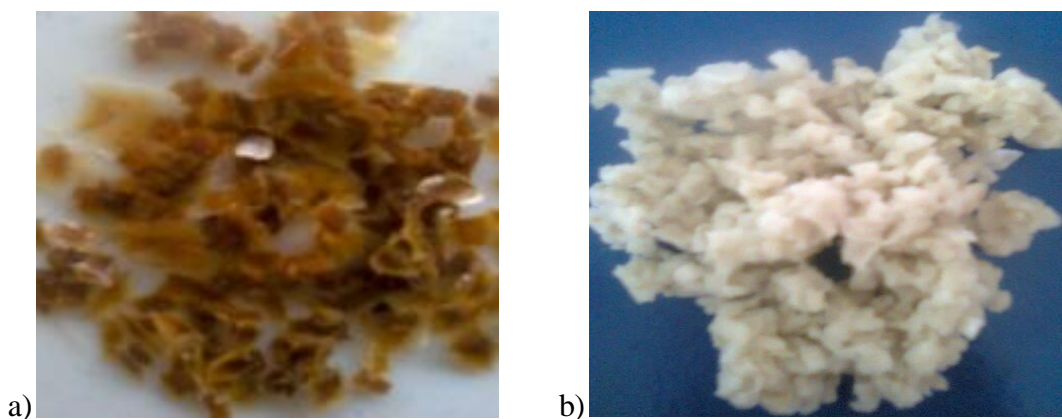
Figure 4.1. Photographs of (a) oven-dried cellulose-g-PAM-co-AA**,** (b) acetone-extracted
cellulose-g-PAM-co-AA

4.1.3 Optimization of Reaction Conditions

4.1.3.1 Effect of the monomer to cross-linker ratio on the formation of polymer hydrogel

The effect of the monomer to cross-linker ratio on grafting cross-linking percentage (GCP), percentage grafting cross-linking efficiency (% GCE) and swelling equilibrium (SEQ) of the

PHG is shown in Table 4.2. In general, GCP, % GCE and water absorbency all increased with increase in cross-linker (*N,N* methylene-*bis*-acrylamide, MBA) and monomer (acrylic acid, AA) content. This observation may be attributed to the increased number of monomer molecules which increased the chances of collision with macro-radicals, resulting in improved grafting. However, optimum values of % GCE and water absorbency were observed at 6.75 % w/v AA content. The observed increase in water absorbency (SEQ) with increased AA content may be attributed to the increased density of hydrophilic groups in the copolymer network (Yu *et al.*, 2011; Sadeghi and Yarahmadi, 2011). The observed decrease in % GCE and SEQ at AA contents above the optimum could be attributed to favoured homopolymerization over graft polymerization, which led to poor grafting and subsequently, less hydrophilic copolymer with a loose network that could not effectively contain water molecules.

Table 4.2. Effect of AA and MBA ratio on GCP, % GCE and water absorbency (SEQ)

Grafting Parameter	AA content (% v/v)	MBA content (% w/v)				
		0.250	0.375	0.500	0.625	0.750
GCP	4.50	Weak	72 (6.0)	126 (5.1)	167 (5.0)	218 (11.0)
	5.75	174 (9.5)	214 (11.5)	253 (14.5)	302 (11.0)	346 (12.5)
	6.75	265 (12.6)	295 (12.0)	371 (16.0)	433 (12.6)	552 (17.5)
	7.75	290 (13.5)	333 (16.0)	413 (13.5)	458 (12.5)	567 (23.0)
	9.00	553 (21.5)	557 (20.5)	559 (23.5)	565 (24.5)	693 (22.0)
% GCE	4.50	Weak	41 (0.6)	68 (2.1)	78 (3.1)	83 (0.6)
	5.75	72 (2.5)	77 (2.6)	80 (3.5)	86 (1.0)	89 (2.0)
	6.75	76 (2.4)	80 (2.5)	85 (3.6)	95 (2.1)	97 (1.0)
	7.75	69 (3.5)	74 (1.6)	83 (3.0)	85 (2.5)	97 (2.5)
	9.00	52 (2.1)	58 (2.5)	60 (3.1)	74 (4.0)	82 (2.1)
SEQ	4.50	Weak	33 (3.1)	55 (2.1)	42 (1.5)	41 (4.4)
	5.75	99 (1.2)	104 (3.5)	100 (3.5)	85 (3.6)	69 (1.5)
	6.75	142 (5.0)	151 (3.0)	156 (5.3)	139 (2.5)	95 (2.1)
	7.75	139 (2.0)	145 (1.5)	107 (4.0)	98 (1.6)	79 (1.0)
	9.00	121 (3.5)	120 (2.2)	108 (3.6)	77 (2.7)	68 (2.6)

Notes: The values in parentheses are standard deviations (n = 3), reaction conditions; degree of neutralization = 80 %, temp. = 80 °C, cellulose = 2 % w/v, APS = 0.25 % w/v, vol. = 40 mL, time = 2 h.

The SEQ increased with MBA content to an optimum value at 0.5 % w/v (Table 4.2), an observation that could be related to the monomer to cross-linker ratio which determines the

cross-link density of the copolymer network (Li *et al*., 2005; Liu *et al*., 2007). The increase in SEQ before the optimum MBA content was attributed to the low cross-link density and hydrophilicity of MBA which enhanced the swelling ratio of the copolymer (Li *et al*., 2005; Liu *et al*., 2007; Laftah and Hashim, 2014). On the other hand, the decrease in swelling equilibrium above the optimum MBA content may have resulted from a highly cross-linked network which decreased the porosity and flexibility of the polymer chains (Laftah and Hashim, 2014; Swantomo *et al*., 2013). Absorption of water is attributed to the balance between the osmotic and dispersive forces (Swantomo *et al*., 2013). The osmotic force impels water molecules into the PHG, while the dispersive force exerted by the polymer chains resists it. The dispersive force increases with increased cross-link density hence, the observed decrease in water absorbency at high MBA content.

4.1.3.2 Effect of the degree of neutralization on the formation of polymer hydrogel

The effect of degree of neutralization (DN) on GCP, % GCE and SEQ is shown in Table 4.3. The GCP and to some extent % GCE decreased with increased DN. This was attributed to the decreased cross-link density of the polymeric network with increasing DN. At low degree of neutralization, the rate of polymerization is enhanced resulting in a high cross-link density and vice versa (Liu *et al*., 2007). The SEQ increased with increased degree of neutralization to an optimum value of 165 g/g at 70 % after which there was a decline. The initial increase could be attributed to decreased cross-link density with increased DN which improved flexibility of polymer chains, whereas the decrease after the optimum could be due to poorly grafted copolymer that resulted in a weak network structure.

Table 4.3. Effect of degree of neutralization (DN) on GCP, %GCE and water absorbency

Grafting	Degree of Neutralization (%)					
Parameter	40	50	60	70	80	90
GCP	331(13.6)	322(11.5)	304(12.5)	293(9.2)	281(10.6)	271(7.4)
% GCE	95(1.2)	90(2.2)	85(2.4)	83(2.6)	84(2.3)	83(2.6)
SEQ	108(2.5)	123(3.4)	142(2.0)	165(4.2)	158(7.6)	112(2.1)

Notes: The values in parentheses are standard deviations (n = 3), reaction conditions; AA = 6.75 % w/v, MBA = 0.5 % w/v, cellulose = 2 % w/v, APS = 0.25 % w/v, temp. = 80 °C, vol. = 40 mL, time = 2 h.

Witono *et al.* (2014) obtained a comparable optimal SEQ value of 114 (g/g) at 50% DN in polymer hydrogel based on cassava starch grafted with polyacrylic acid, neutralized with NaOH and cross-linked with MBA. They observed an increase in SEQ with increased DN which was attributed to increased amount of Na^+ ions attached to macro-molecular chains that increased the osmotic force. The decrease in SEQ after the optimum was linked to dissolution of the hydrogel. Guan *et al.* (2017) obtained higher SEQ value of 859 (g/g) at 75% DN in PHG prepared using carboxymethyl cellulose, acrylamide and acrylic acid neutralized with NaOH. They attributed the higher SEQ to repulsion between ionized carboxylate groups which expanded the molecular chains for accommodating water molecules. These were different from the case in the present study because NH_3 was used to neutralize acrylic acid (Section 3.2.5.1) where hydrophilic group transformed from $-COONH_4$ to $-CONH_2$ on heating (Scheme 4.2).

4.1.3.3 Effect of cellulose content and the total volume of the reaction mixture on the formation of polymer hydrogel

The effect of cellulose content and the total volume of the reaction mixture on GCP, % GCE and SEQ are shown in Table 4.4. The GCP decreased with increase in cellulose content and volume of the reaction mixture. The observation could be attributed to homopolymerization. Cellulose content higher than the optimum favours homopolymer formation because the growing polymer chains are immobile and close to each other. At reaction volumes greater than the optimum, the macro-radicals are farther apart causing increased chain transfer reactions to monomer molecules and subsequently, a poorly grafted copolymer. The % GCE showed a general decrease with increased volume of the reaction mixture although some initial increase was observed at low cellulose contents, followed by a decline at higher cellulose contents. The SEQ increased with increase in cellulose content at a reaction volume of 40 mL to the optimum value of 165 g/g followed by a decline. The observation could be attributed to well grafted copolymers and the hydrophilicity of cellulose. However, cellulose content higher than the optimum value of 2.0 % w/v caused a decrease in SEQ due to the formation of high number of physical entanglements, which acted as additional cross-link points. Mahfoudhi and Boufi (2016) obtained comparable optimum SEQ values of 175, 152 and 145 g/g for cellulose nano-fibrils (CNFs) contents of 3 %, 5 % and 10 % on assessing the effects of CNFs on the swelling properties of poly(acrylic acid-co-acrylamide)/CNFs nano-composite PHG.

Table 4.4. Effect of cellulose content and the volume of the reaction mixture on GCP, % GCE and water absorbency

Grafting Parameter	Reaction vol. (mL)	Amount of Cellulose (%w/v)				
		1.50	1.75	2.00	2.25	2.50
GCP	40	454(13.5)	343(11.3)	306(12.0)	263(10.5)	237(13.0)
	45	434(9.6)	358(12.5)	293(11.3)	258(11.5)	222(10.0)
	50	396(10.7)	296(9.0)	236(13.5)	203(13.8)	203(11.0)
%GCE	40	80(1.4)	82(2.5)	78(1.7)	77(2.1)	75(3.0)
	45	81(2.1)	78(1.6)	76(3.4)	72(3.7)	66(2.2)
	50	67(3.1)	71(2.0)	64(2.7)	60(3.5)	58(3.1)
SEQ	40	122(4.9)	150(5.4)	165(4.0)	130(1.5)	95(1.0)
	45	122(2.5)	122(3.0)	125(2.1)	108(4.0)	95(2.1)
	50	103(4.5)	107(1.0)	104(4.0)	104(1.2)	101(1.8)

Notes: The values in parentheses are standard deviations (n = 3), reaction conditions; AA = 6.75 % w/v, MBA = 0.5 % w/v, APS = 0.25 % w/v, temp. = 80 °C, time = 2 h.

4.1.3.4 Effect of the initiator concentration on the formation of polymer hydrogel

The effect of the initiator (ammonium persulphate, APS) content on GCP, % GCE and SEQ is shown in Table 4.5. The GCP increased with increase in initiator concentration, an observation attributable to increased chances of H abstraction and chain transfer reaction between the monomers and cellulose macro-radicals. However, some decrease in % GCE was observed at high initiator content. This could be attributed to early termination of the growing polymer chains due to generation of excess micro-radical sites which led to a poorly grafted copolymer. The SEQ increased to an optimum value of 165 g/g at 0.25 % w/v APS content, an observation which may be explained by the effect of initiator on the rate of polymerization and molecular weight distribution (MWD) of the copolymer (Li *et al*., 2005; Liu *et al*., 2007; Sadeghi and Yarahmadi, 2011; Sadeghi *et al*., 2013; Laftah and Hashim, 2014). An increase in initiator content beyond the optimum increases the rate of polymerization, but decreases MWD of the copolymer. At APS content lower than the optimum, the initiator is mostly utilized in the generation of macro-radical sites in cellulose where monomers can be grafted, resulting in improved water absorbency. At initiator content higher than the optimum, excess radicals may either lead to homopolymerization or termination through bi-molecular collisions, resulting in low MWD and loose network structure and thus, the observed decrease in swelling equilibrium.

Table 4.5. Effect of the initiator concentration on GCP, %GCE and water absorbency

Grafting	Amount of APS (%w/v)				
Parameter	0.125	0.250	0.375	0.500	0.625
GCP	287(13.6)	305(12.9)	336(13.8)	328(11.2)	353(10.7)
% GCE	80(2.6)	83(1.8)	77(3.7)	74(5.1)	76(2.9)
SEQ	113(7.2)	165(5.0)	131(3.2)	111(3.6)	107(4.5)

Notes: The values in parentheses are standard deviations (n = 3), reaction conditions; AA = 6.75 % w/v, MBA = 0.5 % w/v, temp. = 80 °C, cellulose = 2%, vol. = 40 mL, time = 2 hr.

4.1.3.5 Effect of the reaction temperature on the formation of PHG

The effect of reaction temperatures variation on GCP, % GCE and SEQ is shown in Table 4.6. The GCP and % GCE generally decreased with an increase in the reaction temperatures and the optimum SEQ was attained at 70 °C. The dependence of water absorbency on the reaction temperature was attributed to the balance between chain growth, cross-linking and termination. Below the optimum, an increase in temperature led to a predominant chain growth, whereas temperatures greater than the optimum led to a significant cross-linking and chain termination. High temperatures enhance not only the rate of decomposition of APS but also the kinetic energy of the radical centres and the diffusion of monomers into cellulose macro-radicals (Sadeghi *et al*., 2011). However, temperatures higher than optimum may lead to a poorly grafted copolymer, a phenomenon attributed to: (a) increased rate of termination and chain transfer reactions to monomer molecules, and/or (b) decomposition of ammonium persulphate to yield O_2, a radical scavenger (Sadeghi *et al*., 2013).

Table 4.6. Effect of the variation of reaction temperatures on GCP, %GCE and water absorbency

Grafting	Reaction Temperature (°C)			
Parameter	50	60	70	80
GCP	380(12.1)	320(10.7)	308(11.4)	345(12.8)
% GCE	89(2.8)	82(3.1)	77(3.5)	74(2.4)
SEQ	113(4.0)	140(3.5)	165(4.5)	150(5.6)

Notes: The values in parentheses are standard deviations (n = 3), reaction conditions; AA = 6.75 % w/v, MBA = 0.5 % w/v, cellulose = 2%, APS = 0.25 % w/v, vol. = 40 mL, time = 2 hr.

4.1.4 Characterization of water hyacinth, isolated cellulose and cellulose grafted copolymer

4.1.4.2 FTIR spectroscopy

The FTIR spectra of water hyacinth, isolated cellulose and cellulose-g-PAM-co-AA are displayed in Figure 4.2, and the summary of the spectral bands is indicated in Table 4.7. The spectral bands for both crude WH and purified cellulose were similar, except for a strong band at 1608.6 cm^{-1} assigned to the C=C stretch for the aromatic ring, which diminished in isolated cellulose. The delignification possibly removed lignin, a complex polymer derived from *p*-coumaryl, coniferyl and sinapyl alcohols coupled by aryl-ether bonds and ether cross-links. The intensity of the spectral bands at 1320-1210 cm^{-1} assigned to C-O stretch for alcohol and ether groups also decreased probably due to removal of lignin and hemicellulose. This indicates that lignin and hemicellulose were effectively removed. Grafting of the monomer onto cellulose was confirmed by comparing the FTIR spectrum of cellulose with that of cellulose-grafted PHG. The intense spectral band at 1018.4 cm^{-1} (Figure 4.2a and 4.2b) assigned to the C-O stretch for primary or secondary alcohols was drastically weakened and shifted to 1029.9 cm^{-1} in cellulose-g-PAM-co-AA (Figure 4.2c), implying that most of the -OH groups were involved in grafting. The spectrum of grafted cellulose also showed a broad band between 3700-2500 cm^{-1} assigned to N-H stretching and a strong band at 1541 cm^{-1} assigned to N-H bending for primary amides. These spectral bands are characteristic of the -CONH$_2$ group and hence confirmed the dehydration of ammonium acrylate to acrylamide upon oven drying at 60 °C. The broad band extending from 3700-2500 cm^{-1} is also assigned to alcoholic and carboxylic –OH. The alcoholic -OH may be attributed to crystalline regions of cellulose that is unlikely to take part in grafting unless disrupted to allow penetration of monomers. The penetration of monomers is restricted to amorphous regions where most grafting occurs, though the reactivity of –OH under heterogeneous conditions may be influenced by steric effects from the chemical reagent and supra-molecular structure of cellulose (Roy *et al*., 2009; Swantomo *et al*., 2013; Pönni, 2014). The carboxylic –OH reveals the unneutralized portion of acrylic acid functional groups.
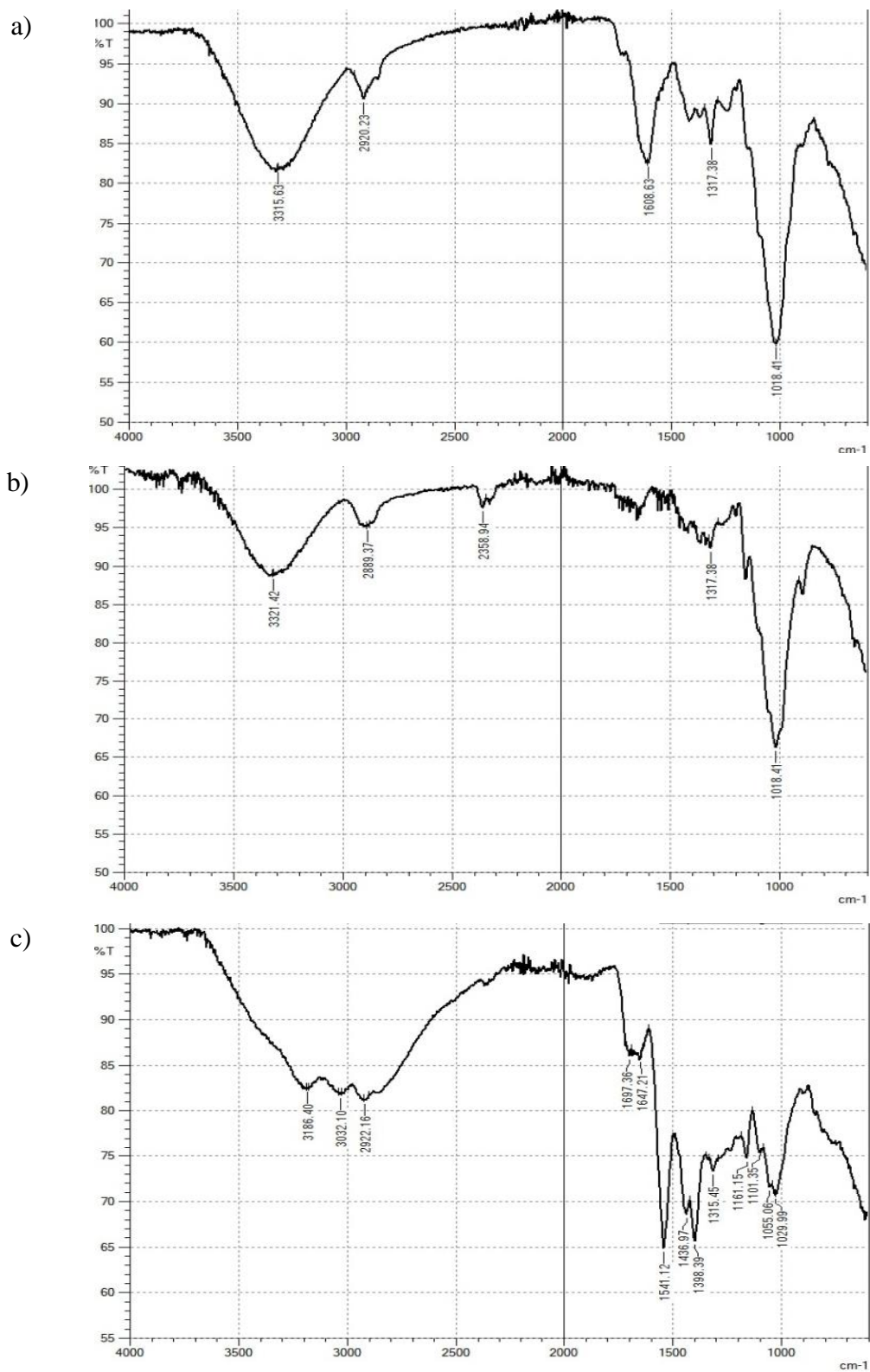
Figure 4.2. FTIR spectra of (a) crude water hyacinth, (b) isolated cellulose (c) water hyacinth cellulose-g-PAM-co-AA

Table 4.7. Summary of the spectral bands

Wave Number (cm^{-1})	Functional group
3700-3000	O-H stretch, alcohol
3700-2500	O-H stretch, carboxylic acid and alcohol
	N-H stretch, amide
2920, 2922, 2889	C-H stretch, SP^3 carbon
1647-1697	C=O stretch, amide
1608	C=C stretch, aromatic ring
1541	N-H bending, 1° amide
1440-1400	O-H bending, carboxylic acid
1320-1210	C-O stretch, alcohol, ether
1300-1000	C-O-C stretch, ether
	C-O stretch, alcohol, carboxylic acid
1018	C-O stretch, 1° or 2° alcohol

4.1.4.3 X-ray diffraction (XRD) analysis

The X-ray diffraction patterns of WH and isolated dry cellulose is presented in Figure 4.3. The crude WH (Figure 4.3a) displayed diffraction peaks at $2\theta = 21.6°$ corresponding to (020) crystallographic plane reflections characteristic of cellulose I, and the bands at $2\theta = 26.5°$, $39.5°$ and $44°$ could be related to cellulose Iβ structure. The isolated cellulose (Figure 4.3b) indicated diffraction peaks at $2\theta = 16°$, $22°$ and $34.5°$ assigned to (110), (200) and (004) crystallographic plane reflections for cellulose I, respectively. The findings are in agreement with observations made by Ago *et al*. (2004), Chen *et al*. (2011), Bai *et al*. (2012), Ambjörnsson, (2013), Gupta *et al*. (2013) and Nam *et al*. (2016). The intense peaks observed in isolated (mercerized) dry cellulose (Figure 4.3b) may be attributed to restructured H-bonds (coalescence) that increased crystallinity of cellulose (Ambjörnsson, 2013; Gupta *et al*., 2013; Pönni, 2014). The transformation of cellulose I to II has been found to occur at NaOH concentration > 10% (w/v) (Gupta *et al*., 2013), and hence transformation in this study was unlikely because of lower concentration of NaOH (2% w/v) used to isolate cellulose (Section, 3.2.3).
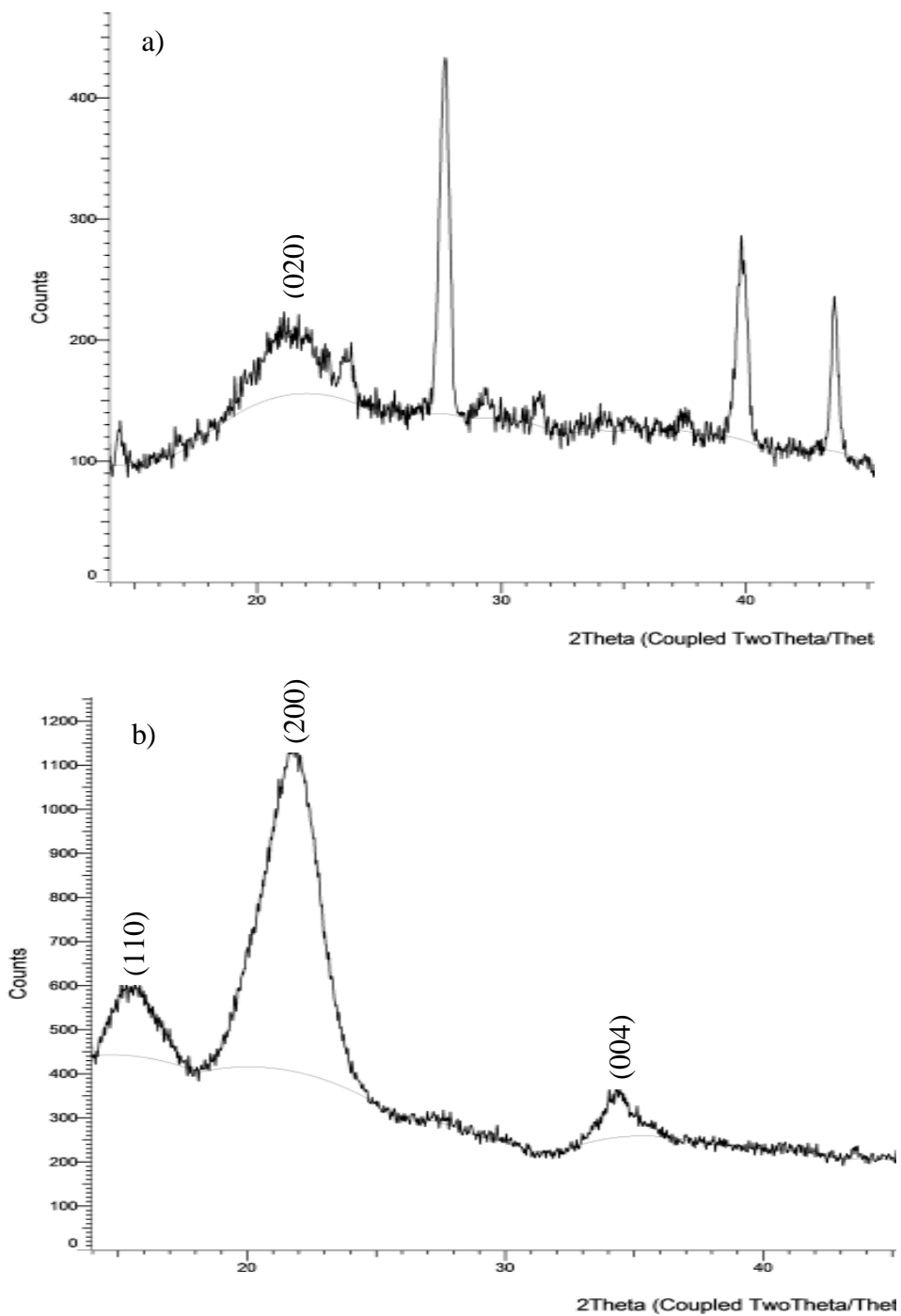
Figure 4.3. Diffractograms of (a) crude water hyacinth, (b) isolated dry cellulose

The diffractograms of copolymer without cellulose and cellulose grafted copolymer are displayed in Figure 4.4. The copolymer without cellulose (Figure 4.4a) displayed an amorphous pattern. Cellulose grafted copolymer (Figure 4.4b) showed a diffraction band of lower intensity

at $2\theta = 22°$ (200) for cellulose I crystalline allomorph, relative to the intensity of the same peak in the isolated cellulose (Figure 4.3b), confirming grafting of monomers onto cellulose fibres. The diffraction band in cellulose grafted copolymer at $2\theta = 26.5°$ (Figure 4.4b) is suggestive of the existence of some crystalline cellulose allomorph that was not fully destroyed during alkali treatment, limiting the accessibility of -OH groups during the polymerization reaction.
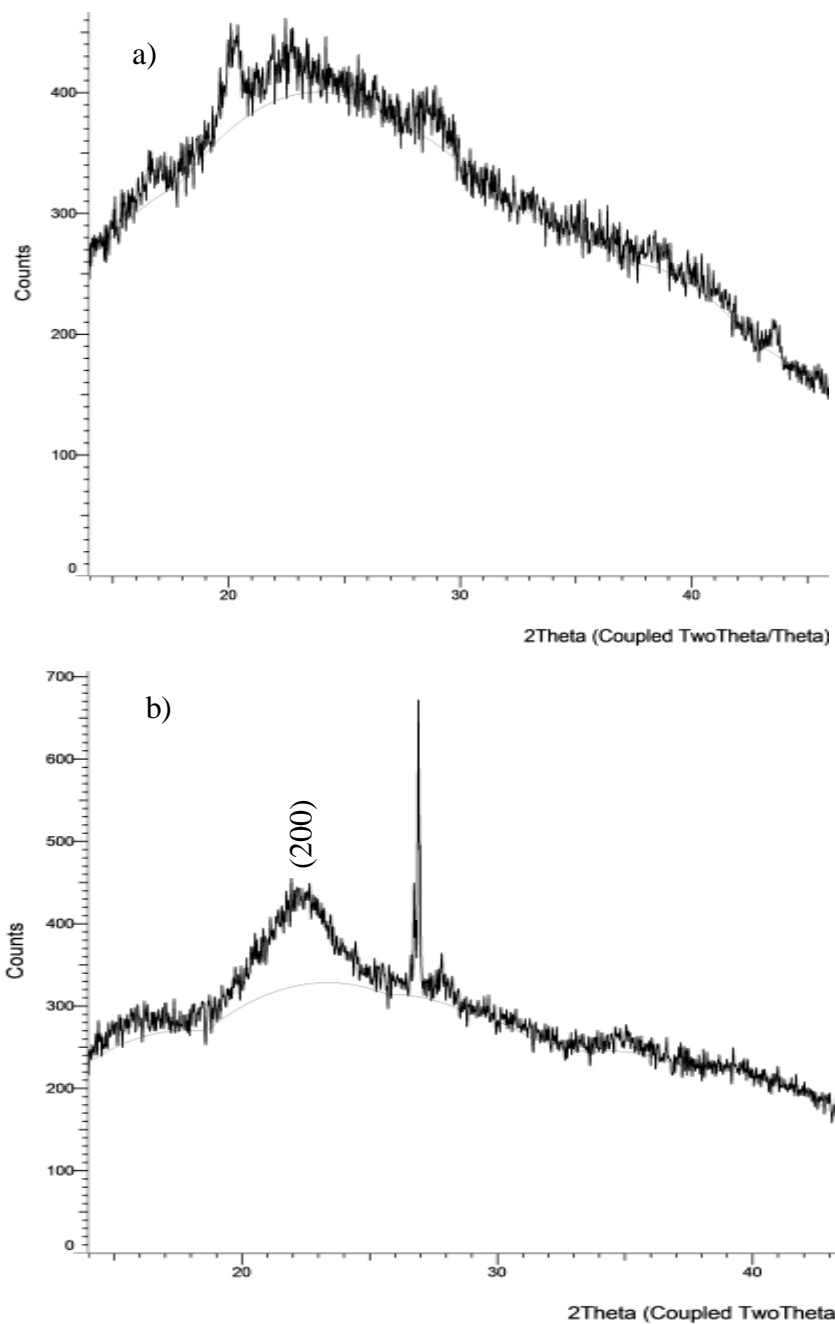
Figure 4.4. Diffractograms of (a) polymer hydrogel without cellulose, (b) cellulose grafted polymer hydrogel.

4.1.4.1 Transmission electron microscopy (TEM) and energy dispersive X-ray (EDX) spectroscopy

High resolution transmission electron microscopy (TEM) images of oven-dried cellulose-g-PAM-co-AA and acetone-extracted cellulose-g-PAM-co-AA polymer hydrogels are shown in Figure 4.5. TEM micrographs of the oven-dried PHG showed a smooth dense material (Figure 4.5a and b), whereas those of acetone-extracted PHG displayed voids and foldings which confirmed the presence of micro-pores (Figure 4.5c and d). Acetone-extracted PHG samples were used in water absorption tests due to higher swelling ratio and faster swelling rate compared to the oven-dried PHG. This suggested that, heating the samples (at 60°C) enhances cross-link density where unneutralized –COOH and unreacted –OH groups of cellulose could possibly interact through H-bonding and also react forming covalent (ester) bonds.
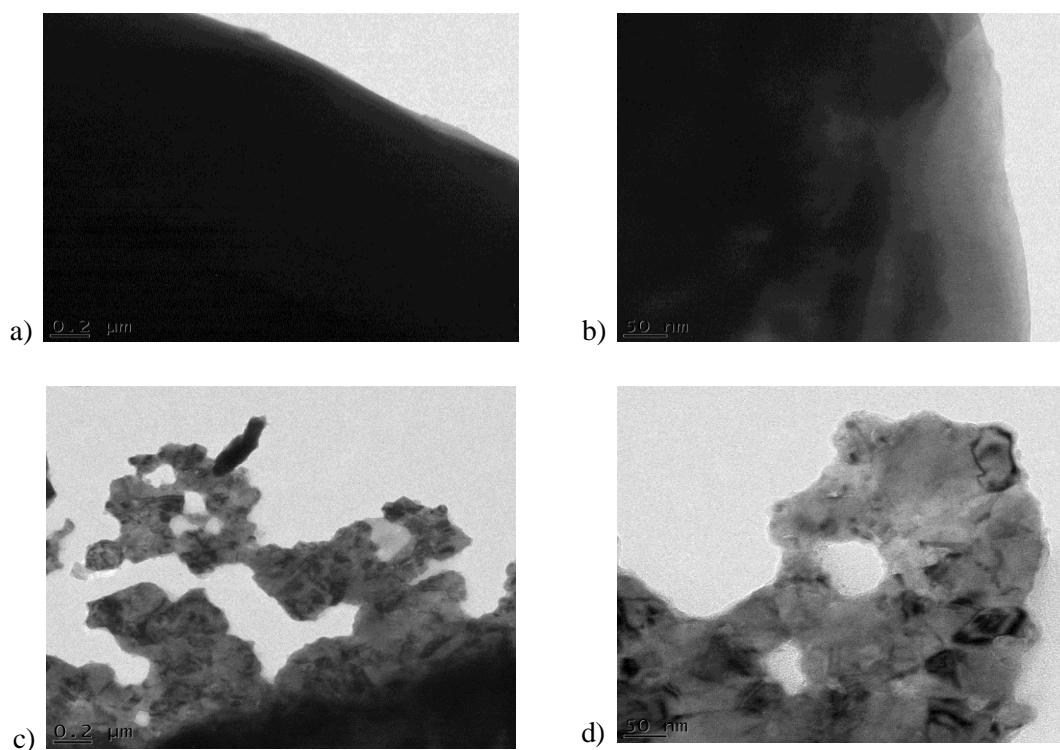
Figure 4.5. TEM micrographs of (a and b) oven-dried cellulose-g-PAM-co-AA, (c and d) acetone-dehydrated cellulose-g-PAM-co-AA, at 0.2 μm and 50 nm scales

Similar observations were made by Sannino *et al.* (2004), who used a phase inversion desiccation technique in acetone to dehydrate a PHG based on sodium carboxymethyl cellulose

and hydroxyethyl cellulose cross-linked with divinyl sulphone. This technique induced a micro-porous structure into the PHG which increased the water absorption and the swelling kinetics due to capillary effects. Simoni *et al*., 2017 obtained smooth and compact micrographs in air-dried PHG samples and attributed it to evaporation of water that led to equilibrium polymeric chain conformation.

The energy dispersive X-ray (EDX) spectrum of cellulose-grafted copolymer is displayed in Figure 4.6. The spectrum revealed an intense carbon band at 0.2 KeV due to cellulose and acrylic chains being the main constituents of the copolymer. Other elements detected were oxygen (0.5 KeV) due to cellulose, sulphur (2.3 KeV) due to ammonium persulphate (radical initiator), Cu (0.9, 8 and 9 KeV) due to the grid used during viewing, while Ca (3.7 KeV) and Fe (6.4 and 7 KeV) could be part of the nutrients absorbed by the WH during growth.
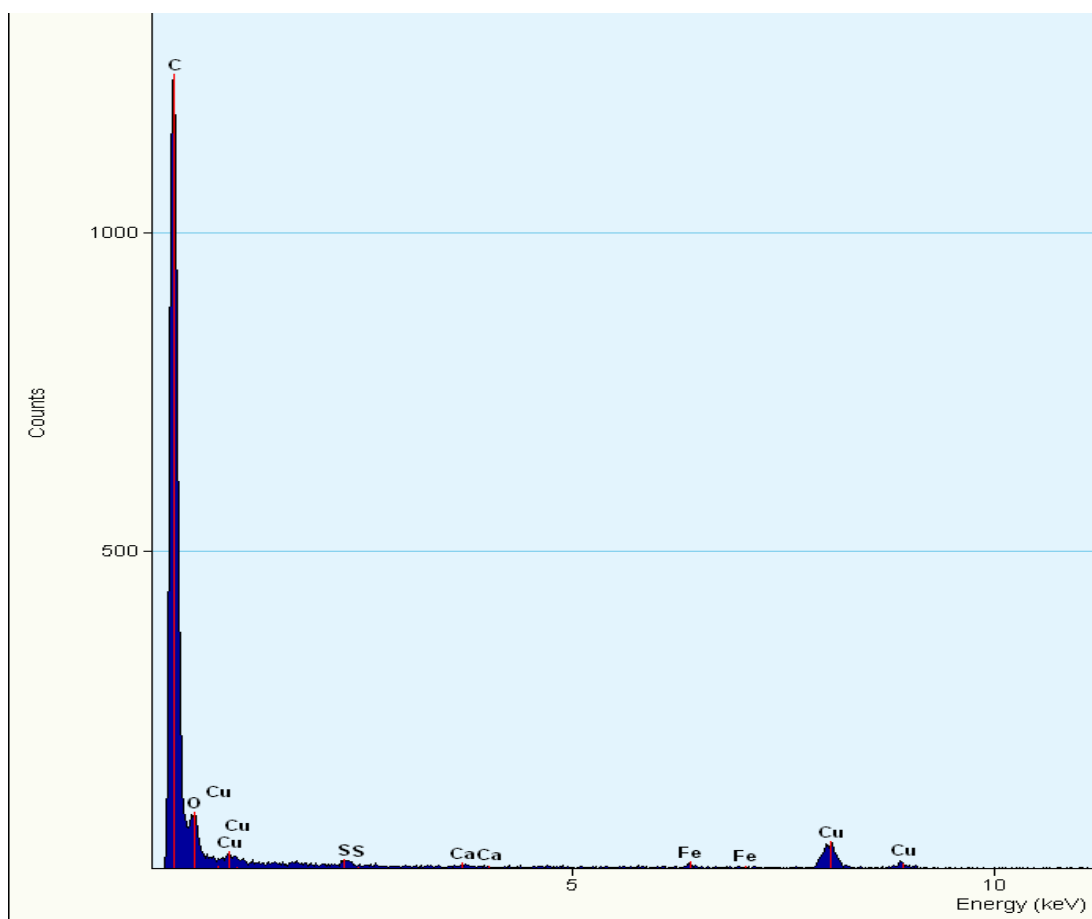
Figure 4.6. EDX of cellulose-g-poly(acrylamide-co-acrylic acid)

The band characteristic of N was not observed as expected and this could be due to absorption by the detector window. The X-ray transmission by Beryllium window is almost 100% for energies > 2 KeV, but it drops to about zero at 0.5 KeV (Liao, 2006), hence X-ray line such as that of N (0.4 KeV) is absorbed. The presence of carbon in the sample is also implicated for low detection of N Kα (X-ray line) because of high mass absorption coefficient value of carbon, 25500 cm^2g^{-1} (Liao, 2006).

4.1.5 Evaluation the factors influencing the swelling of polymer hydrogel

4.1.5.1 Influence of salt solutions on water absorbency

The effect of salt concentration and ionic charge on the swelling equilibrium (SEQ) is shown in Figure 4.7. The SEQ decreased in salt solutions, depending on the nature and the concentration of the metal cation in the order; $Na^+ > Al^{3+} > Ca^{2+}$. This was attributed to lowering of the osmotic pressure, the driving force behind the swelling of the PHG (Laftah *et al*., 2011; Gupta and Shivankumar, 2012; Swantomo *et al*., 2013). Furthermore, multivalent cations may have neutralized the charge at the surface of the PHG by complexing with carboxyamide and carboxylate groups leading to a highly cross-linked network with a small internal free volume as reported by Shi *et al*. (2011) and Livney *et al*. (2003).
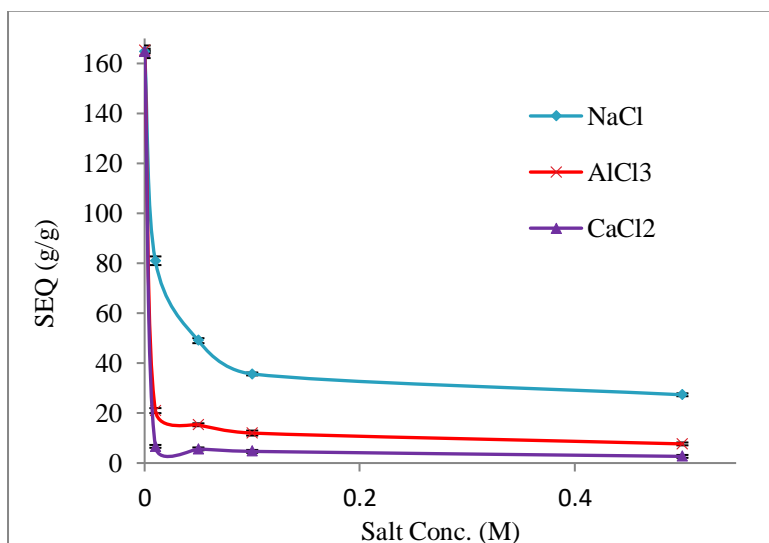
Figure 4.7. Influence of salt concentration and ionic charge of the salt on the swelling of polymer hydrogel: Results are reported as Mean ± SD (n=3)

The SEQ was higher in the presence of trivalent Al^{3+} ions compared to divalent Ca^{2+} ions. The observation may be related to charge density, explained by increased electron pair attraction of strongly co-ordinated water molecules (Livney *et al.*, 2003). Small size and high charge density Al^{3+} ions bind water molecules strongly, co-ordinating them with the O atoms towards the cation and the H atoms protruding. Due to attraction of electron cloud by the cation, the H atoms of co-ordinated water molecules become more positive than bulk water molecules; hence, they are more susceptible to formation of H-bonds with electron pairs of polymer dipolar groups such as carboxylic and amide oxygen. On the other hand, large and low charge density Ca^{2+} ions interfere with the water structure without creating an alternative radial structure (Livney *et al.*, 2003). Gupta and Shivakumar (2012) observed a decrease in SEQ of poly(methacrylic acid-co-acrylamide) PHG from 155 to 30 g/g in aqueous solution containing Na^+ at concentrations ranging from 0.0001 to 1M, and also decreased SEQ with increased cationic charge in the order; $Na^+ > Ca^{2+} > Al^{3+}$, slightly different from the copolymer in the present study. The decrease was attributed to degree of cross-linking which increased with cationic charge and the lowering of the pH of the swelling medium in the case of $AlCl_3$ salt. Shi *et al.* (2011) also observed decreased SEQ values of guar gum-g-poly(sodium acrylate-co-styrene)/attapulgite PHG in the same order; $Na^+ > Ca^{2+} > Al^{3+}$, a phenomenon attributed to the "charge screening effect" and formation of chemical cross-links through complexation of carboxylate groups by multivalent cations.

4.1.5.2 Influence of pH on water absorbency

The effect of pH on the swelling equilibrium (SEQ) of the hydrogel is shown in Figure 4.8. The SEQ values observed in buffer solutions ranged from 20 to 80 g/g, lower than values of 165 g/g and 120 g/g obtained in distilled and tap water, respectively. This indicates that the PHG was sensitive to charged species in the swelling medium. The SEQ increased with increase in pH of the solution up till pH of 10 then declined. The observation was attributed to the existence of ionizable (carboxyl) groups which present electrostatic repulsion to each other, expanding free volume to accommodate more water molecules (Soleimani and Sadeghi, 2012). However, excess NaOH (used to adjust the pH, section 3.2.8.3) may cause a "shielding effect" of Na^+ ions on the carboxylate by lowering the repulsion between them, hence decreasing the free volume. The low SEQ at low pH values relates to high proportion of undissociated -COOH groups characterized by low degree of hydrophilicity and high ability to form H-bonds, resulting in a rigid network.

Similar observations were made by Demitri *et al*. (2013) who evaluated the swelling behaviour of sodium carboxymethyl cellulose/hydroxyethyl cellulose PHG at pH values ranging from 2 to 10. The SEQ increased from 37 to 95 g/g due to dissociation of -COOH groups, which depended on the pH of the swelling medium. Soleimani and Sadeghi (2012) obtained a maximum SEQ value of 95 g/g at pH 8 in PHG based on starch-polyacrylate. Gupta and Shivakumar (2012) obtained higher SEQ value of 160 g/g at pH 7.4. Mahfoudhi and Boufi (2016) observed low SEQ in the pH range of 2-4, which increased from pH 5 to the maximum at pH 7, then declined thereafter.
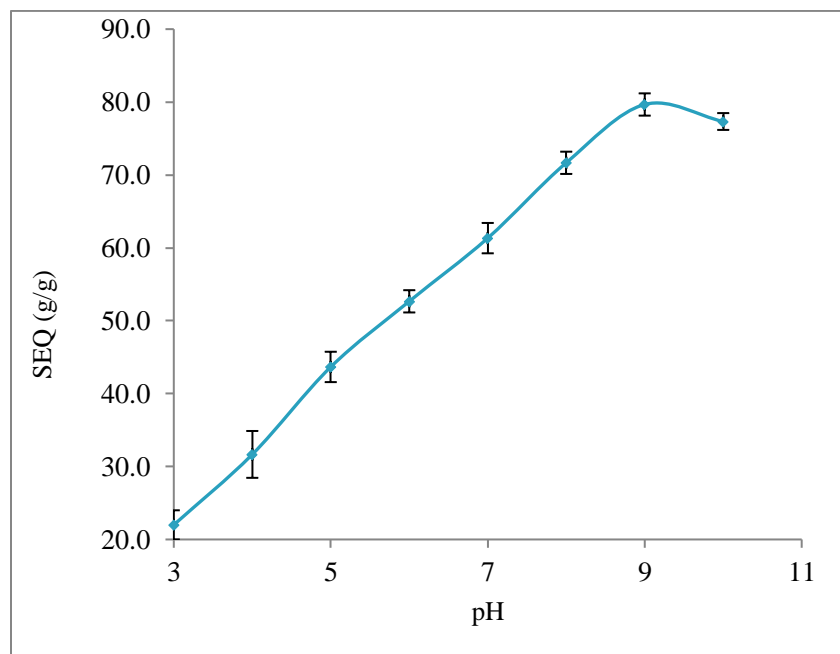
Figure 4.8. Influence of pH on the swelling of PHG: Results are reported as Mean ± SD (n=3)

4.1.5.3 Moisture holding capacity of PHG amended soil

The moisture holding capacity (MHC) of sandy-loam soil amended with different amounts of cellulose grafted copolymer is shown in Figure 4.9. The moisture contents of the amendments were recorded at an average temperature of 24 °C and humidity of 40. The initial values of the MHC ranged from 35 % in the unamended soil to 68 % at 1.5 % ($^W/_W$) copolymer content. A gradual decrease in MHC was observed with time at different rates to near dryness as at 19th day in all the amendments. The copolymer revealed the capacity to absorb and retain moisture in soil and factors such soil pH and the presence of cations may have influenced its water absorbency.

This is an important attribute for the efficient use of water in agriculture. The retention of moisture in soil is attributed to macro-molecular hindrance and hydrophilicity of the copolymer (Demitri *et al.*, 2013), which slows the release of absorbed water. In a similar study, Shahid *et al.* (2012) obtained MHC values ranging from 35 to 65 % in sandy-loam soil amended with 0.1 to 0.4 % poly(acrylic acid-co-acrylamide)/$AlZnFe_2O_4$/K humate nano-composite. The retention of moisture at relatively lower copolymer content was attributed to K humate which enhanced hydrophilicity. Thombare *et al.* (2018) also obtained MHC values ranging from 39.8 to 51.57 % in sandy-loam soil amended with relatively lower copolymer content of 0.1 to 0.3 % guar gum based PHG. The MHC values were proportional to the amount of PHG added to the soil.
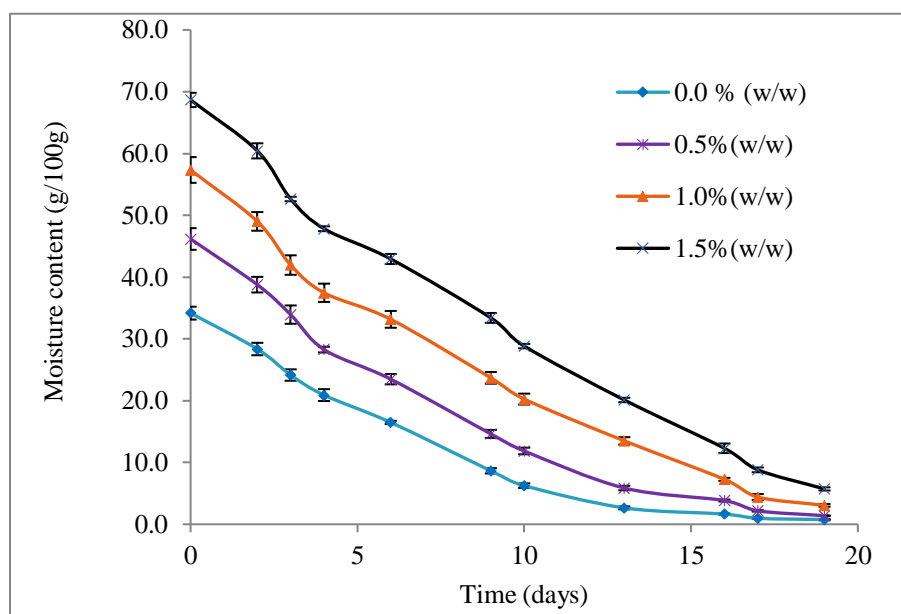
Figure 4.9. Moisture holding capacity of 100 g PHG-amended sandy-loam soil**:** Results are reported as Mean ± SD (n=3).

4.1.6 Biodegradation of polymer hydrogel in soil and by soil microbial isolates

4.1.6.1 Biodegradation of cellulose-grafted-copolymer in soil

The degradation curves of cellulose-g-PAM-co-AA and PHG without cellulose are shown in Figure 4.10. A slow mass loss was observed in cellulose-grafted PHG in the first four weeks followed by a more rapid loss from the 4th to 12th week, after which the curve tends to plateau. No considerable change in mass was observed in the case of PHG without cellulose. After 14 weeks, the mass loss was approximately 25 % for cellulose-g-PAM-co-AA and 5 % for PHG

without cellulose. In a similar study, Laftah and Hashim (2014) obtained a mass loss of about 9.6 % in cotton-g-poly(sodium acrylate-co-acrylic acid) PHG and 0.1 % in PHG without cotton after 14 weeks incubation in soil. The lower mass loss relative to copolymers in the present study was attributed to highly crystalline cotton cellulose and stability of the copolymer. It follows that enhanced degradation of cellulose-g-PAM-co-AA is attributed to low degree of crystallinity of cellulose due to alkali treatment, in addition to amide-N that acted as source of nourishment to the microbes. The half-life ($t_{1/2}$) of cellulose-g-PAM-co-AA calculated from the rate constant of 0.025 week^{-1} (Figure 4.10) was found to be 27 weeks, significantly shorter than that of PAM-co-AA which was found to be 173 weeks. Thombare *et al*. (2018) obtained a relatively higher degradation rate constant of 0.009 day^{-1} and $t_{1/2}$ of 77 days in guar gum-g-polyacrylic acid PHG cross-linked with di-methacrylic acid.
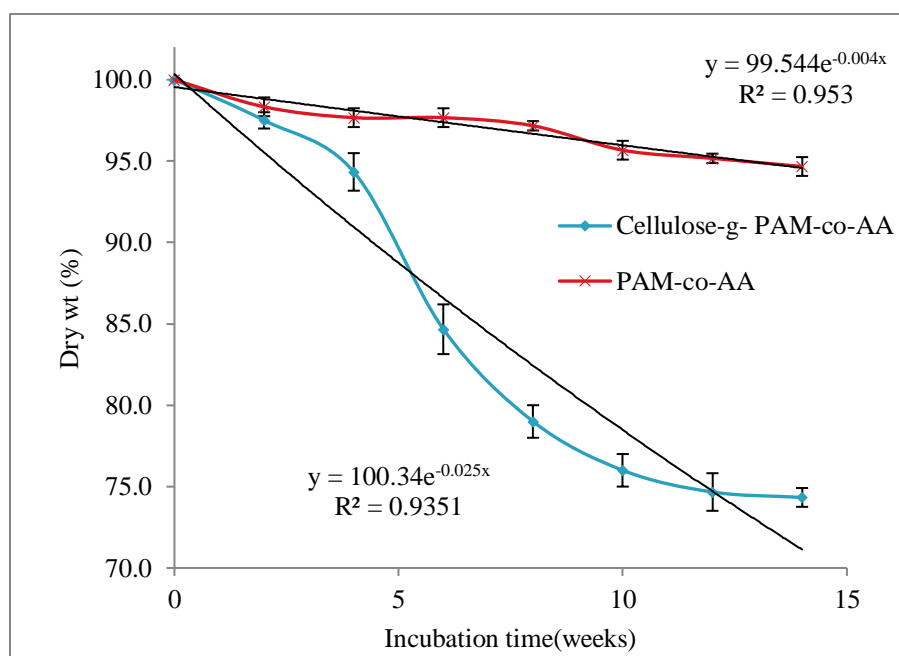
Figure 4.10. Degradation curve of cellulose-grafted PHG and PHG without cellulose**:** Results are reported as Mean ± SD (n=3).

The photographs of swollen PHGs before and after burying in moist soil are displayed in Figure 4.11. The cellulose-grafted PHG changed from whitish to dark-brown colour (Figure 4.11a and b) after 14 weeks in moist soil. The brown colour of cellulose-grafted PHG (Figure 4.11b) was darker than that of PHG without cellulose (Figure 4.11c), an observation which may be revealing

microbial degradation of copolymer chains. Oven-dried samples of unearthed cellulose-grafted PHG transformed from the initial tough solid (Figure 4.1a) to a friable material, whereas PHG without cellulose remained tough. High molecular weight polymer chains are degraded by microbes into monomeric and oligomeric units to enable assimilation (Yu *et al*., 2015). Native soil bacteria (*Pseudomonas, Xanthomonas, Rhodococcus, Klebseilla*) have been found to degrade and utilize polyacrylamide (PAM) as sole source of C and N under both aerobic and anaerobic conditions (Shanker *et al*., 1990; Nawaz *et al*., 1993 and 1994; Yu *et al*., 2015). They secrete PAM-specific intracellular and extracellular *amidase* (*amidohydrolase*) enzyme to hydrolyse the amide group into acrylic acid and ammonia, according to Scheme 4.4 (Kay-Shoemake 1998a and 1998b). Acrylic acid is eventually degraded to carbon dioxide and water. The addition of C sources into PAM has been reported to promote bacterial growth; Yu *et al*. (2015) observed improved degradation efficiency of PAM in culture medium supplemented with glucose. In this case, the grafted cellulose could have enhanced the degradation of the copolymer.

Figure 4.11. Photographs of (a) swollen cellulose-g-PAM-co-AA before burying in moist soil, (b) swollen cellulose-g-PAM-co-AA after 14 weeks in moist soil, (c) swollen PHG without cellulose after 14 weeks in moist soil

$$R-CONH_2 \xrightarrow[\text{H}_2\text{O}]{\textit{Amidase}} R-COO^- \, NH_4^+ \rightleftharpoons R-COOH \, + NH_3$$
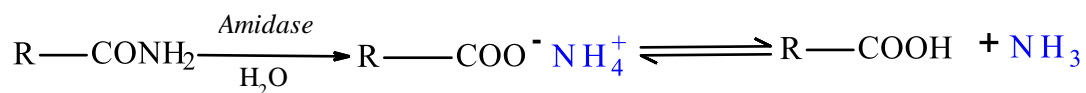
(R denotes macro-molecule)

Scheme 4.4. Enzymatic hydrolysis of acrylamide to carboxylic acid and ammonia

4.1.6.2 Microbial culture and degradation of the copolymer by soil microbial isolates

Of the 5 soil samples incubated in phosphate buffered medium (PBM) supplemented with acrylamide, 3 tested positive for NH_4^+. Acrylamide degrading microbes have been reported in soil contaminated with amides and their derivatives such as herbicides (Nawaz *et al*., 1991). These microbes transform herbicides such as propanil (acrylamilide) to amides and eventually NH_4^+, to support their growth (Nawaz *et al*., 1991). They have been isolated, identified and the *amidase* enzyme purified and characterized (Shanker *et al*., 1990; Nawaz *et al*., 1993 and 1994; Yu *et al*., 2015). The present study focused on utilizing the soil microbial isolates to degrade acrylamide copolymers; therefore, the microbes involved could be more than one species.

Table 4.8 shows the amount of NH_4^+ liberated with time in PBM supplemented with acrylamide and different amounts of the copolymer as the sole source of C and N. The amount of NH_4^+ accumulated in the copolymer supplemented media increased with time to maximum values at 100 h above which some decline were observed. The decrease after the maxima may be attributed to utilization of NH_4^+ by the microbes as N source. The amount of NH_4^+ accumulated in the media for both copolymers increased significantly ($p \leq 0.05$) with the copolymer content (P1 to P3 and CP1 to CP3) from 40 to 100 h. The values recorded in 0.05 % (w/v) copolymer content (P3 and CP3) were in most instances, not significantly different from those observed in 0.06 % (w/v) (P4 and CP4). Significantly higher accumulation of NH_4^+ was observed in the cellulose grafted copolymer CP1 and CP2 from 40 to 100 h, relative to similar content of the copolymer without cellulose P1 and P2. The observation may be attributed to easily accessible cellulose-C which enhanced microbial growth and subsequently, increased amount of enzyme that caused considerable hydrolysis of the amide-N.

The degradation of the copolymers was not compared statistically with that of acrylamide (monomer) due to cross-linked network which must be degraded into monomeric units to enable microbial assimilation. Acrylamide supplemented medium showed low content of NH_4^+ ranging from 1.1 to 1.9 mg/kg in the first 60 h, reflecting the lag phase, which then increased considerably from 20 mg/kg at 80 h to a maximum value of 112.2 mg/kg at 216 h after which it declined.

Table 4.8. Concentration of NH_4^+ (mg/kg) liberated with time (hours) at different copolymer contents

Sample code	6 h	20 h	40 h	60 h	80 h	100 h	168 h	216 h	288 h
AM	0.5 (0.1)	1.1(0.1)	1.5 (0.3)	1.9 (0.2)	20.9(2.0)	54.8(1.9)	95.8(3.3)	112.2(4.2)	93.9(3.0)
P1	6.7(1.6)a	11.1(0.2)a	19.4(1.4)a	17.4(1.0)a	20.9(1.9)a	34.6(1.6)a	21.7(2.4)a	21.1(1.2)a	22.7(0.6)a
P2	10.6(2.3)ab	14.7(1.5)ab	31.6(2.4)b	26.4(1.8)b	37.8(0.4)c	50.4(2.2)c	33.8(2.9)a	33.8(1.7)b	34.3(3.1)b
P3	11.7(2.5)b	22.2(2.8)cd	41.6(1.7)c	56.0(0.9)d	62.8(1.4)e	66.9(0.5)d	63.3(1.6)bc	67.2(7.4)d	64.1(1.0)de
P4	12.3(1.6)b	28.3(1.7)d	56.9(1.5)cd	61.9(2.6)e	64.3(0.8)e	80.3(1.9)e	80.3(3.2)d	64.3(0.6)d	52.3(2.1)c
CP1	12.8(1.7)b	13.3(0.5)ab	30.6(2.4)b	24.1(1.5)b	34.3(1.5)b	42.0(3.7)b	27.7(3.8)a	28.3(1.0)ab	32.3(3.2)b
CP2	13.9(1.2)b	19.2(1.0)bc	41.8(1.6)c	38.9(1.8)c	47.0(1.0)d	60.7(1.8)d	53.3(2.0)b	49.8(2.6)c	56.3(3.2)cd
CP3	13.5(1.9)b	21.1(2.4)c	56.1(2.1)d	51.8(2.0)d	64.6(0.5)e	81.1(2.5)e	57.4(10.3)bc	58.2(0.8)cd	61.7(3.8)de
CP4	14.1(1.9)b	20.7(3.3)c	52.5(2.0)d	53.9(0.8)d	63.3(1.6)e	81.7(2.5)e	68.0(3.7)cd	66.6(4.6)d	65.6(3.4)e

Notes: The values in parentheses are standard deviations (n = 3), different letters in the same column are significantly different (Tukey test; $P \leq$ 0.05 level)

Legend: AM = Acrylamide monomer, 10 mM {0.07 % (w/v)}, P = PAM-co-AA; P1 = 0.02, P2 = 0.04, P3 = 0.05 and P4 = 0.06 (%w/v), CP = Cellulose-g-PAM-co-AA; CP1 = 0.02, CP2 = 0.04, CP3 = 0.05 and CP4 = 0.06 % (w/v)

In related studies on the degradation of acrylamide (monomer) by *Pseudomonas sp.,* Shanker *et al*. (1990) observed the highest accumulation of NH_4^+ after 6 days, at 30°C. Nawaz *et al*. (1993) in *Pseudomonas sp.,* observed maximum NH_4^+ content after 24 h, at 28 °C which decreased to 1.0 mM at 96 h; whereas, *Xanthomonas maltophilia* showed the highest accumulation of NH_4^+ and acrylic acid at 48 h under the same conditions. In both cases, the highest acrylic acid content coincided with the disappearance of acrylamide and decreased with cellular growth. Nawaz *et al*. (1994) in degradation study of 62 mM acrylamide by *Rhodococcus sp.,* observed maximum accumulation of NH_4^+ and acrylic acid after 24 h and a peak cellular growth from 72 to 96 h at 28 °C. The variation in the time taken to achieve maximum NH_4^+ accumulation between the present and previous studies on the acrylamide may be related to the microbial (bacterial) species involved in the degradation and the initial population of microbes in the culture media.

4.2 Formulation of slow release nano-composite fertilizer and evaluating its N mineralization potential

Nano-HA and the formulated slow release nano-NPK fertilizer [water hyacinth cellulose-graft-poly(acrylamide/nano-HA/soluble fertilizer)] composite were characterized. The nutrient release from the fertilizer composite was evaluated in a laboratory soil incubation experiment.

4.2.1 Incorporation of nano-HA into cellulose grafted copolymer

The effect of nano-HA content on water absorbency (SEQ) of cellulose-grafted-copolymer is given in Table 4.9. The introduction of nano-HA into the copolymer at first decreased the swelling equilibrium from 163 to 104 (g/g) followed by a marked increase to 122 (g/g) with increased content of nano-HA to an optimal value at 2.5 % w/v, after which it declined. The initial decrease may be attributed to the rigidity of nano-HA which occupied the voids within the copolymer network, decreasing the free volume for accommodating water molecules. The initial increase in swelling equilibrium could be attributed to –OH groups at the surface of nano-HA which enhanced the hydrophilicity of the copolymer. Nano-HA content higher than the optimum decreased the SEQ. This was attributable to; a) generation of additional cross-link points where the –OH at the surface of nano-HA may react with the monomer (AA) and unneutralized –COOH, reducing flexibility of the co-polymer chains, b) decreased hydrophilic portion of the

composite, that is, poly(acrylamide-co-acrylic acid) with increased nano-HA content and (c) hampered growth of polymer chains by chain transfer mechanism according to Scheme 4.5.

Table 4.9. Effect of nano-HA content on the water absorbency of cellulose grafted copolymer

Nano-HA (% w/v)	Wt. of dry PHG composite (g)	SEQ (g/g)
0.00	3.56 (0.06)	163 (4.9)
0.63	3.62 (0.45)	104 (1.0)
1.25	4.10 (0.02)	106 (1.5)
1.88	4.26 (0.05)	113 (0.6)
2.50	4.55 (0.04)	122 (0.6)
3.75	5.12 (0.04)	100 (2.0)
5.00	5.44 (0.05)	79 (1.5)
6.25	5.82 (0.19)	67 (0.6)
7.50	6.09 (0.14)	57 (1.5)

Note: The values in parentheses are standard deviations (n = 3); reaction conditions; AA = 6.75 % (w/v), MBA = 0.5 % (w/v), cellulose = 2 % w/v, APS = 0.25 % w/v, degree of neutralization = 70 %, total volume = 40 mL and reaction time = 2 hr.
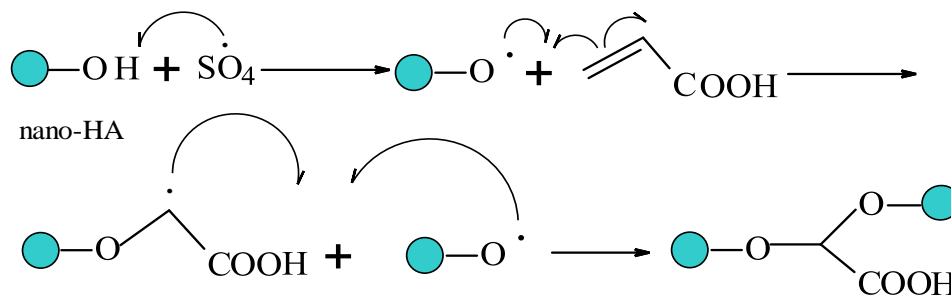
Scheme 4.5. Grafting of nano-HA to acrylic acid (monomer) by chain transfer mechanism

In a similar study, Gao *et al.* (2010) grafted methacrylic acid (MAA) onto HA particle surfaces by esterification reaction according to Scheme 4.6. The monomer (MAA) was then grafted onto etherified HA surface in presence of UV light as the initiator. The characterized product revealed successful grafting of MAA onto HA particles surfaces through a covalent bond. Rashidzadeh *et al.* (2014) evaluated sodium alginate-g-poly (acrylic acid-co-acrylamide)/clinoptilolite and observed increased SEQ from 34 (g/g) to a maximum value of 41 (g/g) after which it declined. They attributed initial increase in swelling equilibrium to repulsive forces between negative

surface charge of clinoptilolite and $-COO^-$ groups of the hydrogel, while the decrease was linked to additional cross-linking and reduced hydrophilicity of the composite with increased clinoptilolite content. Hosseeinzadeh and Sadeghi (2012) on assessing carboxymethyl cellulose-g-poly(sodium acrylate)/kaolin composite observed a decrease in SEQ from 450 to 45 (g/g), an observation attributed to additional cross-linking by kaolin and hindered growth of polymer chains through chain transfer mechanism.
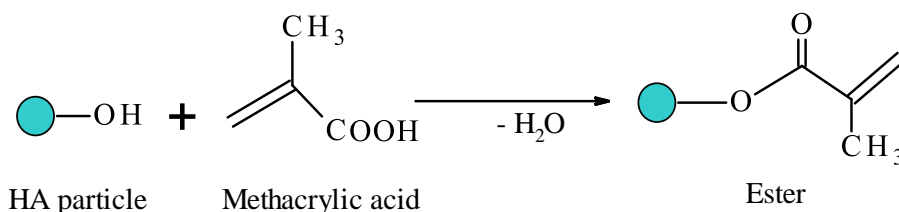
Scheme 4.6. Condensation reaction between the –OH group on HA particles surfaces and -COOH group of methacrylic acid, leading to the formation of an ester (Gao *et al.*, 2010)

4.2.2 Characterization of nano-HA and the formulated slow release nano-composite fertilizer

4.2.2.1 FTIR spectroscopic analysis

The Fourier transform infra-red (FTIR) spectrum of HA nano-particles is shown in Figure 4.12. The absorption bands at 1419 and 875 cm^{-1} correspond to CO_3^{2-} ions, attributed to the physical interaction of HA with CO_2 during the synthesis at ambient conditions (Iyyappan and Wilson, 2013). The spectrum observed in the study is similar to that of Costescu *et al.* (2010), who reported decreased intensity of the peaks related to CO_3^{2-} at high calcination temperatures of 600 and 1000 °C. The broad and weak band at 3600-3000 cm^{-1} and 1635 cm^{-1} is attributed to H-O-H of lattice water (Costescu *et al.*, 2010), and also stretching vibrations of -OH ions in the nano-HA lattice (Cisneros-Pineda *et al.*, 2014; Gayathri *et al.*, 2018). The characteristic bands for PO_4^{3-} group appear at 1022 and 964 cm^{-1} due to stretching vibrations and those at 601 and 563 cm^{-1} corresponding to bending vibrations. The bands characteristic of C-H stretch at 2928 and 2856 cm^{-1} due to -CH_3 and -CH_2 respectively, were found to be absent in the FTIR spectrum. This confirms complete removal of T-X 100 upon washing HA nano-particles with methanol.
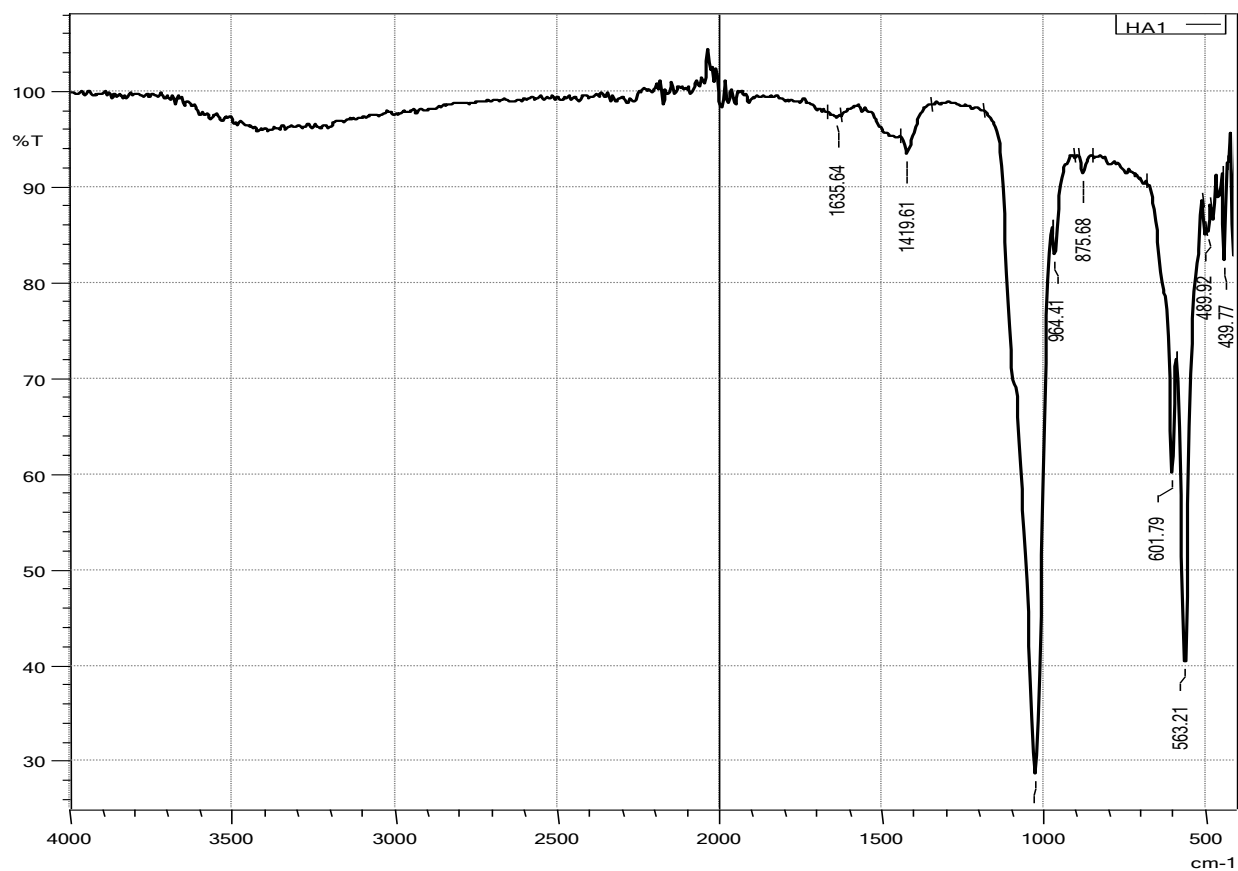
Figure 4.12. FTIR spectrum of hydroxyapatite nano-particles

FTIR spectrum of the fertilizer composite is shown in Figure 4.13. The broad and strong band at 2500-3500 cm^{-1} can be assigned to O-H stretch due to carboxylic acid (acrylic acid) and alcoholic group (cellulose), and also, N-H for amide group (acrylamide). The bands at 3182 and 1543 cm^{-1} are assigned to N-H stretching vibration for primary amide (Bundela and Bajpai, 2008).

Eritsyan *et al.* (2006) and Fernandes *et al.* (2015) proposed radical polymerization reaction mechanism between acrylic acid and urea via the carbonyl carbon (Scheme 4.7). According to these authors, the moderately strong band at 1635 cm^{-1} (Figure 4.13) is assigned to adsorption of NH$_3^+$ and COO$^-$ groups as a result of intra- and inter-molecular interactions between –COOH and –NH$_2$ which lead to the formation of a salt.
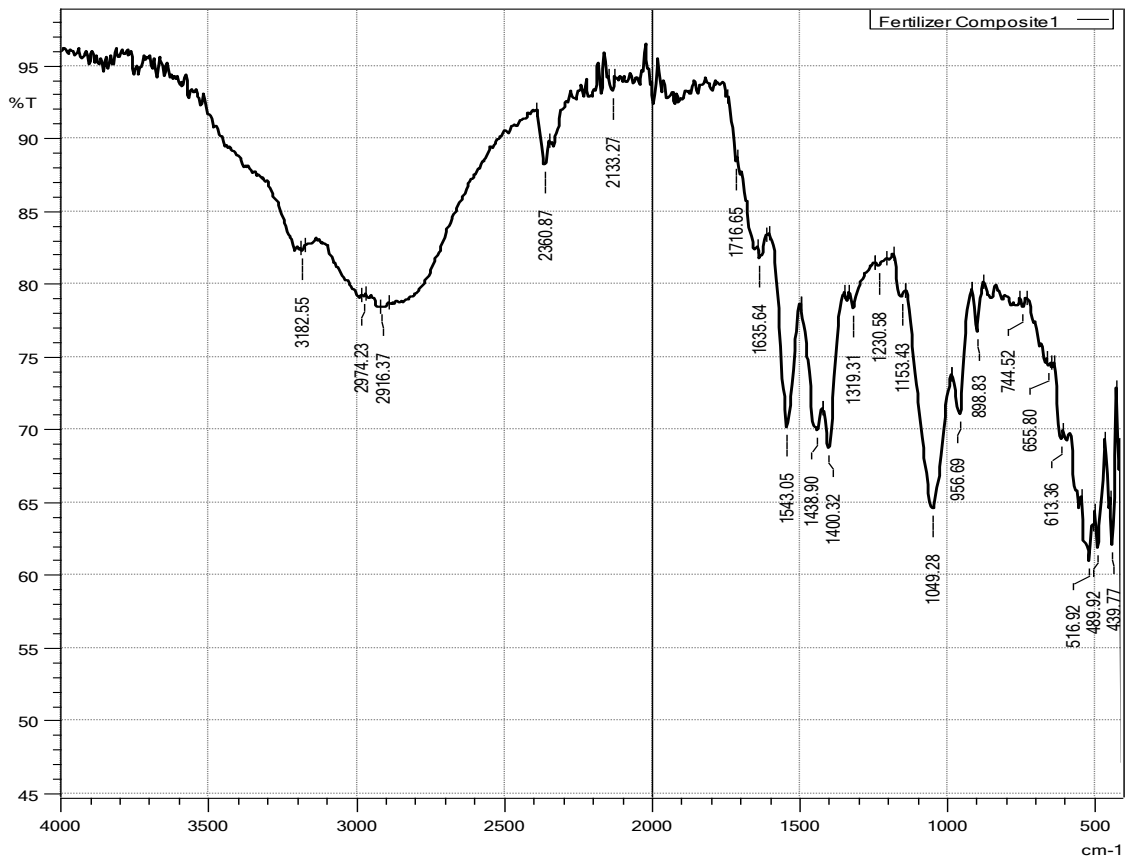
Figure 4. 13. FTIR spectrum of cellulose-g-poly(acrylamide)/nano-HA/soluble fertilizer composite
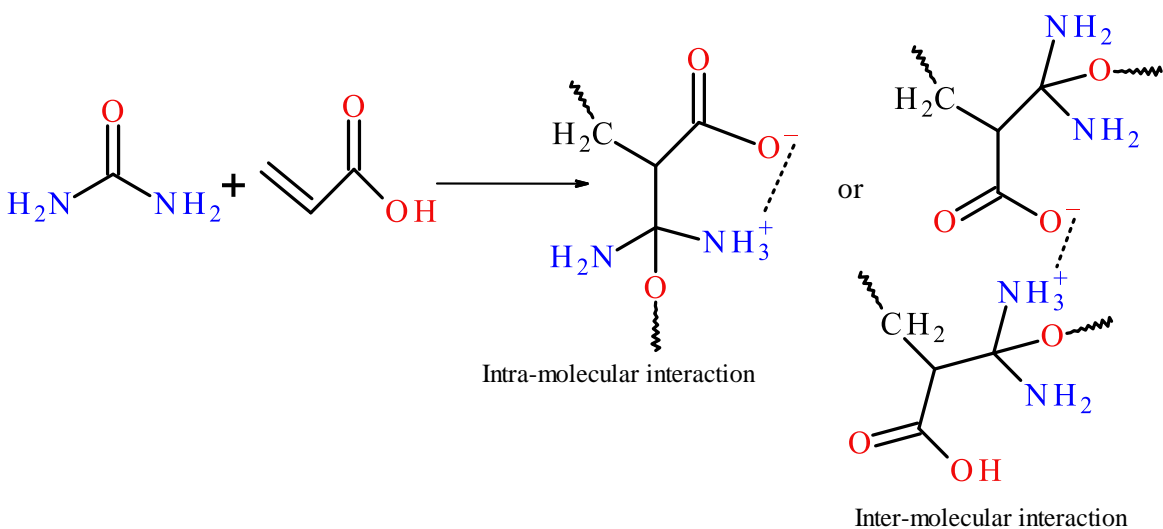
Scheme 4.7. Radical polymerization between urea and acrylic acid

Since acrylic acid was partially neutralized with NH_3, ammonium acrylate could react the same way according to Scheme 4.8. Alongside radical polymerization, condensation reaction between urea and acrylic acid may also occur (Fernandes *et al.,* 2015), yielding a branched co-polymer according to Scheme 4.9.
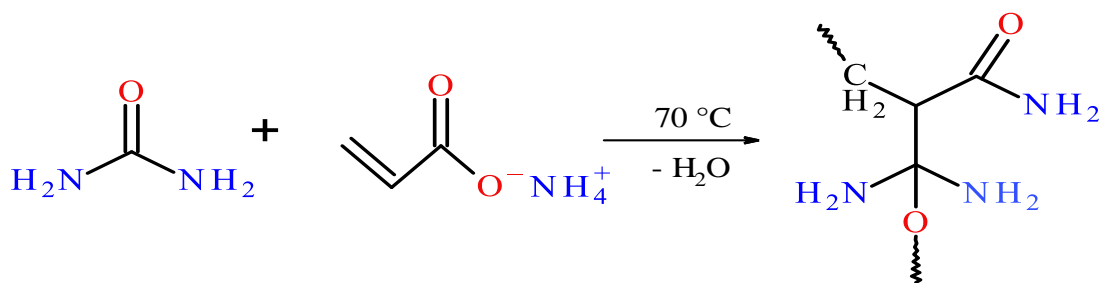
Scheme 4.8. Radical polymerization between urea and ammonium acrylate
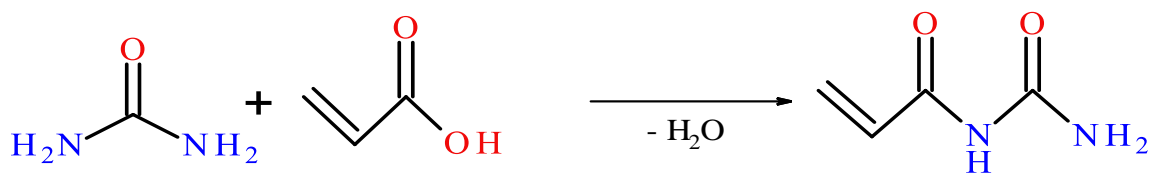
Scheme 4.9. Condensation reaction between urea and acrylic acid

The strong band at 1438-1400 cm^{-1} (Figure 4.13) corresponds to O-H bending vibration for carboxylic acid, revealing incomplete neutralization of acrylic acid. Spectral bands at 1153 to 1049 cm^{-1} are assigned to C-O-C bridging resulting from the reaction between ammonium acrylate (monomer) and the –OH group of cellulose. The band at 898 cm^{-1} is assigned to C-O-C stretch of glucosidic bonds for amorphous cellulose (Synytsya and Novak, 2014). The FTIR peaks from 1049-920 cm^{-1} are assigned to P-O-C (Figure 4.13), suggesting an overlap between bands attributed to C-O-C and P-O-C groups. The peaks at 1049 and 956 cm^{-1} are assigned to P-O-C stretching vibrations, indicating the reaction between –OH groups at the surface of HA nano-particles and the monomer. The bands at 1319 and 516 cm^{-1} (Figure 4.13) are attributed to P=O stretching vibrations for the PO_4^{3-} ion due to $(NH_4)_2HPO_4$, whereas the bands at 613 and 439 cm^{-1} corresponds to SO_4^{2-} ion due to K_2SO_4 i.e., inorganic salts.

From FTIR spectrum of the fertilizer composite, there is an indication of the existence of chemical interactions between (a) the monomer, cellulose and nano-HA, and (b) monomer and urea molecules towards the formation of 3-D network structure. Additionally, due to large surface area of HA nano-particles, Kottegoda *et al.* (2011; 2017) associated the formation of urea-HA nano-hybrid (molar ratio, 6:1) to the existence of H-bonds between –OH group on the surface of HA and –NH$_2$ group of urea.

4.2.2.3 XRD analysis

The X-ray diffraction patterns of nano-HA and cellulose-g-poly(acrylamide-co-AA)/nano-HA composite are presented in Figure 4.14. Nano-HA displayed mainly diffraction bands at 2θ = 26°, 32°, 33°, 34.3°, 39.5°, 46.5°, 49.5° (Figure 4.14a) assigned to (002), (211), (112), (300), (130), (222), (213) crystallographic plane reflections, respectively (Costescu *et al.*, 2010; Mechay *et al.*, 2012; Brundavanam *et al.*, 2013; Ragu and Sakthivel, 2014; Gayathri *et al.*, 2018). The cellulose grafted polymer/nano-HA composite (Figure 4.14b) indicated a weak diffraction band at around $2\theta = 22°$ (200) attributed to cellulose I allomorph, with the rest of the bands being typical of nano-HA crystalline structure.
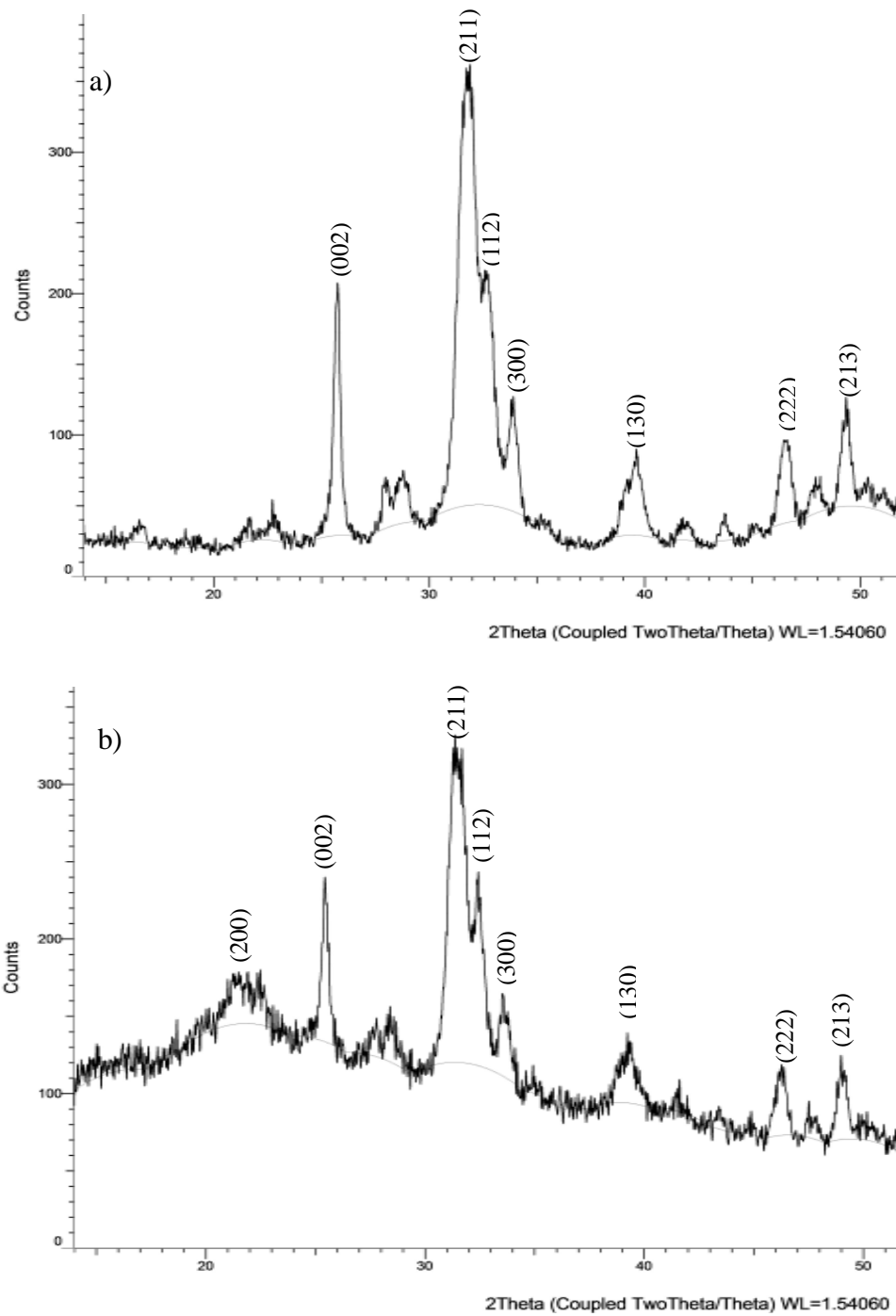
Figure 4.14. Diffractograms of (a) nano-HA, (b) cellulose-g-poly(acrylamide-co-AA)/nano-HA
composite

4.2.2.2 Transmission electron microscopy (TEM) and energy dispersive X-ray (EDX) spectroscopy

The transmission electron microscopy (TEM) micrographs of HA nano-particles and cellulose-g-poly(acrylamide)/nano-HA/soluble fertilizer composite are shown in Figure 4.15. The images of nano-HA displayed rod-shaped nano-particle agglomerates with particle size of less than 50 nm (Figure 4.15a and b). This is consistent with the observation made by Iyyappan and Wilson (2013) who attributed the formation of rod-like nano-HA to hydrophobic ring complex formed through ion-dipole interaction between Ca^{2+} and polyoxyethylene group of TX-100, as shown in Scheme 4.10. The formation of this complex is thought to reduce the transfer rate of Ca^{2+} to the growing nano-HA crystals reducing the particle size under controlled conditions. The formation of nano-rods is also attributed to adsorption of TX-100 onto certain planes of formed crystals leading to growth of nano-particles in a preferential direction. The agglomeration of nano-particles (Figure 4.15a and b) was attributed to high specific surface energy that led to aggregation (Pramanik *et al*., 2009; Ragu and Sakthivel 2014). TEM images of the fertilizer composite (Figure 4.15c and d) showed dispersion of HA nano-particles and the salt crystals. Similarly, Ragu and Sakthivel (2014) observed diminished agglomeration of nano-HA in polymethyl methacrylate/nano-HA composite at about 20 to 50 nm. This was attributed to reduction of surface energy of nano-HA by the polymer through its pendent PO_4^{3-} group.
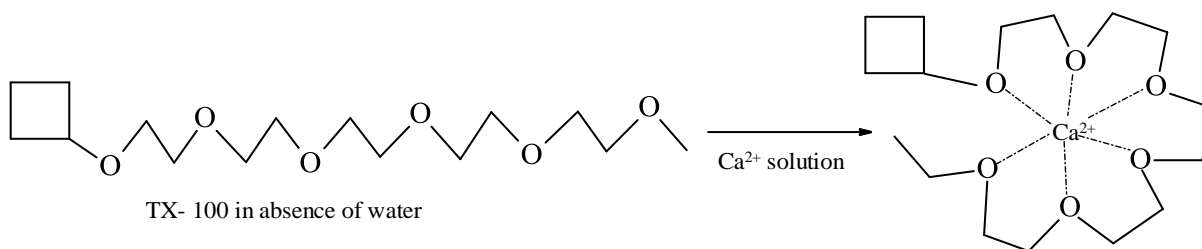
Scheme 4.10. The ion-dipole interaction between Ca^{2+} and polyoxyethylene group of TX-100 leading to formation of hydrophobic complex (Iyyappan and Wilson, 2013)
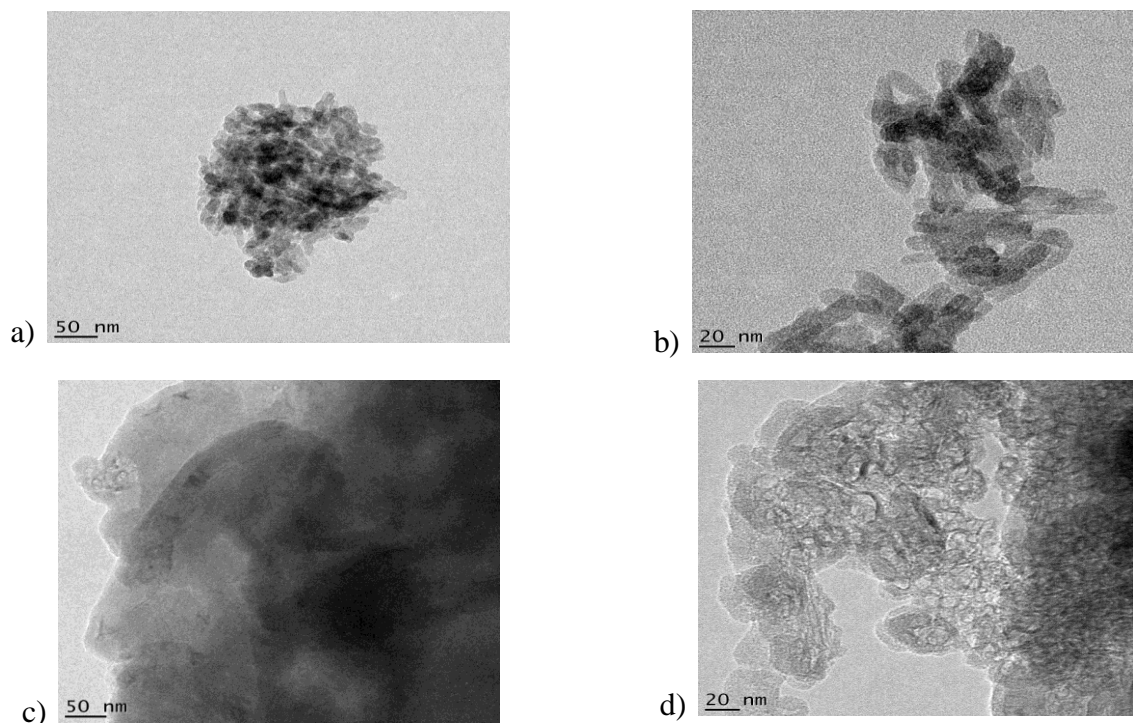
Figure 4.15. TEM micrographs of (a and b) HA nano-particles, (c and d) cellulose-g-poly(acrylamide)/nano-HA/soluble fertilizer) composite, at 50 and 20 nm scales

The energy dispersive X-ray (EDX) spectra of nano-HA and cellulose-g-poly(acrylamide)/nano-HA/soluble fertilizer composite are displayed in Figure 4.16. EDX spectrum of nano-HA displayed the main constituents of sample as calcium (3.7 KeV), phosphorous (2.0 KeV), oxygen (0.5 KeV) and carbon (0.2 KeV) (Figure 4.16a). Ca, P and O are expected in nano-HA lattice, while C may be attributed to the existence of CO_3^{2-} ions. Cisneros-Pineda *et al*. (2014) also obtained a peak due to carbon and attributed it to sensitivity of apatite lattice to the substitution environment of the CO_3^{2-} ions. This substitution can either be type A where CO_3^{2-} ions replace – OH ions, or type B where the CO_3^{2-} ions replace PO_4^{3-} ions (Cisneros-Pineda *et al*., 2014). The same bands were also observed in the fertilizer composite (Figure 4.16b), but the peaks due to oxygen and carbon were more intense than those observed in nano-HA spectrum (Figure 4.16a), an observation attributable to cellulose-grafted copolymer fraction. Sulphur was also detected in the fertilizer composite, which was part of the formulation in K_2SO_4 and ammonium persulphate (radical initiator). The rest of peaks due to Cu (0.9, 8.0 and 9.0 KeV) may have originated from the grid, Te (3.8 KeV) and Si (1.8 KeV) are not related to the constituents of the sample and could have probably originated from metal conductive layers and/or impurities.

94
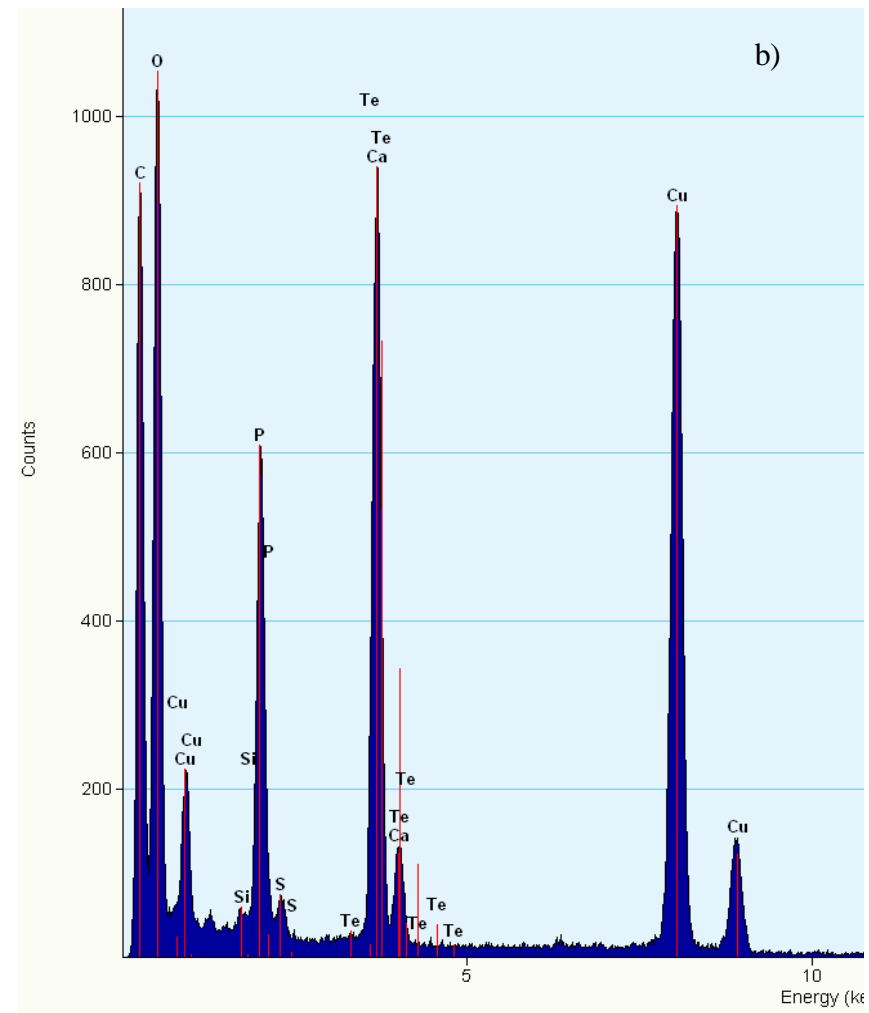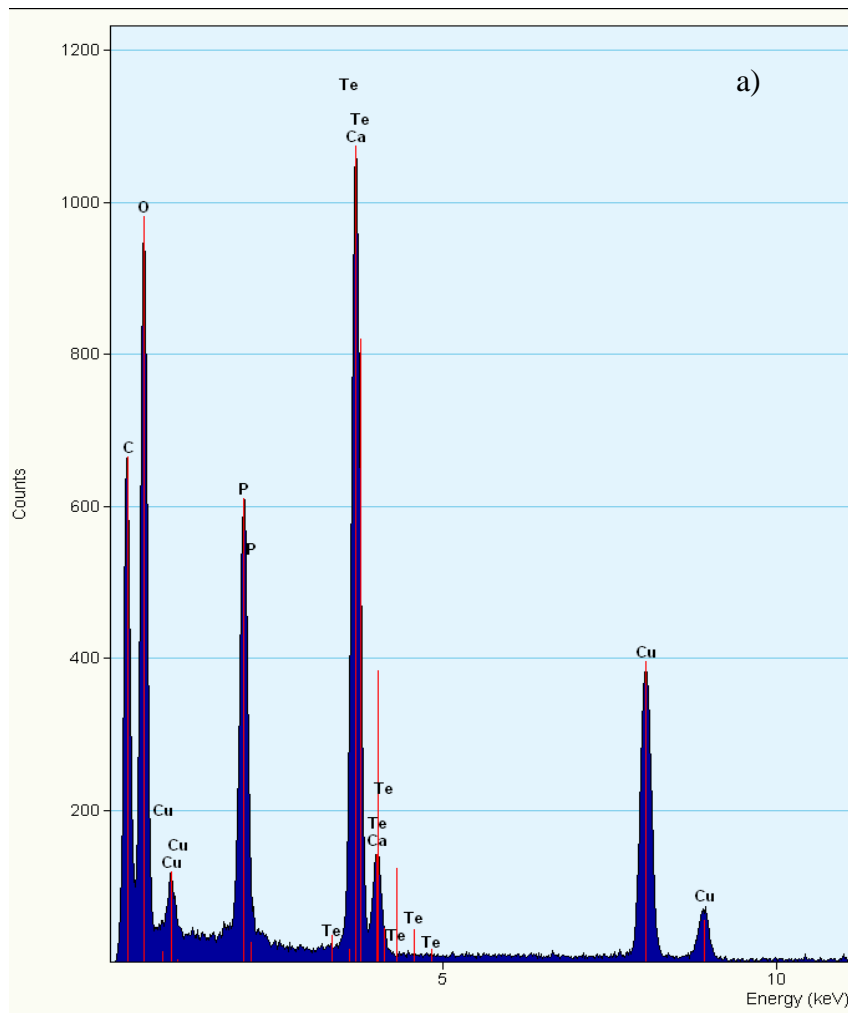
Figure 4.16. EDX spectra of (a) nano-HA, (b) cellulose-g-poly(acrylamide)/nano-HA/soluble fertilizer composite

4.2.3 Chemical characteristics of soil at the onset of incubation experiment

Table 4.10 shows salient characteristics of the soil used in the study. The soils at the site were acidic with low available P content. The soil acidity could be attributed to the humid conditions in central highlands which lead to the leaching of Ca, Mg and K, and other basic cations. Low amounts of available P could be attributed to soil acidity which renders P unavailable through fixation and also, continuous removal by crops.

Table 4.10. Some salient chemical characteristics of soil used in incubation experiment

Parameter	Units	Value
pH (soil: H_2O, 1: 2.5)	-	5.25
pH ($CaCl_2$: 1: 2.5)	-	4.50
Electrical conductivity	ds/m	0.26
Cation exchange capacity	$Cmol(+)\ kg^{-1}$	15.62
Total N	%	0.29
Available P	ppm	8.50
Exchangeable K	$Cmol(+)\ kg^{-1}$	1.10
Ca	$Cmol(+)\ kg^{-1}$	8.51
Mg	$Cmol(+)\ kg^{-1}$	4.26

4.2.4 Nitrogen mineralization

The mineral N (NH_4-N + NO_3-N) content during 16 weeks of incubation is shown in Table 4.11. The results show low mineral-N content in the initial stages of incubation with some decrease in the 4th week, followed by significant increase through the 8th week and a peak at the 12th week then a decline in the 16th week. Low mineralization of N in the initial stages of incubation reflects the lag phase (Deenik and Yost, 2008) associated with immobilization of nutrients by micro-organisms to nourish and diversify their species and biomass (Karuku and Mochoge, 2016; Tambone and Adani, 2017). The inorganic nutrients, sufficient water, carbon sources and trace elements are essential for maintenance and population growth of micro-organisms. The incubation period between the 4th and 12th week relates to microbial exponential growth phase where microbes proliferated and was able to act on the substrate. After they are satiated, the remaining portion of the substrate is mineralized into the soil. The decline in mineral-N content after the 12th week of incubation may be attributed to depletion of mineralizable substrate and

possibility of immobilization by microbes as their population had proliferated during the long incubation period (Karuku, 2019). This mineralization pattern may favour annual crops such as maize, since the uptake of N is slow at establishment, moderate at development and reproductive growth stages, and declines at maturity as plant reaches senescence.

Table 4.11. Concentration of mineral N (NO_3-N + NH_4-N) (ppm) during 16 weeks incubation period

Treatment	Incubation Period (weeks)					
	2	4	8	12	16	Cumulative Mineral-N at 16th wk
Cntrl	43.6a	24.2a	107.2a	145.8a	85.1a	405.8a
T1	50.8ab	33.0b	152.9b	176.6ab	117.9b	531.1b
T2	59.0abc	44.1cd	176.4c	200.1bc	128.4cd	608.0cd
T3	55.0abc	41.5c	189.5cd	192.2bc	119.3b	597.4c
T4	55.3abc	46.0cd	205.1de	266.1e	139.1e	711.7e
T5	63.5bc	42.9c	190.1cde	210.6cd	124.7bcd	631.8cd
T6	58.3abc	48.8cd	211.7e	242.1de	131.2de	692.1e
T7	73.2c	51.7d	184.9cd	207.5bc	129.6d	646.9d

Notes: Different letters in the same column are significantly different ($p \leq 0.05$ level). Cntrl = No treatment, T1= 14: 0: 0, T2 = 13.8: 18.8: 4.6, T3 = 15.4: 20: 4.8, T4 = 16.8: 21.5: 6.2, T5 = 20: 24: 9.7, T6 = 21.3: 25: 11.2, T7 = 24: 22: 11

The release of N from the SRF composites T2 to T6 [cellulose-g-poly(acrylamide)/nano-HA/soluble fertilizer composite] is thought to have occurred in two phases: i) diffusion of urea-N and NH_4-N and ii) hydrolysis of amide-N according to Liu *et al.* (2007). The highest content of mineral-N in the first 4 weeks was observed in conventional fertilizer (T7) and was attributed to the urea-N hydrolysis and release of NH_4-N in DAP. However, no significant difference was observed between T7 and T2 to T6 in the initial period of incubation. This non-significant difference may be attributed to the small particle sizes of SRF composite (<1 mm) that enabled rapid diffusion of the soluble fertilizer into the soil. Thus, the rate of diffusion of soluble N may be decreased by increasing the particle size of the fertilizer composite. Significant higher mineral-N content was observed in T6 in the 8th and 12th week and T4 in the 12th and 16th week, relative to T7. The lower values observed in T7 (relative to T4 and T6) during this period (8th – 16th week) may be attributed to early exposure of NH_4-N to exchangeable sites in the soil and

possibility of immobilization through fixation. The higher mineral-N content in T4 and T6 (than T7) in the later stages of incubation (8th - 12th week) was attributed to its reduced interaction with soil particles in the early stages of incubation and release of hydrolysed amide-N. NH_4^+ fixation occurs in clay soils due to the formation of NH·O bond in the hexagonal holes and the balancing of positive charge deficiency which arises from isomorphous substitution of Si^{4+} and Al^{3+} ions (Chen, 1997). No significant difference in mineral-N content was observed in the 12th week between T7 and T1, T2 and T3, indicating considerable mineralization of N in all SRF treatments. The observed increase in mineral-N contents between the 8th and 16th week in SRF treatments (T1 to T6) may be attributed to release through hydrolysis of amide-N.

The cumulative mineral-N generally increased from T1 to T6 due to increased proportion of soluble fertilizer and decreased content of nano-HA in the fertilizer formulation (Table 3.1). N mineralization is a biological process; hence, its release depends on the chemical constituent of the fertilizer such as N content and C: N ratio (Masunga *et al.*, 2016) as well as lignin and lingo-cellulose ratio, among other factors. The C:N ratio influences mineralization rate, as microorganisms have to immobilize N to break carbon bonds/chains in the organic material for their energy requirement (Dong *et al.*, 2012; Karuku and Mochoge, 2016; Tambone and Adani, 2017). The significant difference observed in T1 mineral-N content compared to all other SRF treatments, from the 4th to the 16th week, was related to the carbon content in the formulation. Slow mineralization of N in T1 (100 % PHG which is composed of carbonaceous material of acrylic and cellulose chains) may have been due to its higher carbon content, compared to other SRF treatments (Table 3.1). The proportion of carbon decreased on incorporating soluble fertilizer and nano-HA into the PHG.

Nevertheless, significantly higher mineral-N content in T1 compared with the control indicates substantial hydrolysis of the amide-N within the incubation period. Cellulose chains being part of the polymer composite provide easily degradable-C to the microorganisms, enhancing breakdown of the copolymer and hence N release. Addition of organic material to PAM-amended soil has been reported to effect degradation through increased microbial activity. Higher amounts of soil aggregating fungi was reported by TonThat *et al.* (2008) in macro-aggregates generated from PAM-wheat residue amended soil compared to the control. Award *et al.* (2012) also reported stimulating effect of synthesized PAM biopolymer (BP) and biochar

(BC) on the decomposition of soil organic matter and maize residue. The workers observed higher enzymatic activities in both BP and BC amended soil compared to the control and, fungi were implicated for contributing largely to plant residue decomposition. Watson *et al*. (2016) observed stimulation of nitrification and C-mineralization in maize straw-amended soil conditioned with PAM, a phenomenon attributed to improved microbial conditions and partial utilization of PAM as a substrate.

Addition of mineral-N from inorganic source to organic fertilizer enhances decomposition of organic material (Abbasi and Khaliq 2016). Further, cultures of bacteria derived from agricultural soils have been reported to utilize PAM as N source (Kay-Shoemake *et al.,* 1998a and 1998b). Bacterial strain (*Pseudomonas putida* H147) studied by Yu *et al.* (2015) showed 31.1 % degradation efficiency of PAM in 7 days and exceeded 45 % under optimum culture conditions. Degraded PAM showed low molecular weight oligomer derivatives while acrylamide monomers did not accumulate. The observed increase in the content of mineral-N in SRF treatments T2 to T6, could be attributed to increased amount of soluble N from DAP and easily hydrolysable N from urea. The microbes were provided with easy source of N and to acquire energy (carbon), the polymer had to be degraded. Polymer medium supplemented with mineral N, liquid paraffin and sucrose has been shown to contribute to PAM degradation and microbial biomass compared to the control (Yu *et al.,* 2015). The significantly ($p \leq 0.05$) lower content of mineral-N observed in SRF treatment T5 relative to T4 and T6 could be attributed to the experimental errors.

Table 4.12 shows ammonium-N and nitrate-N contents during different incubation stages. The NH_4-N content in T7 was significantly higher ($p \leq 0.05$) than T1, T2, T4 and T5 in the 2nd week, whereas for NO_3-N, T7 showed significantly higher value than T1, T3, T4 and T5 in the 4th week of incubation. No significant difference in both NH_4-N and NO_3-N content was observed between T7 and SRF T2, T3 and T5 in the 8th, 12th and 16th week, but significantly higher values were observed in T4 and T6 compared to T7. Significantly higher N content in T7 at early stages of incubation (2nd and 4th week) reveals availability of N which crops may not fully utilize as it may be lost through leaching or fixation by clay minerals, while in SRFs it may be preserved for future use and hence better synchronization. From the 8th to the 16th week, T7 and most of the

SRFs showed nearly equal N content, implying that the plant can utilize N released by SRF more efficiently than T7 which might get depleted sooner due to susceptibility to early losses.

Table 4.12. Concentration of NH_4-N and NO_3-N (ppm) during 16 weeks incubation period

Treatment	Incubation Period in weeks					Cumulative Mineral-N after 16th wks
	2	4	8	12	16	
NH_4-N						
Cntrl	29.4 a	17.1 a	72.5 a	87.0 a	53.3 a	259.0 a
T1	34.0 ab	24.5 b	83.0 ab	99.6 ab	69.3 b	310.3 b
T2	38.8 c	26.8 b	97.4 bc	116.8 bc	78.9 cd	358.7 cd
T3	34.0 ab	25.0 b	95.4 bc	114.5 bc	73.6 bc	342.5 bc
T4	35.1 ab	29.3 b	109.8 c	131.7 c	86.4 d	392.3 bc
T5	35.8 ab	23.5 ab	86.29 ab	103.5 ab	78.9 cd	328.0 bc
T6	38.8 c	28.3 b	113.7 c	136.4 c	78.9 cd	396.1 d
T7	38.8 c	27.9 b	89.5 ab	107.4 ab	73.6 bc	342.6 c
NO_3-N						
Cntrl	14.2 a	7.2 a	34.6 a	58.8 a	31.7 a	146.5 a
T1	16.8 ab	8.7 b	69.9 b	77.0 ab	48.5 b	220.8 b
T2	20.2 abc	17.2 cd	79.1 c	83.3 bc	49.5 cd	249.2 c
T3	20.9 abc	16.5 c	94.1 cd	77.7 bc	45.7 bc	254.9 c
T4	20.2 abc	16.7 c	95.4 de	134.4 e	52.7 e	319.3 d
T5	27.6 bc	19.5 c	103.9 cde	107.1 cd	45.7 bcd	303.8 d
T6	19.4 bc	20.5 cd	98.1 e	105.7 de	52.3 de	295.9 d
T7	34.3 c	23.8 d	95.4 cd	100.1 bc	56.0 d	309.7 d

Notes: Different letters in the same column are significantly different ($p \leq 0.05$ level). Cntrl = No treatment, T1= 14: 0: 0, T2 = 13.8: 18.8: 4.6, T3 = 15.4: 20: 4.8, T4 = 16.8: 21.5: 6.2, T5 = 20: 24: 9.7, T6 = 21.3: 25: 11.2, T7 = 24: 22: 11

NH_4-N content was higher than NO_3-N throughout the incubation. Subsequently, the cumulative NH_4-N content at the end of incubation period recorded higher values than NO_3-N content and generally increased from T1 to T6. No significant difference was observed in cumulative NH_4-N content between T7 and SRF T2, T3, T4 and T5, and also, in the cumulative NO_3-N between T7 and SRF T4, T5 and T6. The higher NH_4-N content compared to NO_3-N may be attributed to the acidity of soil which could have inhibited the growth and activities of nitrifying bacteria. The pH of soil during the incubation period showed some increase in the 12th and 16th week (Table 4.13),

particularly in SRF T2 to T6, though not significant among the treatments. The lowest pH value was 5.15 recorded in the 2nd week, while the highest value was 5.97 recorded in the 16th week. Nitrification (biological oxidation of NH_4^+ to NO_3^-) occurs in soil at pH values ranging from 5.5 to 10.0, optimal at pH value of about 8.5 and inhibited at pH less than 5 (Sahrawat, 2008).

Table 4.13. Soil pH during the incubation period

Treatment	Incubation period (weeks)				
	2	4	8	12	16
Cntrl	5.34 a	5.60 a	5.53 a	5.33 a	5.42 a
T1	5.31 a	5.54 a	5.43 a	5.66 b	5.71 b
T2	5.28 a	5.23 a	5.56 a	5.74 b	5.76 bc
T3	5.21 a	5.69 a	5.30 a	5.63 ab	5.67 b
T4	5.33 a	5.46 a	5.36 a	5.68 b	5.83 bc
T5	5.15 a	5.47 a	5.44 a	5.59 ab	5.71 bc
T6	5.28 a	5.80 a	5.34 a	5.47 ab	5.92 c
T7	5.24 a	5.65 a	5.23 a	5.52 ab	5.68 b

Notes: Different letters in the same column are significantly different ($p \leq 0.05$ level).
Legend: Cntrl = No treatment, T1= 14: 0: 0, T2 = 13.8: 18.8: 4.6, T3 = 15.4: 20: 4.8, T4 = 16.8: 21.5: 6.2, T5 = 20: 24: 9.7, T6 = 21.3: 25: 11.2, T7 = 24: 22: 11

Similar to the current study, Omar and Ismail (1999) observed higher content of NH_4-N than NO_3-N in soil treated with a mixture of urea and $CaCl_2$ or K_2SO_4. The population of bacteria and fungi decreased in both urea and $CaCl_2$ or K_2SO_4 treatments. Soil pH increased in urea amendment, but was decreased in inorganic salt amendments to values lower than that of the control. The toxic effect of urea and inorganic salts reduced when they were applied as a mixture. Giroto *et al.* (2017) observed higher pH values (6.3-7.9) after 42 days of aerobic incubation of soil amended with urea/HA and thermoplastic starch urea/HA compared to that of untreated soil, whereas the pH of soil amended with HA and SSP remained close to the pH of the control (≈ 5). The increase in pH in nano-composite amendments was attributed to high hydrolysis of urea in the soil with low CEC and low buffering capacity. The existence of more of mineral-N in the form of NH_4-N is beneficial because it is not susceptible to leaching losses.

Table 4.14 shows N mineralization potential (N_o), mineralization rate constant (K), coefficient of determination (R^2) and time taken for 50% of potentially mineralizable N $\left(t_{1/2}\right)$, to be

mineralized. T7 had the highest potentially mineralizable nitrogen (N_o) compared to all other treatments though not significantly different from T2, T3, T4, T5 and T6. The low N mineralization observed in SRF treatments may be attributed to slow release of nutrients in the initial stages of incubation. N_o related well to the observed cumulative mineral N as at 16th week of incubation. However, no significant difference was observed for cumulative mineral-N between T7, T2 and T5 at 16th week of incubation, implying that incorporation of soluble fertilizer into the polymer composite enhances mineralization of N. Thus, the significantly higher ($p \leq 0.05$) mineral-N values observed in T4 and T6, relative to T7 may be attributed to improved mineralization leading to release of higher amounts of mineral-N in the later stages of incubation.

Table 4.14. Nitrogen mineralization potential (N_o), mineralization rate constant (K), half-life ($t_{1/2}$) and cumulative mineral nitrogen

Treatment	N_o (ppm)	R^2	K (week^{-1})	$t_{1/2}$ (wks)	Observed cumulative Mineral-N at 16 wk (ppm)
Cntrl	425 a	0.903	0.052	13.3	405 a
T1	495 ab	0.917	0.051	13.6	531 b
T2	576 abc	0.829	0.059	11.7	608 cd
T3	536 abc	0.716	0.051	13.6	597 c
T4	539 abc	0.865	0.056	12.4	712 e
T5	619 bc	0.742	0.060	11.6	632 cd
T6	569 abc	0.910	0.053	13.1	692 e
T7	714 c	0.831	0.057	12.2	647 d

Legend: N_o = Nitrogen Mineralization Potential, K = Mineralization rate constant and $t_{1/2}$ = Time taken for 50 % of potentially mineralizable nitrogen to be mineralized. Cntrl = No treatment, T1= 14: 0: 0, T2 = 13.8: 18.8: 4.6, T3 = 15.4: 20: 4.8, T4 = 16.8: 21.5: 6.2, T5 = 20: 24: 9.7, T6 = 21.3: 25: 11.2, T7 = 24: 22: 11

The coefficient of determination, R^2 ranged from 0.742 to 0.917, indicating a good fit of the experimental data to the single order kinetics model. The mineralization rate constant ranged from 0.051 to 0.056 week^{-1} which resulted in half-life time ($t_{1/2}$) ranging from 11.6 to 13.6 weeks, suggesting that mineralization of most of the N would occur within the growing period of most annual crops of about 20 weeks. The $t_{1/2}$ values obtained in the experiment were similar to the average value of 12.8 weeks reported by Stanford and Smith (1972) on evaluating $t_{1/2}$ of 39

soil types in the USA. Since there was less variation in the $t_{1/2}$ among the treatments, the advantage of SRF over T7 could be attributed to the slow initial N mineralization, leading to release of significantly (p≤0.5) higher amounts in the later stages of incubation. The incubation experiment was however carried out at optimal conditions of moisture, temperature and aeration, for the growth and activity of soil microbes and hence N-mineralization rate might be lower/higher in the field than in the laboratory due to varying conditions that could affect the performance of micro-organisms.

4.2.5 Available phosphorous

Available P at different incubation times is shown in Table 4.15. The lowest P values were recorded in the 4th week, highest in the 8th week and remained nearly constant in the 12th and 16th week of incubation. The decline in P content between the 2nd and 4th week could be attributed to microbial immobilization and adsorption of soluble P into the soil. The increased P availability after 4 weeks in all SRF treatments may be attributed to its release through microbial solubilization of nano-HA and degradation of the copolymer. Insoluble phosphates such as apatite have been shown to be solubilized by native soil micro-organisms. Phosphate solubilizing bacteria (*Pseudomonous, Enterobactor, Anthrobactor*) and fungi (*Aspergillus, Penicillium*) present in the soil and the rhizosphere have been reported to hydrolyze insoluble P by secreting low molecular mass organic acids, to chelate mineral ions or lower the pH (Khan *et al.,* 2014; Alori *et al.,* 2017). Besides organic acids, mineral acids such as HCl, HNO_3 and H_2SO_4 produced by chemoautotrophs and H^{+} pump, for instance in *Penicillium rugulosum* has been reported to solubilize P (Khan *et al.,* 2014). Soil fungi such as mycorrhizae have been shown to be better solubilizers of P than bacteria as they traverse longer distances within the soil and also, produce and secrete more acids such as gluconic, citric, lactic, 2-ketogluconic, oxalic, tartaric and acetic acids (Alori *et al.,* 2017). Additionally, assimilation of NH_4^+ within microbial cells release H^{+} that solubilizes P without production of organic acids. Acidification of microbial cells and their surroundings release P through substitution of H^{+} for Ca^{2+} ions. The release of Ca^{2+} ions into the soil could be the reason for the observed increase in soil pH towards the end of the incubation period (Table 4.13). Ca^{2+} ions are bases and have the effect of neutralizing soil acidity (Mucheru-Muna *et al.,* 2014).

Table 4.15. Content of available P (ppm) at different incubation times (weeks)

Treatment	Incubation period (weeks)				
	2	4	8	12	16
Cntrl	21.0 a	10.4 a	25.3 a	23.9 a	26.1 a
T1	24.1 ab	12.9 abc	25.9 a	26.3 a	28.5 a
T2	24.1 ab	12.5 ab	39.3 b	37.8 b	41.1 b
T3	22.3 ab	13.6 abc	46.5 bc	46.6 c	46.2 bc
T4	26.1 ab	14.4 bc	55.2 cd	54.3 d	51.6 cd
T5	25.6 ab	16.3 cd	63.5 d	66.2 e	66.2 e
T6	27.4 ab	16.3 cd	76.3 e	80.4 f	76.6 f
T7	27.8 b	19.6 d	54.2 cd	53.7 d	54.3 d

Notes: Different letters in the same column are significantly different ($p \leq 0.05$ level).
Legend: Cntrl = No treatment, T1= 14: 0: 0, T2 = 13.8: 18.8: 4.6, T3 = 15.4: 20: 4.8, T4 = 16.8: 21.5: 6.2, T5 = 20: 24: 9.7, T6 = 21.3: 25: 11.2, T7 = 24: 22: 11

No significant difference was observed in the 2nd week between T7 and SRF T1 to T6, while in the 4th week T1 to T4 recorded significantly lower P content compared to T7. From the 8th to 16th week, highest P value was observed in T6 which was also significantly different from all the treatments. The observation could be attributed to solubilization of nano-HA and release of soluble P which was physically protected by the composite from adsorption into the soil in the initial stages of incubation.

Fertilizer composites were quantified to deliver a specific amount of N (50 mgNkg^{-1} of soil) into the soil regardless of NPK formulae, hence the amount of P in the amendments varied as: T2 = 68.1 mgkg^{-1}, T3 = 65 mgkg^{-1}, T4 = 64 mgkg^{-1}, T5 = 60 mgkg^{-1}, T6 = 58.5 mgkg^{-1} and T7 = 54.5 mgkg^{-1} (Table 3.1). The available P increased significantly ($p \leq 0.05$) from T2 to T6, an observation attributed to increased content of soluble P and decreased content of hydroxyapatite. No significant difference was observed between T7 and T4, except in the 4th week, a fact attributed to the balance between the amount of P in the treatment (T7 < T4) and availability in the soil. Nitisols are strong P sorping soils (WRB, 2015) and hence, lower content of P observed in T7, relative to T5 and T6 could be attributed to soil retention capacity which increases with contact time (Naima *et al.,* 2015; Giroto *et al.,* 2017). Slow microbial solubilization of nano-HA and encapsulation by the copolymer composite could have reduced available P time of contact in T5 and T6. No significance difference was observed between the control and T1 since they did

not contain P in the shipments. Due to varied content of P in the amendments (Table 3.1) it was not possible to ascertain the optimum amount to be incorporated into the fertilizer composite.

4.2.6 Exchangeable potassium

Exchangeable K at different incubation times is shown in Table 4.16. The K content showed less variation during the incubation period suggesting a short release time. The small particle size of SRF composite and high water solubility of the K_2SO_4 salt could have enabled faster diffusion of K into the soil. No significant difference ($p \geq 0.05$) was observed between CF T7 and SRF T1 to T6 in the first 4 weeks, but significant difference was observed between the same from the 8th to the 16th week. The control did not differ significantly from T1 throughout the incubation period and this was expected as K was not included in the formulation. The contents of K in the treatments were different (Table 3.1) and hence, just like in P, it was not possible to ascertain the optimum amount to be incorporated into the fertilizer composite.

Table 4.16. Concentrations of exchangeable K (Cmol kg^{-1}) at different incubation times (weeks)

Treatment	Incubation period (weeks)				
	2	4	8	12	16
Cntrl	1.63 a	1.70 a	1.87 a	1.58 a	1.70 a
T1	1.75 ab	1.85 ab	1.90 ab	1.85 a	1.80 a
T2	1.87 ab	1.83 ab	1.98 bc	2.05 b	2.08 b
T3	2.00 ab	1.92 ab	1.90 c	2.06 b	2.18 c
T4	2.05 ab	2.05 bc	1.95 d	2.00 c	1.95 d
T5	2.10 ab	2.10 bc	2.05 d	2.10 d	2.37 e
T6	2.17 ab	2.13 bc	2.25 e	2.17 e	2.27 e
T7	2.10 b	2.07 bc	2.30 d	2.37 c	2.28 d

Notes: Different letters in the same column are significantly different ($p \leq 0.05$ level).
Legend: Cntrl = No treatment, T1= 14: 0: 0, T2 = 13.8: 18.8: 4.6, T3 = 15.4: 20: 4.8, T4 = 16.8: 21.5: 6.2, T5 = 20: 24: 9.7, T6 = 21.3: 25: 11.2, T7 = 24: 22: 11

4.3 Evaluating the effects of formulated nano-NPK slow release fertilizer composite on the performance and yield of maize, kale and capsicum

The performance of the formulated slow release nano-NPK fertilizer [water hyacinth cellulose-graft-poly(acrylamide/nano-HA/soluble fertilizer)] composite relative to the conventional NPK fertilizer on the growth and yield of maize, kale and capsicum was evaluated in a greenhouse experiment.

4.3.1 Physico-chemical characteristics of soil at the onset of the greenhouse experiment

Physico-chemical characteristics of soil that was used in the greenhouse experiment are presented in Table 4.17. The soil is clay-loam according to soil textural triangle and slightly acidic due to moderate leaching of Ca and Mg ions ascribed to humid conditions in the study area. It had low electrical conductivity (ECe) indicating salt free soils and hence good permeability. ECe in sub-humid tropics has been reported to be < 4 dSm^{-1} (Lelago *et al*., 2016) due to sufficient rainfall flashing out base forming cations. Thus, absorption of water in such soil is not a problem to the plants due to low osmotic effect of dissolved salts. CEC was moderate hence satisfactory for crops provided adequate fertilizers are supplied (Landon, 1991). Low organic carbon and organic matter was attributed to low organic materials added to the soil as crop residues are completely removed at harvest. Total N was low, an observation attributed to low external inputs such as plant residues and manure, as well as losses of NO$_3$-N through leaching. The low available P may be attributed to intensive cropping system, mining, imbalanced use of fertilizer and fixation by the kaolinitic clay minerals inherent in this soil. Nitisols have high P fixation capacity (WRB, 2015). High exchangeable K was attributed to predominance of K rich minerals such as mica (Lelago *et al*., 2016), though its availability and depletion may influence crop yields (Kapkiyai *et al*., 1999). Exchangeable Ca and Mg were moderate and attributed to the nature of the parent material. These cations can be depleted through continuous cultivation and subsequent removal by crops and use of acidifying fertilizers (Chimdessa, 2016).

Table 4.17. Some salient physico-chemical characteristics of soil used in the greenhouse experiments

Parameter	Units	Value	Rating (Landon, 1991)
Sand	%	24	-
Silt	%	38	-
Clay	%	38	-
Textural class	-	Clay-loam	-
pH (soil: H_2O, 1: 2.5)	-	5.98	Moderate
Electrical conductivity (ECe)	dSm^{-1}	0.20	Salt free
Cation exchange capacity (CEC)	$Cmol(+) kg^{-1}$	14.5	Moderate
Organic carbon	%	1.40	very low
Organic matter (OM)	%	2.41	Low
Total N	%	0.04	very low
Available P (Melich I)	mg/kg	5.50	very low
Exchangeable K	$Cmol(+) kg^{-1}$	0.82	High
Exchangeable Ca	$Cmol(+) kg^{-1}$	5.10	Moderate
Exchangeable Mg	$Cmol(+) kg^{-1}$	1.65	Moderate

4.3.2 Growth and yield response of maize

Growth parameters and yield of maize are given in Table 4.18. The number of leaves, leaf area and girth increased from the 4th to the 8th week after planting, with some decrease observed in the 12th week in SRF treatments S1-S5 probably due to senescence (Figure 4.19a and b); a phenomenon attributable to heat stress, age related development and N limitation at plant's maturity stage. Senescence is an oxidative process involving degradation of cellular and sub-cellular structures and macro-molecules such as chlorophyll, and mobilization of degradation products such as thylakoid proteo-lipids to other parts of the plant, resulting in decline in photosynthetic rate and subsequent death (Woo *et al*., 2013). No significant difference in the number of leaves was observed in the 4th and 8th week amongst the treatments. In the 12th week, CF2 recorded the highest number of leaves, though insignificant compared to SRF of similar application rate, S4.

Table 4.18. Maize growth parameters and yield

Sample code	No. of Leaves			Total Leaf Area (cm^2)			Height (cm)			Girth (cm)			Grain Yield (Mg/ha)	Biomass (Mg/ha)
	4 w	8 w	12 w	4 w	8 w	12 w	4 w	8 w	12 w	4 w	8 w	12 w		
Cntrl	4.0^a	5.0^a	7.0^a	204^a	637^a	1082^a	14^a	33^a	77^a	2.1^a	2.3^a	2.6^a	0.00^a	2.08^a
S1	6.3^b	7.7^{ab}	7.0^a	775^b	2948^b	2217^b	23^{bc}	75^b	226^b	3.9^b	5.2^b	4.4^b	2.07^b	8.53^b
S2	5.6^{ab}	9.0^{bc}	7.6^{ab}	719^b	4416^c	2988^b	25^{bc}	94^c	254^{bc}	3.5^b	6.3^{bc}	5.3^{bc}	4.10^c	12.27^{bc}
S3	6.3^b	10.0^{bc}	8.3^{ab}	821^b	4650^c	3539^{cd}	21^{bc}	98^c	268^{bc}	3.8^b	6.9^c	6.0^{cd}	5.30^d	12.41^{bc}
S4	6.0^{ab}	9.3^{bc}	8.6^{abc}	809^b	4649^c	4141^{cd}	27^c	102^c	255^{bc}	3.6^b	7.0^c	6.0^{cd}	5.40^{de}	13.30^{bc}
S5	6.0^{ab}	9.7^{bc}	9.0^{abc}	734^b	4593^c	4361^d	24^{bc}	95^c	254^{bc}	3.8^b	7.3^c	6.6^d	6.80^e	14.73^c
CF1	6.5^b	9.5^{bc}	10.0^{bc}	529^{ab}	3892^{bc}	3930^{cd}	24^{bc}	95^c	255^{bc}	3.9^b	6.3^{bc}	5.3^{bc}	3.97^c	12.74^{bc}
CF2	6.0^b	11.0^c	11.0^c	709^b	4715^c	4543^{cd}	22^{bc}	92^c	254^{bc}	4.1^b	6.6^{bc}	6.2^{cd}	6.03^d	12.59^{bc}

Note: Different letters in the same column are significantly different ($P \leq 0.05$ level)

Legend: Cntrl = 0:0:0, S1 = 45:57:17, S2 = 89:114:33, S3 = 134:171:50, S4 = 178:288:66, S5 = 223:285:83, CF1 = 90:90:90, CF2 = 180:180:180

Plant height, leaf area and girth increased generally with fertilizer application rates, though not statistically significant amongst the amendments in the 4th week. In the 8th week, the control had significantly (p≤0.05) lower values compared to S1, S2, S3, S4, S5, CF1 and CF2, while in the 12th week, highest leaf area and girth was observed in CF2 and S5, respectively, though statistically insignificant compared to S3 and S4. Data on growth parameters indicated that the response of maize to SRF (e.g. S4) compared well to that of CF treatment of similar application rate, CF2.

Grain yield increased significantly (p≤0.05) with increased application rate from S1 to S3 where the highest value was recorded at S5 though not statistically different from S4. The control recorded zero yields due to inadequate amounts of N and P in the soil (Table 4.18), suggesting exclusive dependence of maize performance on supplied fertilizer sources. SRF treatments had insignificantly higher grain yields compared to CF treatments with similar application rates such as S2 and CF1. No statistical significance was observed in biomass yield between SRFs (S2, S3, S4, S5) and CFs (CF1 and CF2), implying that, the quantities of nutrients supplied at these rates were sufficient to produce similar biomass. The data thus indicated that SRF improved maize grain yield in the study; though not significant in the cases of growth parameters and dry matter yield (DMY). Hatfield and Parkin (2014) made similar observation when evaluating the effect of enhanced efficiency fertilizers (EEFs) relative to their non-EEF forms on grain yield and biomass of corn. They observed no significant effect of EEFs on the biomass or leaf area indices but, a higher grain yield was recorded in EEFs than non-EEF treatments, an observation related to increased leaf chlorophyll index that increased the ability of corn canopy to capture photosynthetic active radiation (PAR) which was then converted to yields. Unlike the current study, Cahill *et al*. (2010) did not observe increased grain yield in SRF treated corn and wheat, compared with aqueous urea ammonium nitrate treatment.

The growth and development of maize at early stages is shown in Figure 4.17. Maize growth was more vigorous in fertilizer amended soil compared to the control (Figure 4.17a). P deficiency was observed as at the 5th week in the control and S1 treated pots, manifesting itself as purplish color in the stalk (Figure 4.17b). This was also observed in CF1 and CF2 (Figure 4.17c) treated pots, but was less severe compared to the control and S1. The deficiency observed in S1 may be attributed to inadequate supply of P, whereas for CF1 and CF2, P fixation by clays may have

occurred due to direct and prolonged interaction of soluble P with soil particles. The nitisol in the Kenya highlands are dominated by kaolinitic clay (Karuku, 2011, Karuku *et al*., 2012) with high P sorption capacity (WRB, 2015). The kaolinite is a 1:1 type clay mineral with the chemical composition $Al_2Si_2O_5(OH)_4$ (Wei *et al*., 2014). The surface sites of kaolinite contain aluminol groups ($\equiv$Al-OH) located at the edges and the OH-terminated planes of the clay lamellae. This type of clay is often present in the soil alongside Fe oxides, where they tend to associate by forming oxide coatings on the surface of clay mineral (Karuku, 2011; Wei *et al*., 2014). The Al (and Fe) hydrous oxides have the capacity to adsorb large quantities of P added to the soil through; (i) ligand exchange where P anions replace the -OH groups at the surface of Al (and Fe) oxides and hydrous oxides, (ii) precipitation of Al and Fe phosphates at low pH (<4.5–5.0), or the formation of insoluble calcium phosphates at high pH (>6.0) (Haynes and Mokolobate, 2001).
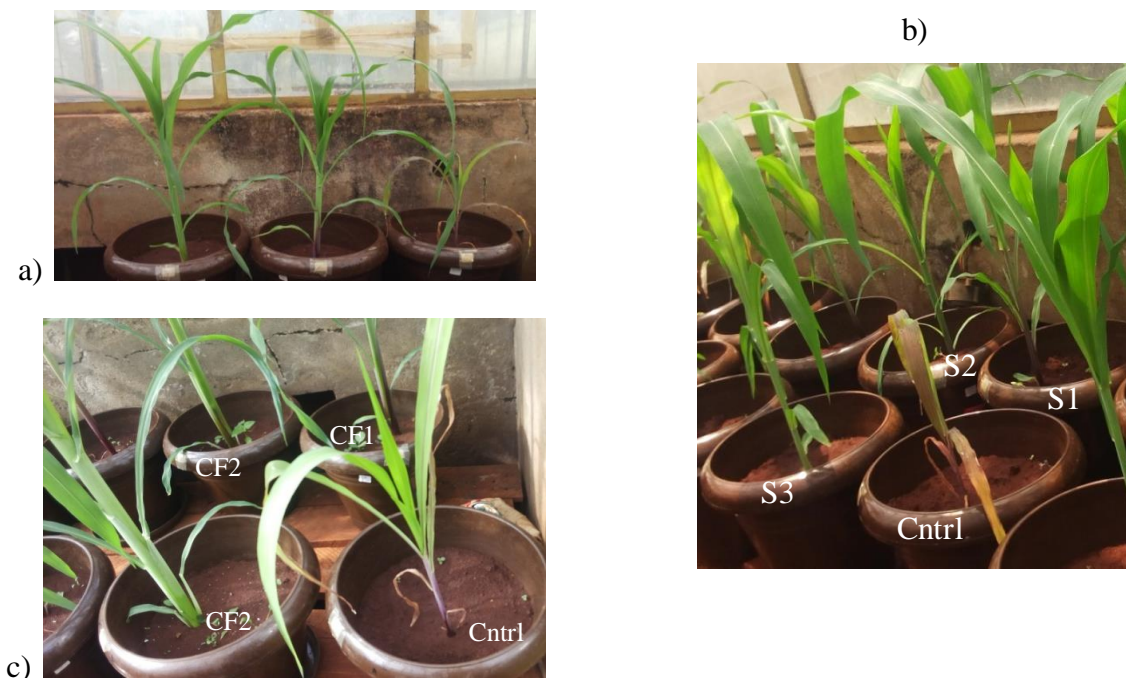
Figure 4.17. Photographs of maize after (a) 3 weeks in SRF treatments; from right to left is the control, S1, S2, (b) 5 weeks in SRF treatment , (c) 5 weeks in CF treatments

Legend: control = 0:0:0, S1 = 45:57:17, S2 = 89:114:33, S3 = 134:171:50, CF1 = 90:90:90, CF2 = 180:180:180

SRFs amendments with rates higher than S2 (i.e., S3, S4 and S5) did not manifest P deficiency, an observation attributed to sustained release of sufficient quantities of soluble P from DAP as well as solubilization of nano-HA through the action of microbes by secreting organic acids such as oxalic, formic, citric and acetic acids to chelate mineral ions or lower the pH (Alori *et al.,* 2017). Plant roots also modify the physico-chemical environment of the rhizosphere through exudation of organic acids and release of proton [H^+] due to the activity of proton pump ATPases located at the root plasmalemma (Houmani *et al*., 2015). The rhizosphere is the zone in soil where plant roots influence microbial activity (Karuku, 2019). Active interaction occurring among the plant roots, soil and microbes within this zone results in increased N mineralization which subsequently, increases the net plant N assimilation (Karuku, 2019).

Plant nutrition is thought to largely influence the release of H^+ and generally, addition of NH_4^+ leads to acidification of rhizosphere due to excess uptake of cations over anions (Wang and Tang, 2018). This acidity within the rhizosphere initiates the dissolution of nano-HA according to Scheme 4.11. The increased concentration of H^+, continuous removal of the reaction products *i.e.,* $H_2PO_4^-$ and Ca^{2+} through crops' uptake (Arcand and Schneider 2006) and neutralization of OH^- by the acidic soil, favor the equilibrium shift to the right, making it a self-propagating process. Microbial degradation of polyacrylamide to polyacrylic acid could also create an acidic environment within the copolymer thus enabling dissolution of P. This formulated Slow Release NPK is therefore a smart fertilizer since the chances of P fixation are reduced due to less duration of its interaction with soil particles.

$$Ca_{10}(PO_4)_6(OH)_2 + 12H^+ \rightleftharpoons 10Ca^{2+} + 6H_2PO_4^- + 2OH^-$$
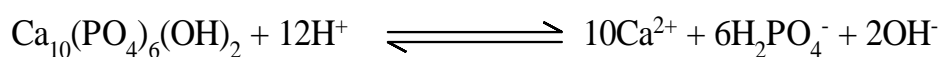
Scheme 4.11. Neutralization reaction expressing the dissolution of nano-HA

The images of maize at mid growing stages are shown in Figure 4.18. N deficiency manifested as yellowing of leaves in CF1 and CF2 is observed in the 8th week (Figure 4.18a). However, this manifestation was not observed in SRF treatments with similar or higher application rates in the same period (Figure 4.18b). This is an indication of low availability of N in CF treatments, attributed to microbial immobilization, leaching losses and/or binding by the soil due to early interaction with the soil particles. Conversely, the N in SRF was physically shielded, thus delaying its interaction with soil particles due to initial slow release of soluble N and later release

of mineralized amide-N. This is advantageous because N requirement by maize is low at establishment, moderate at development and reproductive phases, and declines at maturity. This release synchronizes with plant N requirement, reduces losses thus increasing NUE. Khan *et al.* (2015) in a similar study observed that delayed hydrolysis of urea in Super urea and Agrotain synchronizes N availability with crop's requirement.
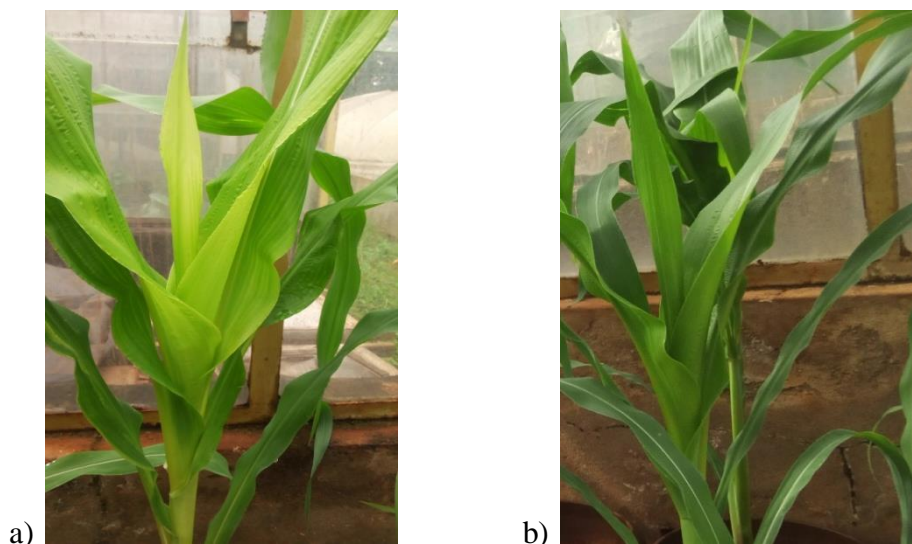
Figure 4.18. Photographs of maize after (a) 8weeks in CF treatment CF1, (b) 8 weeks in SRF treatments

Legend: CF1 = 90:90:90, S2 = 89:114:33

The images of maize at advanced growing stages are shown in Figure 4.19. Leaf senescence was observed in the 12th week both in SRF (Figure 4.19a) and CF treatments (Figure 4.19b), progressing from the lower leaf upwards and more pronounced at low application rates. Senescence enables the degradation of nutrients produced during the growing stages of the leaf and their redistribution to developing seeds and other plant parts (Woo *et al.,* 2013). Leaf senescence in the study occurred earlier than expected towards the end of maturity in maize. Possibly, the amount of N assimilated by plants during development stage may not have been sufficient to build up reserves for utilization in the reproduction stage. N being mobile both in soil and plants, tends to relocate from older to younger leaves, a phenomenon observed by Schildhauer *et al.* (2008) in *Hordeum vulgare* and *Arabidopsis thaliana* deprived of N, a situation later alleviated when these plants were re-supplied with N. Senescence has also been linked to growth conditions such as high temperatures (Hatfield and Prueger, 2015), that induce formation of reactive oxygen species (ROS) such as H_2O_2, $\dot{O}_2^-$ and $\dot{O}H^-$ radicals (De la Haba *et*

al., 2014). Low ROS levels trigger stress defense responses, though they may at times increase to toxic levels, injuring cellular membranes and other cellular components due to oxidative stress and eventually cell death (Wang *et al*., 2013). ROS play a key role in the degradation of lipids and proteins, inactivation of enzymes, pigment bleaching and disruption of DNA strands during senescence (Woo *et al*., 2013; De la Haba *et al*., 2014).

a)   b)
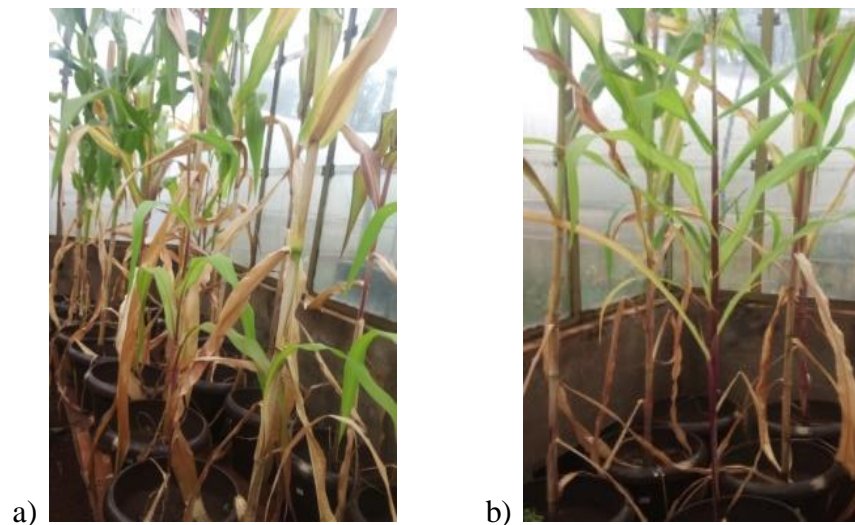
Figure 4.19. Photographs of maize after (a) 12 weeks in SRF treatments, (b) 12 weeks in CF treatments

4.3.3 Growth and yield response of capsicum

Growth parameters, DMY and fruit yields of capsicum are shown in Table 4.19. The highest number of leaves was recorded in S5, while control pots had the lowest. No significant difference in leaf number was observed in the 4th and 12th week between S1, S2, S3, S4, S5, CF1 and CF2, treated pots. In the 8th week, S5 had the highest number of leaves though not significantly different compared to S3 and S4 treated pots. The leaf area, plant height and girth all increased with fertilizer application rates but were not significantly different amongst the amendments (S1-S5, CF1 and CF2). The number of fruits, DMY and fruit yields obtained in treatment with the lowest application rate (S1) relative to the control was however significant (p≤0.05), implying that the amounts of fertilizer applied influenced the performance of capsicum. The highest number of fruits per plant was also recorded in S5 treated pots, though insignificant compared with S3, S4 and CF2 treated pots after mean separation.

Table 4.19. Mean growth parameters, biomass and fruit yield of capsicum

Sample Code	No. of Leaves			Leaf Area (cm^2)			Height (cm)			Girth (cm)			No. of Fruits/ plant	Fruit Yield (Mg/ha)	Biomass (Mg/ha)
	4 w	8 w	12 w	4 w	8w	12 w	4 w	8 w	12 w	4 w	8 w	12 w			
Cntrl	5.4^a	8.0^a	11.2^a	48^a	74 ^{a}	211^a	6.9^a	9.6^a	16.8^a	0.96^a	1.07^a	1.38^a	0.8^a	0.45^a	0.11a
S1	8.6^{ab}	18.3^{ab}	27.0^{ab}	174^{abc}	610^{ab}	1066^{ab}	13.0^a	35.6^b	52.3^b	1.43^{ab}	2.20^b	2.62^b	3.0^b	9.41^b	0.57^b
S2	8.7^{ab}	20.0^{ab}	32.0^{ab}	150^{abc}	640^{ab}	1357^{bc}	13.0^a	35.5^b	57.3^b	1.60^b	2.10^b	2.41^b	3.6^b	18.14^c	0.70^{bc}
S3	10.3^b	23.0^c	35.6^{ab}	225^{bc}	798^{ab}	1435^{bc}	13.3^a	34.6^b	52.7^b	1.40^{ab}	2.25^b	2.51^b	4.0^{bc}	21.53^d	0.83^{bcd}
S4	10.6^b	22.7^c	36.3^b	289^c	885^b	1679^{bc}	14.3^a	39.0^b	50.0^b	1.60^b	2.36^b	2.46^b	4.3^{bc}	23.37^{de}	1.06^{cde}
S5	11.3^b	24.3^c	46.0^b	300^c	986^b	2230^c	12.0^a	32.3^b	58.0^b	1.63^b	2.51^b	2.98^b	5.6^c	25.35^e	1.18^e
CF1	8.7^{ab}	18.5^{ab}	40.5^b	115^{ab}	852^b	1809^{bc}	10.5^a	36.0^b	56.7^b	1.47^{ab}	1.51^b	2.83^b	3.0^b	16.66^c	0.86^{bcd}
CF2	9.5^b	19.5^{ab}	36.0^b	140^{abc}	1042^b	1859^{bc}	10.0^a	35.5^b	52.5^b	1.63^b	2.75^b	3.14^b	4.0^{bc}	21.80^d	0.96^{cde}

Note: Different letters in the same column are significantly different ($P \leq 0.05$ level)

Legend: Cntrl = 0:0:0, S1 = 25:32:9, S2 = 50:64:18, S3 = 75:95:27, S4 = 100:127:36, S5 = 125:159:45, CF1 = 50:50:50, CF2 = 100:100:100

The fruit and DMY were found to increase significantly ($p \leq 0.05$) with increased amount of SRF from S1 to S4, above which significance between S4 and S5 treated pots ceased. Higher fruit and DMY were recorded in SRF S4, relative to CF of similar application rate CF2, though not significant. Reyes *et al.* (2008) made similar observation where capsicum in SRF performed better compared to $CaNO_3$ treatment due to improved availability of N. In a similar experiment, Stagnari and Pisante (2012) observed that urea and $Ca(NO_3)_2$ amendments recorded statistically higher capsicum DMY and fruit yields compared to SRF amendment due to delayed N release contrary to this study. However, the two workers observed that ryegrass DMY was higher in SRF due to later release of N after the removal of capsicum from the field. The authors did not observe any advantage of SRF over CF in capsicum nutrition. Conversely, the current study indicated an improved capsicum DM and fruit yield with SRF over CF amendments though there was insignificant variation in growth parameters.

SRF treated capsicum at the 8th and 14th week after transplanting is shown in Figure 4.20. No deficiency symptoms were observed all through the 4th to 12th week (Figure 20a). However, a pale-greenish color was noted in the 14th week in leaves of SRF treated pots receiving low application rates, S1 and S2 (Figure 4.20b). This suggested insufficient N supply during growth and hence the exhaustion of N reserves at reproduction stage. Plants with application rates higher than S2 (i.e., S3, S4, S5 and CF2) showed no N deficiency symptoms probably due to higher availability and uptake of N leading to high biomass and fruit yields. The leaf color change could also be attributed to senescence at the end of growing period (Woo *et al.*, 2013). Control pots with stunted crop growth at the end of the study period could be attributed to limited N and P as indicated in the initial soil chemical characterization (Table 4.17).

a)

b)

Figure 4.20. Photographs of (a) SRF treated capsicum after 8 weeks, (b) SRF treated capsicum after 14 weeks, from right to left is the control, S1, S2 and S3

Legend: Control = 0:0:0, S1 = 25:32:9, S2 = 50:64:18, S3 = 75:95:27

4.3.4 Growth and yield response of kale

The performance parameters and the yield of kale are shown in Table 4.20. The plant height generally increased with increased fertilizer application rates, though difference was statistically insignificant among the treatments. No significant difference was observed in the girth as well at the 4th week since transplanting among the fertilizer treatments S1 to S5, CF1 and CF2. The highest girth size was recorded in S5 treatment in the 8th week, though not significant compared to S2 to S4, CF1 and CF2. In the 12th week after planting, S5 treatment had significantly the highest girth (P≤0.05) compared to all other treatments. The difference in the cumulative number of leaves was however not significant among all the amendments (S1 to S5, CF1 and CF2). The cumulative leaf area increased significantly (P≤0.05) with increased fertilizer application rate, with S5 treatment having the highest value recorded. However, this S5 value was not significantly different compared to S3 and S4. Generally, the effect of SRF on growth parameters was not significantly different from that of CF treatments; hence, either can substitute the other, though SRF is more beneficial as it improves soil health and resilience over time.

The cumulative kale fresh weight also increased significantly (P≤0.05) with increased application rates with the highest value again recorded in S5. No significant difference in the cumulative fresh weight was observed between SRF and CF treated pots with similar application rates. However, significantly higher biomass (P≤0.05) was observed in SRF treatments S2 and S4, compared to CF treatments with similar rates; CF1 and CF2. This was attributed to higher P content in SRF shipments (S2 and S4) compared to CF (CF1 and CF2) (Table 3.2). This invariably increased the availability and assimilation of P, with a greater portion coming from nano-HA. Further, the copolymer fraction of SRF composite may have conditioned the soil through increased water holding capacity, providing favorable microbial conditions that enhanced N mineralization and assimilation by kale. In similar studies, Li *et al*. (2013) obtained insignificantly higher biomass yield in zeolite SRF compared to CF treatment with the same nutrient content and attributed it to enhanced NUE and reduced nutrient loss.

Table 4.20. Mean growth parameters and yield of Kale

Treatment	Height (cm)			Girth (cm)			Cum. No. of Leaves	Cum. Leaf Area(cm^2)	Cum. Fresh wt (Mg/ha)	Biomass (Mg/ha)
	4 w	8 w	12 w	4 w	8 w	12 w				
Cntrl	6.0^a	10.0^a	10.8^a	1.2^a	1.83^a	1.57^a	9.4^a	250^a	1.04^a	0.18^a
S1	10.3^a	17.3^a	20^{ab}	2.53^b	3.24^b	3.35^b	16.7^{ab}	1482^b	7.30^b	1.31^b
S2	9.70^a	18.6^{ab}	22^{ab}	3.31^b	4.61^{bc}	4.92^{bc}	19.6^b	2316^c	12.47^c	2.35^{cd}
S3	15.0^a	31.0^{ab}	35^{ab}	3.06^b	4.29^{bc}	4.82^{bc}	22.3^b	3531de	16.15^{bc}	3.05^d
S4	11.0^a	23.7^{ab}	25^{ab}	3.33^b	4.92^c	5.23^c	20.0^b	3912^{ef}	18.66^{cd}	2.96^d
S5	10.7^a	24.7^{ab}	35^{ab}	2.35^b	5.13^c	7.01^d	22.0^b	4596^e	22.40^d	3.06^d
CF1	6.6^a	14.0^{ab}	17^{ab}	2.91^b	4.40^{bc}	4.24^{bc}	19.0^{ab}	2705^c	14.67^{bc}	1.71^{bc}
CF2	7.5^a	15.5^{ab}	24^{ab}	3.31^b	4.40^{bc}	5.50^{bc}	22.5^b	2909^{cd}	18.23^{bc}	1.86^{bc}

Note: different letters in the same column are significantly different ($P\leq 0.05$ level)
Legend: Cntrl = 0:0:0, S1 = 31:40:11, S2 = 62:79:23, S3 = 93:119:34, S4 = 124:159:46, S5 = 155:199:57, CF1 = 63:63:63, CF2 = 126:126:126

Figure 4.21 shows kale growth in SRF amended soil at 7th and the 8th week after transplanting. The vegetative growth of kale was increased in SRF fertilizer amendment. The effect was more pronounced at higher application rate, but the control was stunted (Figure 4.21a). P deficiency was observed in kale (Figure 4.21b) plots that received the lowest application rate. The lower leaves had yellowish and purplish coloration, subsequently becoming necrotic, originating from the leaf tip (Figure 4.21c). These observations indicated deficiency of N, P and K, respectively.

a)

b)

c)

Figure 4.21. Photographs of (a) 7 weeks old SRF treated kale, from right to left is the control, S1 and S2, (b) 8 weeks old SRF treated kale, S1, (c) Kale leaf with signs of nutrient deficiency

Legend: Control = 0:0:0, S1 = 31:40:11, S2 = 62:79:23

4.3.5 Plant tissue and soil nutrient content at harvest of the crops

The plant tissue and soil nutrient contents post-harvest of the three crops are shown in Table 4.21. Significantly higher (≤0.05) N content in capsicum tissues was observed in both SRF and CF treatments with the highest rates, compared with the control. This implies that there was sufficient N amounts at these application rates. NPK content in plant tissues was not significantly different in most of the amendments (S1-S5, CF1 and CF2) relative to the control, an observation attributable to the utilization of these nutrients in biomass, fruits and grains production. N is an essential constituent of amino acids and proteins; P promotes root development and plays a key role in metabolic processes as the main constituent of energy compounds in nucleic acids and phospholipids, while K is involved in physiological processes such as osmoregulation, assimilate transport and enzyme activation (Wang *et al*., 2013; Yayeh *et al*., 2017). The nutrients may have been utilized by plants to improve their general health and yields.

Soil pH, total N and K content had no significant difference between the control and the amendments post-harvest. Significantly higher P (P≤0.05) relative to the control was observed in S4 and S5 where maize was harvested. This observation was attributable to residual nano-HA. For the soil where capsicum and kale were harvested, the highest P contents were also recorded in S5 whereas the lowest values were observed in the controls, though not significant. Nonetheless, the levels of total N and available P in S5, were too low to support plant's growth according to Landon (1991).

Table 4.21. Maize, capsicum and kale tissue, and soil nutrient contents after harvest

Treatment	Plant tissue nutrient content			Soil nutrient content			
	N (g/kg)	P (g/kg)	K (g/kg)	pH	% N	P (mg/kg)	K (Cmol/kg)
Maize							
Cntrl	2.6^a	0.75^a	7.91^{abc}	6.27^{ab}	0.09^a	8.67^a	0.83^a
S1	2.8^{ab}	0.77^a	7.49^a	6.40^{ab}	0.13^{ab}	13.26^{ab}	1.40^{ab}
S2	5.7^{ab}	0.82^a	7.76^{ab}	6.23^{ab}	0.13^{ab}	12.71^{ab}	1.30^{ab}
S3	2.7^{ab}	0.77^a	9.53^{bcd}	6.27^{ab}	0.15^a	10.57^{ab}	1.25^{ab}
S4	3.0^{ab}	0.74^a	10.46^{cd}	6.14^a	0.16^{ab}	15.63^b	1.20^{ab}
S5	4.3^{ab}	0.80^a	10.36^{cd}	6.18^a	0.11^{ab}	23.15^c	1.41^{ab}
CF1	2.0^a	0.77^a	9.73^{cd}	6.08^a	0.13^{ab}	10.64^{ab}	1.15^{ab}
CF2	2.7^{ab}	0.79^a	9.74^{cd}	6.40^{ab}	0.11^{ab}	12.85^{ab}	1.04^{ab}
Capsicum							
Cntrl	3.3^a	0.81^a	12.58^a	6.26^{abc}	0.11^{ab}	6.72^a	1.34^a
S1	4.9^{abc}	0.86^a	15.50^a	6.51^{bc}	0.15^{ab}	13.55^{ab}	1.55^{ab}
S2	5.1^{abc}	0.76^a	14.41^a	6.66^c	0.17^b	10.71^{ab}	1.53^{ab}
S3	5.4^{abc}	0.86^a	13.96^a	6.32^{abc}	0.11^{ab}	11.15^{ab}	1.50^{ab}
S4	3.7^{ab}	0.84^a	13.91^a	6.13^{ab}	0.10^{ab}	14.51^{ab}	1.72^{ab}
S5	6.0^{bc}	0.87^a	13.90^a	6.02^a	0.17^b	19.14^{ab}	1.46^{ab}
CF1	5.0^{abc}	0.85^a	12.30^a	6.16^{ab}	0.10^a	11.15^{ab}	1.47^{ab}
CF2	6.5^c	0.90^a	12.90^a	6.46^{abc}	0.13^{ab}	17.95^{ab}	1.95^{ab}
Kale							
Cntrl	19.2^{abc}	2.30^a	18.77^{ab}	6.19^a	0.10^a	8.07^a	0.83^a
S1	17.3^a	2.21^a	19.21^{ab}	6.45^a	0.11^a	10.43^a	1.39^{ab}
S2	18.5^{ab}	2.75^a	19.27^{ab}	6.08^a	0.13^a	11.70^a	1.27^{ab}
S3	16.9^a	2.82^a	17.61^a	6.45^a	0.13^a	11.70^a	1.33^{ab}
S4	22.3^{abc}	3.00^a	18.67^{ab}	6.58^a	0.11^a	10.93^a	1.40^{ab}
S5	24.5^{bc}	2.66^a	19.38^{ab}	5.97^a	0.11^a	14.63^a	1.21^{ab}
CF1	20.7^{abc}	2.59^a	18.71^{ab}	6.27^a	0.11^a	9.55^a	1.11^{ab}
CF2	25.5^c	2.50^a	22.30^{ab}	6.13^a	0.12^a	11.35^a	1.51^{ab}

Note: Different letters in the same column for each crop, are significantly different ($P \leq 0.05$ level)

Legend: Cntrl = 0:0:0, S1 = 25:32:9, S2 = 50:64:18, S3 = 75:95:27, S4 = 100:127:36, S5 = 125:159:45, CF1 = 50:50:50, CF2 = 100:100:100

Figure 4.22 shows the residual fertilizer composite after harvest of crops at the end of the experiment. The plant's roots penetrated into the fertilizer composite, suggestive of direct nutrient uptake. The copolymer composite material also lost its hydrophilicity, an indication of microbial degradation of hydrophilic amide group that causes swelling (Laftah and Hashim, 2014). Oven-dried sample transformed from initial strong material, enough to withstand adverse

conditions/ rough handling, to easily pulverizable material suggestive of degraded copolymer chains.

Figure 4.22. Fertilizer composite in the soil after crop harvest

The nutrient content of the composite material after harvesting the crops is shown in Table 4.22. No statistical significance was observed among the SRF treatments after harvesting the crops. N and P contents in SRF composite were not completely exhausted by crops, which may in the long term, improve the soil quality, an added advantage over CF which is susceptible to leaching and fixation. The residual composite could also enhance further degradation of the remaining polymeric portion because the microbes require sufficient amounts of N and P and a carbon (energy) source for maintenance and growth (Karuku and Mochoge, 2016).

Table 4.22. Nutrient content (n=9) of the composite material after crop harvest

Treatment	N(g/kg)	P(g/kg)	K(g/kg)
S1	89 a	6.48 a	1.07 a
S2	95 ab	6.99 ab	1.10 a
S3	100 ab	6.95 ab	1.08 a
S4	106 ab	7.55 ab	1.16 a
S5	100 ab	8.41 ab	1.12 a

Note: Different letters in the same column are significantly different ($P \leq 0.05$ level)
Legend: S1 = 25:32:9, S2 = 50:64:18, S3 = 75:95:27, S4 = 100:127:36, S5 = 125:159:45

4.3.6 Formulated fertilizer optimal application rate recommendations

The yield response regression curves for kale, capsicum and maize are given in Figure 4.23. The R^2 value ranged from 0.97 to 0.99 indicating good fit of the experimental data to the quadratic regression model. The crop yields at agronomic optimal application rates (AOAR) are presented in Table 4.23. The agronomic optimal application rates of SRF were found to be generally higher compared to CF treatments. This implies that the soil may take higher dosage of SRF and plants could utilize the nutrients efficiently, whereas in CF, the nutrients may be lost through leaching or denitrification processes, fixed by the soil particles or bound to soil organic matter into unavailable forms. Further, the associated injury or "burning" of the root hairs of young plants at high application rates is unlikely in SRF due to its slow release nature. The crop yields at agronomic optimal rates were also found to be higher in SRF compared to CF treatments, an indication of improved NUE. As observed in the regression curves (Figure 4.23), untreated soil recorded near zero crop yields due to insufficient supply of N and P (Table 4.17).

The determination of AOAR in similar studies are commonly carried out in the field experiments using conventional fertilizers with focus directed towards a single nutrient such as N. For example, Wang *et al*. (2014) determined optimal N rate for summer maize in 91 sites in a 2 year field experiment and reported increased grain yield with application rate to an optimum value above which it declined. Poffenbarger *et al*. (2017) also evaluated crop response to N rate and obtained agronomic optimum of N rates for a continuous maize system and for maize in rotation with soybean. The workers found a mean difference between the yields at agronomic optimal N rate and the yield at zero N rate of 6.6 Mgha^{-1} for maize following maize and 4.8 Mg ha^{-1} for maize following soybean.
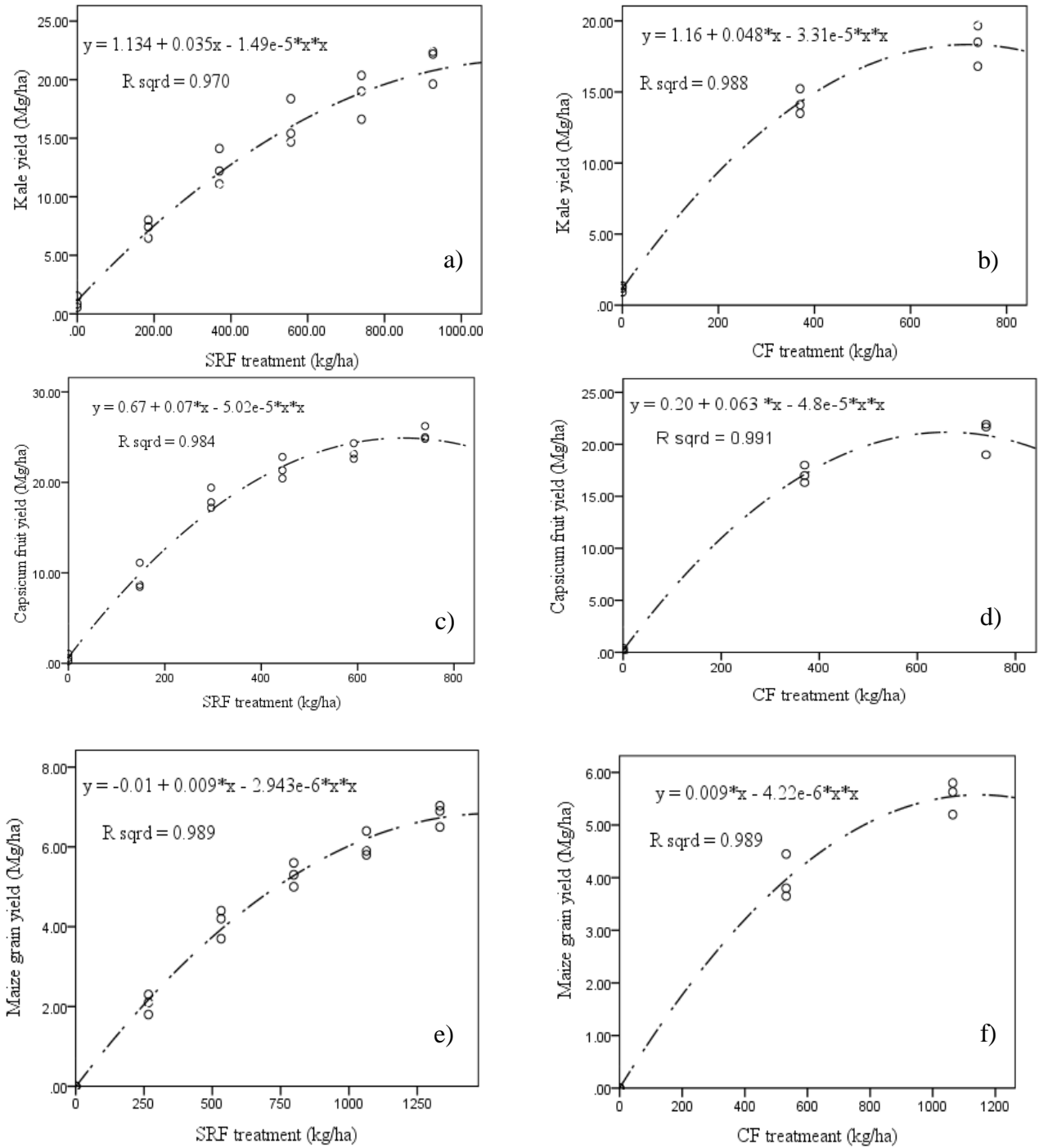
Figure 4.23. Yield response regression curves; (a) SRF and (b) CF treated kale; (c) SRF and (d) CF treated capsicum; (e) SRF and (f) CF treated maize

Table 4.23. The crop yields at agronomic optimal application rates

Treatment	Kale		Maize		Capsicum	
	AOAR (Mg ha^{-1})	Fresh wt. yield ($kg\,ha^{-1}$)	AOAR (Mg ha^{-1})	Grain yield ($kg\,ha^{-1}$)	AOAR (Mg ha^{-1})	Fruit yield ($kg\,ha^{-1}$)
SRF	1175	21.8	1529	7.0	697	25.1
CF	725	18.6	1066	5.4	656	20.9

Legend: SRF = slow release fertilizer, CF = commercial fertilizer, AOAR = agronomic optimal
application rates

CHAPTER FIVE

5.0 CONCLUSION AND RECOMMENDATIONS

5.1 CONCLUSION

Acrylic monomers were grafted onto swollen cellulose isolated from water hyacinth by radical polymerization to form cellulose-g-PAM-co-AA polymer hydrogel. FTIR spectra revealed purification of cellulose from water hyacinth and grafting of the monomer onto cellulose. High resolution TEM images displayed a micro-porous structure in acetone-dehydrated PHG. The X-ray diffraction (XRD) spectrum of cellulose grafted copolymer showed more of amorphous structure relative to that of cellulose.

The influence of reaction conditions on grafting was assessed using grafting parameters, namely, GCP, % GCE and water absorption. The optimized product was obtained at 6.5 % w/v AA content, 0.5 % w/v MBA content, 70 % degree of neutralization, a reaction volume of 40 mL, 2 % cellulose content and a temperature of 70 °C. The highest water absorbency in distilled water was 165 g/g, and hence the copolymer exhibited superabsorbent properties. The water absorbency of the copolymer was influenced by the presence, concentration and nature of ions present. The cellulose grafted copolymer revealed significant hydrolysis of amide-N in the microbial culture, displayed biodegradability and the potential to absorb and retain water in the soil. These are important features for potential agricultural applications such as formulation of slow release fertilizers and soil conditioning.

A slow release nano‐composite fertilizer was formulated and characterized. FTIR spectroscopy revealed existence of chemical interaction between nano-HA, urea molecules and the copolymer structure. Besides forming part of copolymeric network, nano-HA was physically entrapped within the copolymer as indicated by XRD spectra. Energy dispersive X-ray (EDX) spectra revealed the constituents of nano-composite to be mainly C, O, Ca and P, while N was not detected by this method.

Nano-composite fertilizer was assessed for release of nutrients using laboratory incubation experiment. The incubation experiment revealed low mineral-N content in the first 4 weeks and a

126

peak at the 12th week corresponding to the most active and nutrient demand stages of development and reproduction of most crops, hence proper synchronization of SRF. The highest mineral-N content was observed in conventional fertilizer (CF) in the first 4 weeks, whereas between the 8th and 16th week, both CF and SRF showed similar mineral-N content with some SRFs, for instance T4 and T6, releasing significantly higher amounts. Single first-order kinetics model predicted well N mineralization and the half-life time ($t_{1/2}$) showed less variation among the treatments. Low contents of P were observed in the first 4 weeks, increased to a maximum in the 8th week and remained constant thereafter. Availability of P increased significantly in SRF with increased content of soluble P and decreased content of nano-HA. The specific objective of the study was achieved and SRF T5 and T6 could provide synchronized release N and P, although the release of K was almost immediate. The SRF composite would be more suitable for use in annual crops and should be applied during planting, so as to match nutrient release with crop uptake.

The effect of formulated nano-composite fertilizer on the performance and yield of maize, kale and capsicum was evaluated in a greenhouse experiment. The performance parameters had no significant difference amongst the SRF and CF treatments with similar application rates. However, SRF showed increased maize grain yield, capsicum fruit numbers and DMY, and increased kale DMY, though none was significantly different from CF treatments. The crops depended mainly on the external supply of nutrients and deficiency was observed in all crops at low application rates. N deficiency was observed in CF treated maize (CF1 and CF2) as at the 8th week but not in SRFs of similar (S2) or higher rates. This probably suggests synchrony of N release in SRF with crop's requirement.

The agronomic optimal application rates of SRF were higher than CF, suggesting enhanced NUE even at higher SRF doses. S5 though the agronomic optimal rate for capsicum, was slightly higher than S5 for both maize and kale. CF2 was the optimal rate for the three test crops and hence, the study objective realized. SRF can therefore replace CF as it is more eco-friendly, easy to synchronize and thus promoting NUE and environmental protection.

5.2 RECOMMENDATIONS

i). Morphological characterization of cellulose grafted copolymer and SRF nano-composite should be studied further using scanning electron microscopy (SEM).

ii). The release of nutrients from nano-composite fertilizer was based on laboratory incubation experiment and evaluation should be done under field conditions before they can be recommended with confidence.

iii). The growth conditions in the greenhouse may influence the performance of maize as indicated by early leaf senescence and hence, further study should be carried out under field conditions to authenticate the data and observations made.

REFERENCES

Abate, T., Mugo, S., De Groote, H. and Regassa, M.W. (2015), Maize in Kenya: Chance for Getting Back to Former Glory? DT Maize (CIMMYT), **4**(3): 1-3.

Abbasi, M.K. and Khaliq, A. (2016), Nitrogen mineralization of a loam soil supplemented with organic–inorganic amendments under laboratory incubation, *Frontiers in Plant Science*, **7**: 1038.

Abbasi, M.K., Musa, N. and Manzoor, M. (2015), Mineralization of soluble P fertilizers and insoluble rock phosphate in response to phosphate-solubilizing bacteria and poultry manure and their effect on the growth and P utilization efficiency of chilli (*Capsicum annuum L.*), *Biogeosciences,* **12**: 4607–4619.

Abdel-Halim, E.S. (2014), Chemical modification of cellulose extracted from sugarcane bagasse: Preparation of hydroxyethyl cellulose, *Arabian Journal of Chemistry,* **7**: 362–371.

Ago, M., Endo, T. and Hirotsu, T. (2004), Crystalline transformation of native cellulose I to cellulose II polymorph by a ball milling method with specific water, *Cellulose*, **11**: 163-167.

Ahmed, E.M. (2015), Hydrogel: Preparation, characterization and applications: A review, *Journal of Advanced Research,* **6**(2): 105-121.

Alberto, C., Patrícia, A., Marisa, M., José C. and Fernando, S. (2010), Brazilian sedimentary zeolite use in agriculture, *19th World Congress of Soil Science, Soil Solutions for a Changing World,* Brisbane, Australia, pp 37-40.

Alori, E.T., Glick, B.R. and Babalola, O.O. (2017), Microbial phosphorus solubilization and its potential for use in sustainable agriculture, *Frontiers in Microbiology*, **8**: 971.

Åmand, L-E. and Tullin, C.J. (1999), The Theory Behind FTIR analysis, Department of Energy Conversion, Chalmers University of Technology, Sweden,

Ambjörnsson, H.A. (2013), Mercerization and enzymatic pretreatment of cellulose in dissolving pulps, *Dissertation,* Karlstad University, **22**, ISSN 1403-8099.

Anderson, J.M. and Ingram, J.S. (1993), Tropical Soil Biology and Fertility, A Handbook of Methods, 2nd Ed., *CAB International*, Wallingford, Oxon, UK. pp. 70.

Annicchiarico, G., Caternolo, G., Rossi, E. and Martiniello, P. (2011)**,** Effect of manure *vs.* fertilizer inputs on productivity of forage crop models, *International Journal of Environmental Research and Public Health,* **8:** 1893-1913.

Arcand, M.M. and Schneider, K.D. (2006), Plant- and microbial-based mechanisms to improve the agronomic effectiveness of phosphate rock: A review, *Anais da Academia Brasileira de Ciências,* **78**(4): 791-807.

Aswathy, U.S., Sukumaran, R.K., Devi, G.L., Rajasree, K.P., Singhania, R.R. and Pandey, A. (2010), Bio-ethanol from water hyacinth biomass: An evaluation of enzymatic saccharification strategy, *Bioresource Technology,* **101**(3): 925-930.

Award, Y.M., Blagodatskaya, E., Ok, Y.S. and Kuzyakov, Y. (2012), Effect of polyacrylamide, biopolymer and biochar on decomposition of soil organic matter and plant residues as determined by ^{14}C and enzyme activities, *European Journal of Soil Biology*, **48:** 1-10.

Bachmaier, M. and Gandorfer, M. (2012), Estimating uncertainty of economically optimum N fertilizer rates, *International Journal of Agronomy*, **2012:** Article ID 580294, 10 pgs.

Bai, H., Wang, X., Zhou, Y. and Zhang, L. (2012), Preparation and characterization of poly(vinylidene fluoride) composite membranes blended with nano-crystalline cellulose, *Progress in Natural Science: Materials International,* **22**(3): 250-257.

Bandyopadhyay-Ghosh, S., Ghosh, S.B. and Sain, M. (2015), The use of biobased nanofibres in composites, *Biofiber Reinforcements in Composite Materials, Elsevier,* pp. 571-647

Basak, B.B. and Biswas, D.R. (2009), Influence of potassium solubilizing microorganism (*Bacillus mucilaginosus*) and waste mica on potassium uptake dynamics by Sudan grass (*Sorghum vulgare Pers*.) grown under two alfisols, *Plant and Soil,* **317**: 235–255.

Bélanger, G., Walsh, J.R., Richards, J.E., Milburn, P.H. and Ziadi, N. (2000), Comparison of three statistical models describing potato yield response to nitrogen fertilizer, *Agronomy Journal*, **92**: 902–908.

Bologna, L.S., Andrawes, F.F. and Barvenik, F.W. (1999), Analysis of residual acrylamide in field crops, *Journal of Chromatographic Science,* **37**: 240-244.

Bremner, J.M. (1996), Total nitrogen, in: Sparks, D.L. (Eds), Methods of Soil Analysis, Part 3: Chemical Methods, *Soil Science Society of America and American Society of Agronomy,* Madison, Wisconsin, pp. 1085-1086.

Brundavanam, R.K., Poinern, G.J. and Fawcett, D. (2013), Modelling the crystal structure of a 30 nm sized particle based hydroxyapatite powder synthesised under the influence of ultrasound irradiation from X-ray powder diffraction data, *American Journal of Materials Science*, **3**(4): 84-90.

Bunaciu, A.A., Udriştioiu, E.G. and Aboul-Enein, H.Y. (2015), X-Ray diffraction: instrumentation and applications, *Critical Reviews in Analytical Chemistry,* **45**(4): 289-299.

Bundela, H. and Bajpai, A.K. (2008), Designing of hydroxyapatite-gelatin based porous matrix as bone substitute: Correlation with biocompatibility aspects, *Polymer Letters,* **2**(3): 201–213.

Cahill, S., Osmond, D., Weisz, R. and Heiniger, R. (2010), Evaluation of alternative nitrogen fertilizers for corn and winter wheat production, *Agronomy Journal,* **102**(4): 1226–1236.

Carlmark, A., Larsson, E. and Malmstrom, E. (2012), Grafting of cellulose by ring-opening polymerization: A review, *European Polymer Journal*, **48**: 1646–1659.

Chai, Q., Jiao, Y. and Yu, X. (2017), Hydrogels for biomedical applications: Their characteristics and the mechanisms behind them: A review, *Gels,* **3**(6): 1-15.

Chao, C., Zideng, G., Xiaoyun, Q. and Shuwen, H. (2013), Enhancement of the controlled-release properties of chitosan membranes by cross-linking with suberoyl chloride, *Molecules,* **18**: 7239-7252.

Charoenpanich, J. (2013). Removal of acrylamide by microorganisms, in: Yogesh, P. and Prakash R. (Eds), Applied bioremediation - active and passive approaches, *Intech Open Science.*

Chen, C., Gao, Z., Qiu, X. and Hu, S. (2013), Enhancement of the controlled-release properties of chitosan membranes by cross-linking with suberoyl chloride, *Molecules,* **18**: 7239-7252.

Chen, G., Varanasi, P., Li, C., Liu, H., Melnichenko, Y.B., Simmons, B.A. Kent, M.S. and Singh, S. (2011), Transition of cellulose crystalline structure and surface morphology of biomass as a function of ionic liquid pretreatment and its relation to enzymatic hydrolysis, *Biomacromolecules*, **12**(4): 933-941.

Chen, J.F. (1997), Adsorption and diffusion of ammonium in soils, in; Zhu Z., Wen, Q., Freney, J.R. (Eds), Nitrogen in Soils of China, *Development in Plant Soil Sciences,* **74.** *Springer*, Dordrecht, The Netherlands.

Chen, W., Feng, Y., Ruimin, F. and Yun, X. (2015), Isolation of Polyacrylamide-degrading Bacteria from Dewatered Sludge, *International Journal Environmental Research and Public Health,* **12**: 4214-4230.

Chimdessa, D., (2016), Soils characteristics in maize based farming system of Western Oromia, Ethiopia, *Journal of Energy and Natural Resources*, **5**(4): 37-46.

Chiu, Y.C, Larson, J.C., Isom, A.J. and Brey, E.M. (2010), Generation of porous poly(ethylene glycol) hydrogels by salt leaching, *Tissue Engineering, Part C; Methods,* **16**(5): 905-12.

Cisneros-Pineda, O.G., Kao, W.H., Loría-Bastarrachea, M.I., Veranes-Pantoja, Y. Cauich-Rodríguez, J.V. and Cervantes-Uc, J.M. (2014), Towards optimization of the silanization process of hydroxyapatite for its use in bone cement formulations, *Materials Science and Engineering,* C, **40**: 157–163.

Costescu, A., Pasuk, I., Ungureanu, F., Dinischiotu, A., Costache, M., Huneau, F., Galaup, S., Le Coustumer, P. and Predoi, D. (2010), Physico-chemical properties of nano-sized hexagonal hydroxyapatite powder synthesized by sol-gel, *Digest Journal of Nanomaterials and Biostructures,* **5**(4): 989-1000.

Davidson, D., Verma, M.S. and Gu, F.X. (2013), Controlled root targeted delivery of fertilizer using an ionically cross-linked carboxymethyl cellulose hydrogel matrix, *SpringerPlus,* **2**: 318.

De la Haba, P., De la Mata, L., Molina, E. and Agüera, E. (2014), High temperature promotes early senescence in primary leaves of sunflower (*Helianthus annuus L.*) plants, *Canadian Journal of Plant Science*, **94**: 659669.

Deenik, J.L. and Yost, R.S. (2008), Nitrogen mineralization potential and nutrient availability from five organic materials in an atoll soil from the Marshall Islands, *Soil Science,* **173**(1): 54-68.

Demitri, C., Scalera, F., Madaghiele, M., Sannino, A. and Maffezzoli, A. (2013), Potential of cellulose-based superabsorbent hydrogels as water reservoir in agriculture, *International Journal of Polymer Science,* **2013**: Article ID 435073, 6 pgs.

DeRosa, C., Monreal, C., Schnitzer, M., Walsh, R. and Sultan, Y. (2010), Nanotechnology in fertilizers, *Nature Nanotechnology,* **5**(2): 91-94.

Dong, W., Zhang, X., Wang, H., Dai, X., Sun, X., Qiu, W. and Yang, F. (2012), Effect of different fertilizer application on the soil fertility of paddy soils, in red soil region of Southern China, *PLoS ONE,* **7**(9): e44504.

Doyle, W.M. (1992), Principles and applications of Fourier transform infrared (FTIR) process analysis; Technical Note AN–906 Rev. C; *Hellma Axiom*, Inc.: Plainview, NY, USA, pp. 1–24.

Druilhe, Z., and Barreiro-Hurlé, J. (2012), Fertilizer subsidies in sub-Saharan Africa, ESA Work, Paper No. 12-04, Rome, Food and Agricultural Organization (FAO).

Edgar, O.N., Gweyi-Onyango, J.P. and Korir, N.K. (2017), Plant Row Spacing Effect on Growth and Yield of Green Pepper *(Capsicum annuum L.)* in Western Kenya, *Archives of Current Research International,* **7**(3): 1-9.

Ekebafe, L.O., Ogbeifun, D.E. and Okieimen, F.E. (2011), Polymer Applications in Agriculture, *Biokemistri,* **23**(2): 81-89.

Eritsyan, M.L., Gyurdzhyan, L.A., Melkonyan, L.T. and Akopyan, G.V. (2006), Copolymers of acrylic acid with urea, *Russian Journal of Applied Chemistry,* **79**(10): 1666-1668.

Fan and Xiaolin, (2009), Research and development of controlled-release fertilizers as high efficient nutrient management materials in China**,** *The Proceedings of International Plant Nutrition Colloquium XVI,* University of California Davis.

Fernandes, B.S., Pinto, J.C, Cabral-Albuquerque, E.M. and Fialho, R.L. (2015), Free-radical polymerization of urea, acrylic acid and glycerol in aqueous solutions, *Polymer Engineering and Science,* **55**(6):1219-1229.

Fertilizer Manual, 3rd Edition (1998), United Nations Industrial Development Organization (UNIDO) and International Fertilizer Development Center (IFDC), *Kluwer Academic Publishers,* Dordrecht, The Netherlands.

Gachene, C.K.K. (1989), Soils of the erosion research farm, Kabete Campus, *Department of Agricultural Engineering,* University of Nairobi.

Gao, J., Huang, B., Lei, J. and Zheng, Z. (2010), Photografting of methacrylic acid onto hydroxyapatite particles surfaces, *Journal of Applied Polymer Science*, **115**: 2156–2161.

Gaskell, M. and Smith, R., (2007), Nitrogen sources for organic vegetable crops, *Hortechnology,* **17**(4): 431–441.

Gayathri, B., Muthukumarasamy, N., Velauthapillai, D., Santhosh, S.B. and Asokan, V. (2018), Magnesium incorporated hydroxyapatite nanoparticles: Preparation, characterization, antibacterial and larvicidal activity, *Arabian Journal of Chemistry,* **11**: 645-654.

Ge, S., Zhu, Z. and Jiang, Y. (2018), Long-term impact of fertilization on soil pH and fertility in an apple production system, *Journal of Soil Science and Plant Nutrition,* **18**(1): 282-293.

Girisuta, B., Danon, B., Manurung, R., Janssen, L. and Heeres, H. (2008), Experimental and kinetic modelling studies on the acid-catalysed hydrolysis of the water hyacinth plant to levulinic acid, *Bioresource Technology,* **99**: 8367–8375.

Giroto, A.S., Guimarães, G.F., Foschini, M. and Ribeiro, C. (2017), Role of slow-release nanocomposite fertilizers on nitrogen and phosphate availability in soil, *Scientific Reports*, **7**: 46032.

Glendon, W.G. and Doni, O.R. (2002), Particle-size analysis, in: Dane J.H. and Topp G.C. (Eds), Methods of soil analysis. Part 4: Physical methods, *Soil Science Society of America, Inc.,* Madison, WI. pp. 255–293.

Goetz, L.A. (2012), Preparation and analysis of crosslinked lignocellulosic fibres and cellulose nanowhiskers with poly(methyl-vinyl ether-co-maleic acid)–polyethylene glycol to create novel water absorbing materials, *Doctorate Dissertation*, *Georgia Institute of Technology.*

González-Henríquez, C.M., Pizarro, G.C., Sarabia-Vallejos, M., Terraza, C.A**.** and López-Cabaña, Z.E. (2014), In situ-preparation and characterization of silver-HEMA/PEGDA hydrogel matrix nanocomposites: Silver inclusion studies into hydrogel matrix, *Arabian Journal of Chemistry,* in press, http://dx.doi.org/10.1016/j.arabjc.2014.11.012, Available 13th Sept., 2019.

Good, A.G., and Beatty, P.H. (2011), Fertilizing nature: A tragedy of excess in the commons, *PLoS Biology*, **9**(8): e1001124.

Guan, H., Li, J., Zhang, B., Yu, X. (2017), Synthesis, properties, and humidity resistance enhancement of biodegradable cellulose-containing superabsorbent, *Journal of Polymers*, **2017**: Article ID 3134681, 8 pgs.

Guertal, E.A. (2009), Slow-release nitrogen fertilizers in vegetable production: A review, *HortTechnology,* **19**(1): 16-19.

Guezennec, A.G., Michael, C., Bru, K., Touze, S., Desroche, N., Mnif, I. and Motelica-Heino, M. (2015), Transfer and degradation of polyacrylamide-based flocculants in hydrosystems: A review, *Environmental Science and Pollution Research,* **22**(9): 6390-6406.

Guo, M., Liu, M., Hu, Z., Zang, F. and Wu, L. (2005), Preparation and properties of a slow release NP compound fertilizer with superabsorbent and moisture preservation, *Journal of Applied Polymer Science,* **96**: 2132-2138.

Gupta, N.V. and Shivankumar, H.G. (2012), Investigation of swelling behaviour and mechanical properties of a pH sensitive superporous hydrogel composite, *Iranian Journal of Pharmaceutical Research,* **11**(2): 481-493.

Gupta, P.K., Uniyal, V. and Naithani, S. (2013), Polymorphic transformation of cellulose I to cellulose II by alkali pretreatment and urea as an additive, *Carbohydrate Polymers*, **94**: 843–849.

Gürdağ, G. and Sarmad, S. (2013), Cellulose graft copolymers: Synthesis, properties and applications, in: Kalia, S., Sabaa, M. (Eds), Polysaccharide based graft copolymers, *Springer,* Berlin, Heidelberg, pp. 15-57.

Hacker, M.C., Krieghoff, J. and Mikos, A.G. (2019), Synthetic Polymers, in: *Principles of Regenerative Medicine (3rd Ed.)*, *Elsevier*, Amsterdam, The Netherlands, pp. 559-590.

Hall, A. (1993), Application of the indophenol blue method to the determination of ammonium in silicate rocks and minerals, *Applied Geochemistry,* **8**: 101-105.

Hanqin, T., Chaoqun, L., Jerry, M., Wei R., Yao, H., Xiaofeng, X., Liu, M., Zhang, C., Chen, G. and Pan, S. (2012), Food benefit and climate warming potential of nitrogen fertilizer uses in China, *Environmental Research Letters,* **7**: 044020.

Hartinee, A., Hanafi, M.M., Shukor, J. and Mahmud, T.M. (2010), Model comparisons for assessment of NPK requirement of upland rice for maximum yield, *Malaysian Journal of Soil Science,* **14**: 15-25.

Hatfield, J.L. and Parkin, T.B. (2014), Enhanced efficiency fertilizers: Effect on agronomic performance of corn in Iowa, *Agronomy Journal,* **106**: 771-780.

Hatfield, J.L. and Prueger, J.H. (2015), Temperature extremes: Effect on plant growth and development temperature extremes: Effect on plant growth and development, *Weather and Climate Extremes,* **10**: 4-10.

Haynes, R.J. and Mokolobate, M.S. (2001), Amelioration of Al toxicity and P deficiency in acid soils by additions of organic residues: A critical review of the phenomenon and the mechanisms involved, *Nutrient Cycling in Agroecosystems*, **59**: 47–63.

Hosseeinzadeh, H. and Sadeghi, M. (2012), Preparation and swelling behaviour of carboxymethylcellulose-g-poly(sodium acrylate)/kaolin super absorbent hydrogel composites, *Asian Journal of Chemistry,* **24**: 85-88.

Houmani, H., Rabhi, M., Abdelly, C. and Debez, A. (2015), Implication of rhizosphere acidification in nutrient uptake by plants: Cases of potassium (K), phosphorous (P) and iron (Fe), in: Hakeem, K.R. (Ed.), Crop production and global environmental issues, *Springer, Cham,* pp. 103-111.

Inaba, K., Kobayashi, S., Uehara, K., Okada, A., Reddy, S.L. and Endo, T. (2013), High resolution X-ray diffraction analyses of (La,Sr)MnO3/ZnO/Sapphire(0001) double heteroepitaxial films. *Advances in Materials Physics and Chemistry*, **3**(1): Article ID 30348, 18 pgs.

Istirokhatun, T., Rokhati, N., Rachmawaty, R., Meriyani, M., Priyanto, S. and Susanto, H. (2015), Cellulose isolation from tropical water hyacinth for membrane preparation, *Procedia Enviromental Sciences,* **23**: 274-281.

Iyyappan, E. and Wilson, P. (2013), Synthesis of nanoscale hydroxyapatite particles using Triton X-100 as an organic modifier, *Ceramics International,* **39**: 771–777.

Jaetzold, R., Schmidt, H., Hornetz, B. and Shisanya, C. (2006), Farm management handbook of Kenya Vol. II., Natural conditions and farm management information (2nd Ed.) Part A: West Kenya, Subpart A1: Western Province, *Ministry of Agriculture Kenya in Cooperation with the German Agency for Technical Cooperation (GTZ)*, Nairobi, Kenya.

Jafari, N. (2010), Ecological and socio-economic utilization of water hyacinth, *Eichhornia crassipes*, *Journal of Applied Science and Environmental Management,* **14**(2): 43-49.

Jaggard, K.W., Qi, A. and Ober, E.S. (2010), Possible changes to arable crop yields by 2050: A review, *Philosophical Transactions of the Royal Society*, B, **365**: 2835–2851.

Jayachandran, V. and Kwon, S. (2010), Effect of temperature on isolation and characterization of hydroxyapatite from Tuna (*Thunnus obesus*) bone, *Material*s, **3**: 4761-4772.

Jeng, A. and Vagstad, N. (2009), Potential nitrogen and phosphorous leaching from soils fertilized with meat and bone meal, *Acta Agriculturae Scandinavica, Section B: Soil and Plant Science,* **59**(3): 238-245.

Joutey, N.T., Bahafid, W., Sayel, H. and Ghachtouli, N.E. (2013), Biodegradation: Involved microorganisms and genetically engineered microorganisms, in: Chamy R. and Rosenkranz, F. (Eds), Biodegradation - Life of Science, *IntechOpen,* pp 289-320.

Kabiri, K. and Zohuriaan-Mehr, M.J. (2004), Porous superabsorbent hydrogel composites: synthesis, morphology and swelling rate, *Macromolecular Materials and Engineering,* **289**(7): 653-661.

Kaco, H., Zakaria, S., Razali, N.F., Chia, C.H., Zhang, L. and Sani, S.M. (2014), Properties of cellulose hydrogel from kenaf core prepared via pre-cooled dissolving method, *Sains Malaysiana,* **43**(8): 1221-1229.

Kapkiyai, J.J., Karanja, N.K., Qureshi, J.N., Smithson, P.C. and Woomer, P.L. (1999), Soil organic matter and nutrient dynamics in a Kenyan nitisol under long-term fertilizer and organic input management, *Soil Biology and Biochemistry,* **31**: 1773-1782.

Karuku, G.N. (1989), Nitrogen forms in soils, and effect of lime, nitrogen and phosphorus salts on nitrogen mineralization, *MSc. Thesis,* University of Nairobi.

Karuku, G.N. (2011), Effect of cover crop residue management practices on soil moisture conservation and validation of CROPWAT model for predicting water use requirements for tomato crop in Kabete, Kenya, *PhD Thesis,* University of Nairobi.

Karuku, G.N. (2019), Effect of lime, N and P salts on nitrogen mineralization, nitrification process and priming effect in three soil types, andosols, luvisols and ferralsols, *Journal Agriculture and Sustainability*, **12**(1): 74-106.

Karuku, G.N. and Mochoge, B.O. (2016), Nitrogen forms in three Kenyan soils nitisols, luvisols and ferralsols, *International Journal for Innovation Education and Research,* **4**(10): 17-30.

Karuku, G.N. and Mochoge, B.O. (2018), Nitrogen mineralization potential (N$_o$) in three Kenyan soils, nitisols, ferralsols and luvisols, *Journal of Agricultural Science,* **10**(4): 60-78.

Karuku, G.N., Gachene, C.K., Karanja, N., Cornelis W. and Verplancke, H. (2014a), Use of CROPWAT model to predict water use in irrigated tomato (*Lycopersicon esculentum*) production at Kabete, Kenya, *East African Agriculture and Forestry Journal*, **80**(3): 175-183.

Karuku, G.N., Gachene, C.K., Karanja, N., Cornelis, W. and Verplancke, H. (2014b), Effect of different cover crop residue management practices on soil moisture content under a tomato crop (*Lycopersicon esculentum*), *Tropical Subtroptropical Agroecosystems,* **17**(3): 509 -523.

Karuku, G.N., Gachene, C.K., Karanja, N., Cornelis, W., Verplancke, H. and Kirochi, G. (2012), Soil hydraulic properties of a nitisol in Kabete, Kenya, *Tropical and Subtropical Agroecosystems,* **15**: 595-609.

Karuku, G.N., Kimenju, J.W. and Verplancke, H. (2017), Farmers' perspectives on factors limiting tomato production and yields in Kabete, Kiambu County, Kenya, *East African Agriculture and Forestry Journal,* **82**(1): 70-89.

Kay-Shoemake, J.L., Wartwood, M., Lentz, R. and Sojka, R. (1998a), Polyacrylamide as an organic nitrogen source for soil micro-organisms with potential effects on inorganic soil nitrogen in agricultural soil, *Soil Biology and Biochemistry,* **30**(8-9): 1045-1052.

Kay-Shoemake, J.L., Wartwood, M., Sojka, R. and Lentz, R. (1998b), Polyacrylamide as a Substrate for Microbial Amidase Culture and Soil, *Soil Biology and Biochemistry*, **30**(13): 1647-1654.

Kenya Economic Report (2017), Sustaining Kenya's economic development by deepening and expanding economic integration in the region, *Kenya Institute for Public Policy Research and Analysis (KIPPRA)*, Nairobi, Kenya.

Khan, A.Z., Afzal, M., Muhammad, A., Akbar, H., Khalil, S.K., Wahab, S. and Noor-ul-Amin, (2015), Influence of slow release urea fertilizer on growth, yield and N uptake on maize under calcareous soil conditions, *Pure and Applied Biology,* **4**(1): 70-79.

Khan, M.S., Zaidi, A. and Ahmad, E. (2014), Mechanism of phosphate solubilization and physiological functions of phosphate-solubilizing microorganisms, in: Khan, M.S., Zaidi, A., Musarrat, J. (Eds), Phosphate solubilizing microorganisms, *Springer, Cham.*

Kimetu, J.M., Mugendi, D.N., Bationo, A., Palm, C.A., Mutuo, P.K., Kihara, J., Nandwa, S. and Giller, K. (2007), Partial balance of nitrogen in a maize cropping system in humic nitisol of Central Kenya, in: Bationo A., Waswa B., Kihara J., Kimetu J. (Eds), Advances in Integrated Soil Fertility Management in sub-Saharan Africa: Challenges and Opportunities, *Springer,* Dordrecht, The Netherlands, pp. 521–530

Kisinyo, P.O., Othieno, C.O., Gudu, S.O., Okalebo, J.R., Opala, P.A., Ng'etich W.K., Nyambati, R.O., Ouma, E.O., Agalo, J.J., Kebeney, S.J., Too, E.J., Kisinyo, J.A. and Opile, W.R. (2014), Immediate and residual effects of lime and phosphorus fertilizer on soil acidity and maize production in western Kenya, *Experimental Agriculture,* **50**(1): 128–143.

Kivaisi, A. and Mtila, M. (1997), Production of biogas from water hyacinth (*Eichhornia crassipes*) (Mart) (Solms) in a two-stage bioreactor, *World Journal of Microbiology and Biotechnology,* **14**: 125-131.

Kottegoda, N., Manaweera, I., Madusanka, N. and Karunaretne, V. (2011), A green slow-release fertilizer composition based on urea-modified hydroxyapatite nano-particles encapsulated wood, *Current Science,* **101**(1): 73-78.

Kottegoda, N., Sandaruwan, C., Piryrashana, G., Siriwardhana, A., Rathnayake, A.U., Arachchige, D.M.B., Kumarasinghe, A.R., Dahanayake D., Karunaratne, V. and Amaratunga, G.A.J. (2017), Urea-hydroxyapatite nanohybrid for slow release of nitrogen, *ACS Nano,* **11**(2): 1214-1221.

Krivanek, O.L., Ursin, J.P., Bacon, N.J., Corbin, G.J., Dellby, N., Hrncirik, P., Murfitt, M.F., Own, C.S. and Szilagyi, Z.S. (2009), High-energy-resolution monochromator for aberration-corrected scanning transmission electron microscopy/electron energy-loss spectroscopy, *Philosophical Transactions of the Royal Society: A,* **367**: 3683–3697.

Kumar C.G., Pombala, S., Poornachandra, Y. and Agarwal, S.V. (2016), Synthesis, characterization, and applications of nanobiomaterials for antimicrobial therapy, *Nanobiomaterials in Antimicrobial Therapy, Elsevier,* **6**: 103-152,

Laftah, W.A. and Hashim, S. (2014), Synthesis, optimization, characterization and potential agricultural application of polymer hydrogel composites based on cotton microfiber, *Chemical Papers,* **68**(6): 798-808.

Laftah, W.A., Hashim, S. and Ibrahim, A.N. (2011), Polymer hydrogels: A review, *Polymer-Plastics Technology and Engineering,* **50**(14): 1475-1486.

Landon, J.R. (1991), Booker Tropical Soil Manual: A handbook for soil survey and agricultural land evaluation in the tropics and subtropics, *Longman,* Essex, New York, USA, pp. 113-141.

Lelago, A., Mamo, T., Haile, W. and Shiferaw, H. (2016), Assessment and mapping of status and spatial distribution of soil macronutrients in Kambata Tembaro zone, Southern Ethiopia, *Advances in Plants and Agriculture Research,* **4**(4): 00144.

Leye, A.S. and Omotayo, A.E. (2014), Mineralization rates of soil forms of nitrogen, phosphorus, and potassium as affected by organomineral fertilizer in sandy loam, *Advances in Agriculture,* **2014**: 1-5, Article ID 149209.

Li, A., Liu, R. and Wang, A. (2005), Preparation of starch-graft-poly(acrylamide)/attapulgite superabsorbent composite, *Journal of Applied Polymer Science,* **98**: 1351–1357.

Li, Y., Sun, Y., Liao S., Zou, G., Zhao, T., Chen, Y., Yang J. and Zhang, L. (2017), Effects of two slow-release nitrogen fertilizers and irrigation on yield, quality, and water-fertilizer productivity, *Agricultural Water Management,* **186**(31): 139-146

Li, Z., Zhang, Y. and Li, Y. (2013), Zeolite as slow release fertilizer on spinach yields and quality in a greenhouse test, *Journal of Plant Nutrition,* **36**(10): 1496-1505.

Lin, P-C., Lin, S., Wang, P.C. and Sridhar, R. (2014), Techniques for physicochemical characterization of nanomaterials, *Biotechnology Advances,* **42**(4): 771-726.

Liu, M., Liang, R, Zhan, F., Liu, Z. and Niu, A. (2007), Preparation of superabsorbent slow release nitrogen fertilizer by inverse suspension polymerization, *Polymer International,* **56**: 729–737.

Livney, Y.D., Portnaya, I., Faupin, B., Ramon, O., Cohen, Y., Cogan, U. and Mizrahi, S. (2003), Interactions between inorganic salts and polyacrylamide in aqueous solutions and gels, *Journal of Polymer Science: Part B; Polymer Physics,* **41**: 508–519.

Luce, M.S. Grant, C.A., Zebarth, B.J., Ziadi, N., O'Donovan, J.T., Blackshaw, R.E., Harker, K.N., Johnson, E.N., Gan, Y., Lafond, G.P., May, W.E., Khakbazan M. and Smith, E.G. (2015), Legumes can reduce economic optimum nitrogen rates and increase yields in a wheat–canola cropping sequence in western Canada, *Field Crops Research,* **179**: 12–25.

Lui, R. and Lal, R. (2014), Synthetic apatite nanoparticles as a phosphorus fertilizer for soybean (*Glycine max*), *Scientific Reports, Environmental Sciences,* **4**: 5686.

Maddonni, G.Á. and Martínez-Bercovich, J. (2014), Row spacing, landscape position and maize grain yield, *International Journal of Agronomy,* **2014**: Article ID 195012, 12 pgs.

Mahfoudhi, N. and Boufi, S. (2016), Poly(acrylic acid-co-acrylamide)/cellulose nanofibrils nanocomposite hydrogels: Effects of CNFs content on the hydrogel, *Cellulose,* **23**: 3691-3701.

Makokha, S., Kimani, S., Mwangi, W., Verkuij, H. and Musembi, F. (2001), Determinants of fertilizer and manure use in maize production in Kiambu district, Kenya, *Mexico, D.F.: International Maize and Wheat Improvement Center, Kenya Agricultural Research Institute.*

Malmström, E. and Carlmark, A. (2012), Controlled grafting of cellulose fibres: An outlook beyond paper and cardboard, *Polymer Chemistry,* **3**: 1702-1713.

Marturi, N. (2013), Vision and visual servoing for nanomanipulation and nanocharacterization in scanning electron microscope, *Micro and nanotechnologies/Microelectronics*, Universit́e de Franche-Comt́e, English.

Mastronardi, E. Mckeague, M. Monreal, C. and DeRosa, M. (2013), Development and application of crop exudate specific aptamers, *Journal of Biomolecular Structure and Dynamics*, **31**(1): 89.

Masunga, R.H, Uzokwe, V.N., Mlay, P.D., Odeh, I., Singh, A., Buchan, D. and De Neve, S. (2016), Nitrogen mineralization dynamics of different valuable organic amendments commonly used in agriculture, *Applied Soil Ecology,* **101**: 185–193.

Mateus, P.A., Barrias, C.C., Ribeiro, C., Ferraz, M.P. and Monteiro, F.J. (2007), Comparative study of nano-hydroxyapatite microspheres for medical applications, *Journal of Biomedical Materials Research,* **86**A: 483-493.

Mathenge M.K. (2009), Fertilizer types, availability and consumption in Kenya, Tegemeo Institute, Egerton University; *Paper presented at the 6th National Fertilizer Conference in Kenya, on "Towards Increased Use of Fertilizer and Improved Seed for Food Security and Economic Growth,"* *KARI headquarters, Nairobi, Kenya, August 20-21, 2009.*

Mauyo, L.W., Wanyama, J., Lusweti, C. and Nzomoi, J. (2011), Innovativeness of common interest groups in North Rift Kenya: A Case of Trans-Nzoia District. In: Bationo, A., Waswa, B., Okeyo, J., Maina, F., Kihara J. (Eds), Innovations as Key to the Green Revolution in Africa, *Springer,* Dordrecht, The Netherlands.

Mechay, A., Feki, H.L, Schoenstein, F. and Jouini, N. (2012), Nanocrystalline hydroxyapatite ceramics prepared by hydrolysis in polyol medium, *Chemical Physics Letters*, **541**: 75-80.

Mehlich, A. (1953), Determination of P, Ca, Mg, K, Na and NH_4, *North Carolina Soil Testing Laboratory,* Raleigh, University of North Carolina.

Milani, P., França, D., Balieiro, A.G. and Faez, R. (2017), Polymers and its applications in agriculture, *Polímeros,* **27**(3): 256-266.

Ministry of Agriculture, Livestock and Fisheries, State Department of Agriculture (2014), Soil suitability evaluation for maize production in Kenya, *National Accelerated Agricultural Inputs Access Programme (NAAIAP), Kenya Agricultural Research Institute (KARI), Department of Kenya Soil Survey Report.*

Monreal, C.M., DeRosa, M., Mallubhotla, S.C., Bindraban, P.S. and Dimkpa, C. (2015), Nanotechnologies for increasing the crop use efficiency of fertilizer-micronutrients, *Biology and Fertility of Soils,* **52**: 423.

Montalvo, D., McLaughlin, M.J., and Degryse, F. (2015), Efficacy of hydroxyapatite nanoparticles as phosphorus fertilizers in andisols and oxisols*, Soil Science Society of America Journal,* **79**: 551–558.

Montazeri, L., Jafar, J., Mohammad, A., Shahin, B. and Sayfoddin, J. (2010), Hydrothermal synthesis and characterization of hydroxyapatite and fluorhydroxyapatite nano-size Powders, *Biomedical Materials,* **5**: 045004.

Montgomery, E.G. (1911), Correlation studies in corn, *Nebraska Agricultural Experiment Station*, *Annual Report*, **24:** 108-159.

Mourdikoudis S., Pallares, R.M. and Thanh N.T.K. (2018), Characterization techniques for nanoparticles: comparison and complementarity upon studying nanoparticle properties, *Nanoscale,* **10**: 12871-12934.

Mucheru-Muna, M., Mugendi, D., Pypers, P., Mugwe, J., Kungu, J., Vanlauwe, B. and Merckx, R. (2014), Enhancing maize productivity and profitability using organic inputs and mineral fertilizer in Central Kenya small-hold farms, *Experimental Agriculture,* **50**(2): 250-269.

Mukaratirwa-Muchanyereyi, N., Kugara, J. and Zaranyinka, M.F. (2016), Surface composition and surface properties of water hyacinth (*Eichhonia crassipes*) root biomass: Effect of mineral acid and organic solvent treatments, *African Journal of Biotechnology,* **15**(21): 897-909.

Mullen, R.W. (2011), Nutrient cycling in soils: nitrogen, in: Hatfield, J.L., Sauer, T.J. (Eds), Soil Management: Building a Stable Base for Agriculture, *American Society of Agronomy and Soil Science Society of America,* Madison, WI, pp. 67–78.

Murphy, J. and Riley, J.P. (1962), A modified single solution method for the determination of phosphate in natural waters, *Analytica chimica acta,* **27**: 31-36

Muthoni, J.J., Shimelis, H. and Melis, R. (2013), Potato production in Kenya: Farming systems and production constraints, *Journal of Agricultural Science,* **5**(5): 182-197.

Naderi, M. and Danesh, S. (2013), Nano-fertilizers and their roles in sustainable agriculture, *International Journal of Agriculture and Crop Sciences,* **5**(19): 2229-2232.

Naima, B., Leila, H. and Adil, M. (2015), Effect of incubation period of phosphorous fertilizer on some properties of sandy soil with low calcareous content, Southern Algeria, *Asian Journal of Agricultural Research,* **9**(3): 123-131.

Nam, S., French, A.D., Condon, B.D., and Concha, M. (2016), Segal crystallinity index revisited by the simulation of X-ray diffraction patterns of cotton cellulose Iβ and cellulose II, *Carbohydrate Polymers*, **135**; 1–9.

Nawaz, M.S., Franklin, W. and Cerniglia, C.E. (1993), Degradation of acrylamide by immobilized cells of a *Pseudomonas sp*. and *Xanthomonas maltophilia, Canadian Journal of Microbiology,* **39**(2): 207-212.

Nawaz, M.S., Franklin, W., Campbell, W.L., Heinze, T.M. and Cerniglia, C.E. (1991), Metabolism of acrylonitrile by *Klebseilla pneumonia, Archives of Microbiology,* **156**: 231-238.

Nawaz, M.S., Khan, A.A., Seng, J.E., Leakey, J.E., Siitonen, P.H. and Cerniglial, C.E. (1994), Purification and characterization of an amidase from an acrylamide-degrading *Rhodococcus sp*., *Applied and Environmental Microbiology,* **60**(9): 3343-3348.

Nduati, M., Ncube, P., Roberts, S. and Vilakazi, T. (2015), Non-confidential final draft report: Market inquiry on fertilizer in Kenya, *Competition Authority of Kenya (CAK) and Centre for Competition, Regulation and Economic Development (CCRED),* University of Johannesburg.

Nelson, E.W. and Sommers, L.E. (1996), Total carbon, organic carbon and organic matter, in: D.L. Sparks (Ed.), Methods of soil analysis, Part 3: Chemical methods, *Soil Science Society of America,* Inc., Madison, WI.

Noellsch, A.J., Motavalli, P.P., Nelson, K.A. and Kitchen, N.R. (2009), Corn response to conventional and slow-release nitrogen fertilizers across a Claypan landscape, *Agronomy Journal,* **101**(3): 607-614.

OECD (Organisation for Economic Co-operation and Development) (1993a), Second meeting of the OECD experts on polymer definition: Chairman's report [ENV/MC/CHEM/RD(93)4]; April, 1993, Paris, France.

OECD (Organisation for Economic Co-operation and Development) (1993b), Third meeting of the OECD experts on polymers: Chairman's report [ENV/MC/CHEM/RD(93)4]; April, 1993, Tokyo, Japan.

Ojeda, J.J. and Dittrich, M. (2012), Fourier transform infrared spectroscopy for molecular analysis of microbial cells, in: Navid, A. (Eds), Microbial Systems Biology (Methods and Protocols)*, **881**: 187-211, Humana Press, Totowa, NJ.

Oleg, D.N. and Yefimov, N.A. (2019), Powder characterization and testing, in: Handbook of Non-Ferrous Metal Powders (2nd Ed.), *Elsevier,* pp. 3-62.

Omar, S.A. and Ismail, M.A. (1999), Microbial populations, ammonification and nitrification in soil treated with urea and inorganic salts, *Folia microbiologica,* **44**(2): 205-212.

Pandey, S.K. and Singh, H. (2011), A simple, cost-effective method for leaf area estimation, *Journal of Botany,* **2011**: Article ID 658240, 6 pgs.

Pang, X., Zeng H., Liu, J., Wei, S. and Zheng, Y. (2010), The properties of nanohydroxyapatite materials and its biological effects, *Material Sciences and Applications,* **1**: 81-90.

Pataquiva-Mateus, A.Y., Ferraz, M.P. and Monteiro, F.J. (2013), Nanoparticles of hydroxyapatite: Preparation, characterization and cellular approach: An overview, *Revista Mutis*, **3**(2): 43-57.

Poffenbarger, H.J., Barker, D.W., Helmers, M.J,, Miguez, F.E., Olk, D.C., Sawyer, J.E., Six, J., Castellano, M.J. (2017), Maximum soil organic carbon storage in Midwest U.S. cropping systems when crops are optimally nitrogen-fertilized, *PLoS ONE,* **12**(3): e0172293.

Poletto, M., Junior, H.L. and Zattera, A.J. (2014), Native cellulose: Structure, characterization and thermal properties, *Molecules,* **7**: 6105-6119.

Pönni, R. (2014), Changes in accessibility of cellulose for kraft pulps measured by deuterium exchange, *Aalto University Publication Series, Doctoral Dissertations* 68/2014.

Pramanik, N., Mishra, D., Banerjee, I., Maiti, T.K., Bhargava, P. and Pramanik, P. (2009), Chemical synthesis, characterization, and biocompatibility study of hydroxyapatite/chitosan phosphate nanocomposite for bone tissue engineering applications, *International Journal of Biomaterials,* **2009:** Article ID 512417, 8 pgs.

Puntel, L.A., Sawyer, J.E., Barker, D.W., Dietzel, R., Poffenbarger, H., Castellano, M.J., Moore, K.J., Thorburn, P. and Archontoulis, S.V. (2016), Modeling long-term corn yield response to nitrogen rate and crop rotation, *Frontiers in Plant Science,* **7**: 1-18.

Qiu, X. and Hu, S. (2013), "Smart" Materials based on cellulose: A review of the preparations, properties, and applications, *Materials,* **6**: 738-781.

Ragu, A. and Sakthivel, P. (2014), Synthesis and characterization of nano hydroxyapatite with polymethyl methacrylate nanocomposites for bone tissue regeneration, *International Journal of Science and Research*, **3**(11): 2282-2285.

Rahman, M., Das, B., Miah, M. and Ahmad, H. (2008), Fixation of urea to poly(acrylamide-maleic acid) and nitrogen release behaviour of the product: A comparison with urea and control, *Bulgarian Journal of Agricultural Science*, **14**(4): 373-380.

Rambo, M.K. and Ferreira, M.M. (2015), Determination of cellulose crystallinity of banana residues using near infrared spectroscopy and multivariate analysis, *Journal of the Brazilian Chemical Society,* **26**(7): 1491-1499.

Rashidzadeh, A., Olad, A., Salari, D. and Reyhanitabar, A. (2014), On the preparation and swelling properties of hydrogel nanocomposite based on sodium alginate-g-Poly (acrylic acid-co-acrylamide)/clinoptilolite and its application as slow release fertilizer, *Journal of Polymer Research,* **21**: 344.

Ray, R.C. and Singh, R.P. (1989), Leaf area estimation in capsicum (*Capsicum annuum* L.), *Scientia Horticulturae,* **39**(3): 181-188.

Reales-Alfaro, J.G., Trujillo, L.T., Arzuaga-Lindado, G., Castaño-Peláez, H.I. and Polo-Córdoba, A.D. (2013), Acid hydrolysis of water hyacinth to obtain fermentable sugars, *Ciencia, Tecnología* y *Futuro,* **5**(2): 101-112.

Reddy, P.P. (2014), Plant growth promotion rhizobacteria for horticultural crop protection, *Springer,* New Delhi, India, pp.17-30.

Ren, J., Kong, W. and Sun, R. (2014), Preparation of sugarcane bagasse poly(acrylic acid-co-acrylamide) hydrogels and their applications, bagasse acrylic absorbent, *BioResources,* **9**(2): 3290-3303.

Reyes, L.M., Sanders, D.C. and Buhler, W.G. (2008), Evaluation of slow-release fertilizers on bell pepper, *HorTechnology,* **18**(3): 393-396.

Rezania, S., Din, M.F., Kamaruddin, S.F., Taib, S.M., Singh, L., Yong, E.L. and Dahalan, A.F. (2016), Evaluation of water hyacinth (*Eichhornia crassipes*) as a potential raw material source for briquette production, *Energy,* **111**: 768-773.

Rop, K., Karuku, G.N., Mbui, D., Michira, I. and Njomo, N. (2018), Formulation of slow release NPK fertilizer (cellulose-graft-poly (acrylamide)/nano-hydroxyapatite/soluble fertilizer) composite and evaluating its N mineralization potential, *Annals of Agricultural Sciences,* **63**: 163-172.

Roy, D., Semsarilar, M., Guthriea, J. and Perrier, S. (2009), Cellulose modification by polymer grafting: A review, *RSC, Chemical Society Reviews,* **38**(7): 1825–2148.

Sadeghi, M. and Yarahmadi, M. (2011), Synthesis and properties of biopolymer based on carboxymethyl cellulose-g-poly(N-vinyl pyrollidin-co-2-acrylamido-2-methyl propan sulfonic acid as superabsorbent hydrogels, *Oriental Journal of Chemistry,* **27**(1): 13-21.

Sadeghi, M., Safari, S., Shahsavari, H., Sadeghi, H. and Soleimani, F. (2013), Effective parameters onto graft copolymer based on carboxymethyl with acrylic monomer, *Asian Journal of Chemistry,* **25**(9): 5029-5032.

Sadeghi, M., Soleimani, F. and Yarahmadi, M. (2011), Chemical modification of carboxymethyl cellulose via graft copolymerization and determination of the grafting parameters, *Oriental Journal of Chemistry,* **27**(3): 967-972.

Sagadevan, S. and Koteeswari, P. (2015), Analysis of structure and surface morphology, optical and electrical properties of copper nano-particles, *Journal of Nanomedicine Research*, **2**(5): 00040.

Sahrawat, K.L. (2008), Factors affecting nitrification in soils, *Communication in Soil Science and Plant Analysis,* **39**(9-10): 1436-1446.

Salami, A., Kamara, A.B. and Brixiova, Z. (2010), Smallholder Agriculture in East Africa: Trends, constraints and opportunities, working papers series No. 105, *African Development Bank,* Tunis, Tunisia.

Salariana, M., Solati-Hashjin, M., Goudarzi, A. Shafiei, S.S., Salarian, S. and Nemati, Z.A. (2008), Effect of surfactant in formation of nano-rods under hydrothermal conditions, *Iranian Journal of Phamacuetical Sciences,* **4**(2): 157-162.

Sannino, A., Demitri, C. and Madaghiele, M. (2009), Biodegradable cellulose-based hydrogels: Design and applications: A review, *Materials,* **2**: 353-373.

Sannino, A., Mensitieri, G. and Nicolais, L. (2004), Water and synthetic urine sorption capacity of cellulose based hydrogels under a compressive stress field, *Journal of Applied Polymer Science,* **91**(6): 3791-3796.

Saputra, A.H., Hapsari, M. and Pitaloka, A.B. (2015), Synthesis and characterization of CMC from water hyacinth cellulose using isobutyl-isopropyl alcohol mixtures as reaction medium, *Contemporary Engineering Sciences,* **8**(33): 1571-158.

Savci, S. (2012), An Agricultural Pollutant: Chemical Fertilizer, *International Journal of Environmental Science and Development*, **3**(1): 77-80.

Schildhauer, J., Wiedemuth, K. and Humbeck K., (2008), Supply of nitrogen can reverse senescence processes and affect expression of genes coding for plastidic glutamine synthetase and lysine-ketoglutarate reductase/saccharopine dehydrogenase, *Plant Biology,* **10**(1): 76-84

Shahid, S.A., Qidwai, A.A., Anwar, F., Ullah, I. and Rashid, U. (2012), Effects of a novel poly(AA-co-AAm)/AlZnFe2O4/potassium humate superabsorbent hydrogel nanocomposite on water retention of sandy loam soil and wheat seedling growth, *Molecules*, **17**: 12587-12602.

Shanker, R., Ramakrishna, C. and Seth, P.K. (1990), Microbial degradation of acrylamide monomer, *Archives of Microbiology,* **154**: 192-198.

Shen, J., Yuan, L., Zhang, J., Li, H., Bai, Z, Chen, X., Zhang, W. and Zhang, F. (2011), Phosphorus dynamics: From soil to plant, *Plant physiology,* **56**: 1997-1005.

Shi, X., Wen, W. and Ai-Qin, W. (2011), Effect of surfactant on porosity and swelling behaviors of guar gum-g-poly(sodium acrylate-co-styrene)/Attapulgite superabsorbent hydrogels, *Colloids and Surfaces B: Biointerfaces,* **88**: 279–286.

Sihag, S., Pathak, H. and Jaroli, D.P. (2014), Factors affecting the rate of biodegradation of polyaromatic hydrocarbons, *International Journal of Pure & Applied Bioscience,* **2**(3): 185-202.

Simoni R.C., Lemes G.F., Fialho S., Gonçalves O.H., Gozzo A.M., Chiaradia V., Sayer, C., Shirai, M.A. and Leimann, F.V. (2017), Effect of drying method on mechanical, thermal and water absorption properties of enzymatically crosslinked gelatin hydrogels, *Anais da Academia Brasileira de Ciências*, **89**(1): 745-755.

SiunChee, T., ChinEng, O., Yuen, K.H. and Beow, C.Y. (2013), Cellulose and its application in biomolecules purification, *International Research Journal of Applied and Basic Sciences*, **7**(5): 267-276.

Smith D.J. (2008), Development of aberration-corrected electron microscopy, *Microscopy and Microanalysis,* **14**: 2–15.

Sojka, R.E., Entry, J.A. and Fuhrmann, J.J. (2006), The influence of high application rates of polyacrylamide on microbial metabolic potential in an agricultural soil, *Applied Soil Ecology,* **32**: 243–252.

Soleimani, F. and Sadeghi, M. (2012), Synthesis of pH-sensitive hydrogel based on starch-polyacrylate superabsorbent, *Journal of Biomaterials and Nanobiotechnology*, **3**: 310-314.

Sombroek, W.G., Braun, H.M. and Van Der Pouw, B.J. (1982), The exploratory soil map and agro climatic zone map of Kenya, 1980 scale 1: 1,000,000. Exploratory Soil Survey Report No. E1, *Kenya Soil Survey,* Nairobi, Kenya

Stagnari, F. and Pisante, M. (2012), Slow release and conventional N fertilizers for nutrition of bell pepper, *Plant, Soil and Environment,* **58**(6): 268–274.

Stanford, G. and Smith, S.J. (1972), Nitrogen mineralization potentials of soils, *Soil Society of America Journal,* **36**(3): 465-472.

Stanford, G., Carter S.J. and Smith, S.J. (1974), Estimates of potentially mineralizable soil nitrogen based on short term incubations, *Soil Science Society of America Proceedings,* **38**(1): 99-102.

Swantomo, D., Rochmadi, Basuki K. and Sudiyo, R. (2013), Synthesis and characterization of graft copolymer rice straw cellulose-acrylamide hydrogels using gamma irradiation, *Atom Indonesia*, **39**(2): 57-62.

Synytsya, A. and Novak, M. (2014), Structural analysis of glucans: A review, *Annals of Translational Medicine,* **2**(2): 17.

Tambone, F. and Adani, F. (2017), Mineralization from digestate in comparison to sewage sludge, compost and urea in a laboratory incubation soil experiment, *Journal of Plant Nutrition and Soil Science,* **180**: 355-365.

Tayebi, L. and Moharamzadeh, K. (2017), Introduction to oral and dental tissue engineering, *Biomaterials for Oral and Dental Tissue Engineering, Elsevier,* pp. 3-6.

Thombare, N., Mishra, S., Siddiqui, M.Z., Jha, U., Singh, D. and Mahajanc, G.R. (2018), Design and development of guar gum based novel, superabsorbent and moisture retaining hydrogels for agricultural applications, *Carbohydrate Polymers,* **185**: 169–178.

Titus, D., Samuel, E.J.J. and Roopan, S.M. (2019), Nanoparticle characterization techniques, *Green Synthesis, Characterization and Applications of Nanoparticles*, *Elsevier,* pp. 303-319.

Tiwari, J.N., Tiwari, R.N. and Kim, K.S. (2012), Zero-dimensional, one-dimensional, two-dimensional and three-dimensional nanostructured materials for advanced electrochemical energy devices, *Progress in Materials Science,* **57**: 724–803

Ţolescu, C. and Horia, I. (2010), Polymer conditioned fertilizers, *U.P.B. Sci. Bull., Series B,* **72**(2): 1-14.

Tolescu, C., Neamtu, C., Raceanu, G., Popescu, M. and Iovu, H. (2009), Polymeric micro-structures for slow release of fertilizers, *Materiale Plastice,* **46**(4): 387-392.

TonThat, T.C., Busscher, W.J., Novak, J.M., Gaskin, J.F. and Kim, Y. (2008), Effects of polyacrylamide and organic matter on microbes associated to soil aggregation of Norfolk loamy sand, *Applied Soil Ecology,* **40**: 240- 249.

Wada, M., Heux, L. and Sugiyama, J. (2004), Polymorphism of cellulose I family: reinvestigation of cellulose IV$_I$, *Biomacromolecules*, **5**(4): 1385-1391.

Wang, G.L., Ye, Y.L., Chen, X.P. and Cui, Z.L. (2014), Determining the optimal nitrogen rate for summer maize in China by integrating agronomic, economic and environmental aspects, *Biogeosciences,* **11**: 3031–3041.

Wang, J., Zheng, Y. and Wang, A. (2010), Synthesis and swelling behaviors of poly(sodium acrylate)/hydroxyapatite superabsorbent nanocomposites, *Advanced Materials Research,* **96**: 227-232.

Wang, M., Guo, L. and Sun, H. (2019), Manufacture of biomaterials, in: Encyclopedia of Biomedical Engineering, *Elsevier*, pp. 116-134.

Wang, M., Zheng, Q., Shen, Q. and Guo, S. (2013), The critical role of potassium in plant stress response, *International Journal of Molecular Science,* **14**(4): 7370-7390.

Wang, X. and Tang, C. (2018), The role of rhizosphere pH in regulating the rhizosphere priming effect and implications for the availability of soil-derived nitrogen to plants, *Annals of Botany,* **121**(1): 143-151.

Watson, C., Singh, Y., Iqbal, T., Knoblauch, C., Simon, P. and Wichern, F. (2016), Short-term effects of polyacrylamide and dicyandiamide on C and N mineralization in a sandy loam soil, *Soil Use and Management,* **32**: 127–136.

Wei, S., Tan, W., Liu, F., Zhao, W. and Weng, L. (2014), Surface properties and phosphate adsorption of binary systems containing goethite and kaolinite, *Geoderma*, **213**: 478–484.

Witono, J.R., Noordergraaf, I.W., Heeres, H.J. and Janssen, L.P. (2014), Water absorption, retention and the swelling characteristics of cassava starch grafted with polyacrylic acid, *Carbohydrate Polymers,* **103**: 325-332.

Woo, H.R., Kim, H.Y., Nam, H.G. and Lim, P.O. (2013), Plant leaf senescence and death – regulation by multiple layers of control and implications for aging in general, *Journal of Cell Science,* **126**(21): 4823–4833.

WRB (World Reference Base) for Soil Resource (2015), International soil classification for naming soils and creating legends for maps, *World Soil Resources Report,* **106**.

Yayeh, S.G., Alemayehu, M., Haileslassie, A. and Dessalegn, Y. (2017), Economic and agronomic optimum rates of NPS fertilizer for irrigated garlic (*Allium sativum L.*) production in the highlands of Ethiopia, *Cogent Food and Agriculture,* **3**: 1333666.

Yu, F., Fu, R., Xie, Y. and Chen W. (2015), Isolation of polyacrylamide-degrading bacteria from dewatered sludge, *International Journal of Environmental Research and Public Health,* **12**: 4214-4230.

Yu, Y., Liu, L., Kong, Y., Zhang, E. and Liu, Y. (2011), Synthesis and properties of N-maleyl chitosan cross-linked poly(acrylic acid-co-acrylamide) superabsorbents, *Journal of Polymers and the Environment,* **19**(4): 926-934.

Yuan, S., Jia, L., Qinyan, Y., Qian, L. and Baoyu, G. (2014), Adsorption of ammonium and phosphate by feather protein based semi-interpenetrating polymer networks hydrogel as a controlled-release fertilizer, *Environmental Technology*, **35**(4): 446–455.

Yuejin, W., Xiaoyu, N., Zhengyan, W., Lin, W., Guannan, Q. and Lixiang, Y. (2013), A novel slow-release urea fertilizer: Physical and chemical analysis of its structure and study of its release mechanism, *Biosystems Engineering,* **1159**: 274-282.

Yusong, P. and Dangsheng, X. (2010), Preparation and characterization of nano-hydroxyapatite/polyvinyl alcohol gel composites, *Journal of Wuhan University of Technology-Material Science Education,* **25**(3): 474-478.

Zaman, M., Nguyen, M.L., Blennerhassett, J.D. and Quin, B.F. (2008), Reducing NH_3, N_2O and NO_3–N losses from a pasture soil with urease or nitrification inhibitors and elemental S-amended nitrogenous fertilizers, *Biology and Fertility of Soils*, **44**: 693–705.

Zeroual, Y. and Kossir, A. (2012), Smart fertilizers for sustainable agriculture: The state of the art and the recent developments, *25th AAF International Fertilizer Technology Conference and Exhibition,* Morocco.

Zhang, J., Wang, Q., and Wang, A. (2007), Synthesis and characterization of chitosan-g-poly(acrylic acid)/attapulgite superabsorbent composites, *Carbohydrate Polymers*, **68**: 367–374.

Zhang, Y., Xu, W., Duan, P., Cong, Y., An, T. and Yu, N. (2017), Evaluation and simulation of nitrogen mineralization of paddy soils in Mollisols area of North East China under water logged incubation, *PLoS ONE*, **12**(2): 1-19.

Zhong, K., Lin, Z-L. and Zheng, X-L. (2013), Starch derivative-based superabsorbent with integration water-retaining and controlled release fertilizers, *Carbohydrate Polymers,* **92**: 1367-1376.

Zhu, Y.L., Zayed, A.M., Qian, J-H., de Souza, M. and Terry, N. (1999), Phytoaccumulation of trace elements by wetland plants: II. Water hyacinth, *Journal of Environmental Quality*, **28**: 339-344.

Zohuriaan-Mehr, M.J. and Kabiri, K. (2008), Superabsorbent polymer materials: A review, *Iranian Polymer Journal*, **17**(6): 451-477.

INTERNET REFFERENCES

http://agritech.tnau.ac.in/agriculture/agri_nutrientmgt_fertilizers.html, Available 11th March, 2019.

http://www.nafis.go.ke/vegetables/kales/, Available 25th March, 2019.

https://blog.phenom-world.com/what-is-sem, Available 23rd August, 2019.

https://serc.carleton.edu/research_education/geochemsheets/techniques/SEM.html, Available 23rd August, 2019.

https://www.innerfidelity.com/content/hard-core-diy-scanning-electron-microscope

Liao, Y. (2006). Practical electron microscopy and database. An online book. http://www.globalsino.com/EM/, Available 20th March, 2019.

Liu, G., Zotarelli, L., Li, Y., Dinkins, D., Wang, Q., Ozores-Hampton M. (2014). Controlled-release and slow-release fertilizers as nutrient management tools, http://edis.ifas.ufl.edu/pdffiles/HS/HS125500.pdf, Available 26th March, 2019.

Olson-Rutz, K., Jones, C. and Dinkins, C.P., (2011), Enhanced efficiency fertilizers, *Montana State University Extension*, http://landresources.montana.edu/soilfertility/documents/PDF/pub/EEFEB0188.pdf , Available 25th August, 2019.

Oseko E. and Dienya T. (2015), Fertilizer consumption and fertilizer use by crop (FUBC) in Kenya, 2010-2013, https://africafertilizer.org/wp-content/uploads/2017/05/FUBC-Kenya-final-report-2015.pdf, Available 25th August, 2019.

Shoals, M. (2012), Kenya Fertilizer Assessment, The African Fertilizer and Agribusiness Partnership, IFDC. https://africafertilizer.org/wp-content/uploads/2017/04/Kenya-Fertilizer-Market-Assessment-IFDC-AFAP-June-2012.pdf, Available 25th August, 2019.

APPENDICES

Appendix 1. a) Water hyacinth (WH) in Nairobi dam, b) Solvent extracted WH

Appendix 2. a) 1st bleaching of WH with NaOCl, b) Alkaline treatment with NaOH

Appendix 3. a) 2ⁿᵈ bleaching, b) Acid hydrolysis using 1 M HCl

Appendix 4. a) Washing of cellulose fibres using filter cloth, b) Swollen cellulose fibres

Appendix 5. a) Cellulose pulp, b) Oven dried cellulose fibers

Appendix 6. a) Swollen WH cellulose-g-poly(acrylamide-co-AA), b) Soxhlet extraction of homopolymer using acetone

Appendix 7. a) Nano-HA powder, b) Swollen WH cellulose-g-poly(acrylamide-co-AA)/nano-
HA composite

Appendix 8. a) Swollen PHG without cellulose, b) Oven dried PHG without cellulose